Army Institute Of Technology (AIT), Dighi Camp, Pune - 15.
Director : 7249250115, Joint Director : 7249250117, Principal : 7249250186
Exch : 7249250183, 7249250184, 7249250185
Website : www.aitpune.com Email : ait@aitpune.edu.in
Recognised by AICTE and DTE Maharashtra and affiliated to Savitrabai Phule Pune University

2.4.2 Percentage of Full time teachers with NET / SET / Ph.D / D.Sc. / D.Litt. / L.L.D during the last 5 years

Faculty Details

- Course work
- PhD Certificate
- Copy of Publication

Note:

The coursework of Dr. P.B. Karandikar (E&TC), Dr. Umesh Vandeorao Awasarmol (Mechanical), and Dr. Ashok Kr Singh (ASGE) has not been included, as it was not part of their PhD curriculum.

Army Institute Of Technology (AIT), Dighi Camp, Pune - 15.
Director : 7249250115, Joint Director : 7249250117, Principal : 7249250186
Exch : 7249250183, 7249250184, 7249250185
Website : www.aitpune.com Email : ait@aitpune.edu.in
Recognised by AICTE and DTE Maharashtra and affiliated to Savitrabai Phule Pune University

ONWARD TO GLORY

Dr. P B Karandikar (E&TC)

- PhD Certificate
- Publication Copy

EN14-00009

Savitribai Phule Pune University

(Formerly University of Pune)

We, the Chancellor, the Vice Chancellor and the Members of the Management Council and the Academic Council of the Savitribai Phule Pune University certify that

Karandikar Parashuram Balwant

Mother's Name : Bhagyashree

having been examined and found duly qualified for the degree of

Doctor of Philosophy

(Electrical)

The said degree has been conferred on him. In testimony whereof is set the seal of the said University.

आम्ही, सावित्रीवाई फुले पुणे विद्यापीठाचे कुलपति, कुलगुरु आणि व्यवस्थापन परिषद व विद्या परिषद सदस्य, प्रमाणित करितो की,

करंदीकर परशुराम बळवंत

आईचे नाव : भाग्यश्री

विद्यावाचस्पति

(इलेक्ट्रिकल)

पदवीस पात्र झाल्यावद्दल त्यांना ही पदवी प्रदान करण्यात येत आहे. याची साक्ष म्हणून विद्यापीठाची अधिकृत मुद्रा येथे अंकित करण्यात येत आहे.

सावित्रीबाई फुले पुणे विद्यापीठ

02nd March 2015

EN14-00009

Vice Chancellor

Journal of Energy Storage 68 (2023) 107829

Contents lists available at ScienceDirect

Journal of Energy Storage

journal homepage: www.elsevier.com/locate/est

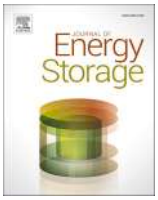

Research papers

Analysis of asymmetrical supercapacitor with horizontally configured electrodes

Sangram Gite [a], R.S. Ambekar [a], S.B. Abrish Aaditya [b], Sarang Joshi [c], P.B. Karandikar [b,*]

[a] Bharati Vidyapeeth University College of Engineering, Pune, India
[b] Army Institute of Technology, Pune, India
[c] AISSMS Institute of Information Technology, Pune, India

ARTICLE INFO

Keywords:
Energy
Storage
Horizontal
Asymmetrical
Supercapacitor

ABSTRACT

Energy is available in several forms but its use to humans is predominantly in the electrical form. Since electrical energy is not immediately consumed post conversion, energy storage devices are required for its storage. This reinforces the importance of research in electrical energy storage devices. Till date, very few energy storage devices have been developed for commercial use. Asymmetrical supercapacitors are the newest addition to this list and have the potential to replace conventional energy storage devices in times to come. They can be further classified based on their electrode orientation namely horizontally and vertically configured electrodes. Research has been conducted on asymmetrical supercapacitors with horizontally configured electrodes as they have a better performance over vertically configured electrode. Analysis of asymmetrical supercapacitor with horizontally configured electrodes through statistical modelling approach is presented in the paper which is useful in setting electrode parameter values during the manufacture of this device. Electrode material loading on current collector of both electrodes is found to be affecting specific-capacitance values; they also add to nonlinearity in the device. Metal oxide contents are an addition to the interaction effect. Modelling approach adopted has provided better insights as to how various electrode parameters interact and in turn affect the specific capacitance. Presented research work also brings out need of extra negative plate or bigger size negative plate in asymmetrical supercapacitors. Findings of this research work can be used as basis for study of other electrical energy storage devices such as battery, fuel cell etc.

1. Introduction

There are various types of energy, such as thermal energy, hydro energy, nuclear energy, solar energy, and many more. Every aspect of society requires energy in various forms and quantities for their daily activities. Energy consumption is expected to rise in coming generations, making energy storage of the most convenient form of energy is critical. Energy in electrical form is the most convenient to generate, transmit and store. Electrical energy is traditionally stored in batteries. Recently a lot of research work is being carried out in the development of hybrid energy storage systems [1]. Various types of supercapacitors which can be referred to as family of supercapacitors are the latest addition to electrical energy storage devices. Supercapacitors have the main advantage of extremely long life. Supercapacitors have very good cyclic stability, high power density, and specific-capacitance. Nowadays research is being carried out extensively for better performance of supercapacitors by developing electrode materials. Asymmetrical Supercapacitor (ASC) is also reported in some literature. Various materials and modelling methods are important aspects of this device. Vertical electrode structure has been analyzed using statistical modelling approach [2]. Various types of biomass-based carbon have been tried in many electrical energy storage devices with limited success [3,4]. Study related to conducting polymer and carbon based nanomaterials have been reported [5]. Mainly electric double-layer supercapacitors are used as they are made from various carbon materials such as activated carbon, which have the advantage of a very high surface area and good conductivity. Recent studies have shown that anode made from carbon nano-materials, carbon black, aero gels, graphene with additions by transition metal oxide exhibits larger capacitance. Flexible hybrid supercapacitor with remarkable electrochemical performance is one of the key findings in recent past [6]. Designing a high energy-density and flexible asymmetric supercapacitor by electrode

* Corresponding author.
E-mail addresses: abrishaditya_21417@aitpune.edu.in (S.B.A. Aaditya), pbkarandikar@aitpune.edu.in (P.B. Karandikar).

https://doi.org/10.1016/j.est.2023.107829
Received 3 February 2023; Received in revised form 4 May 2023; Accepted 22 May 2023

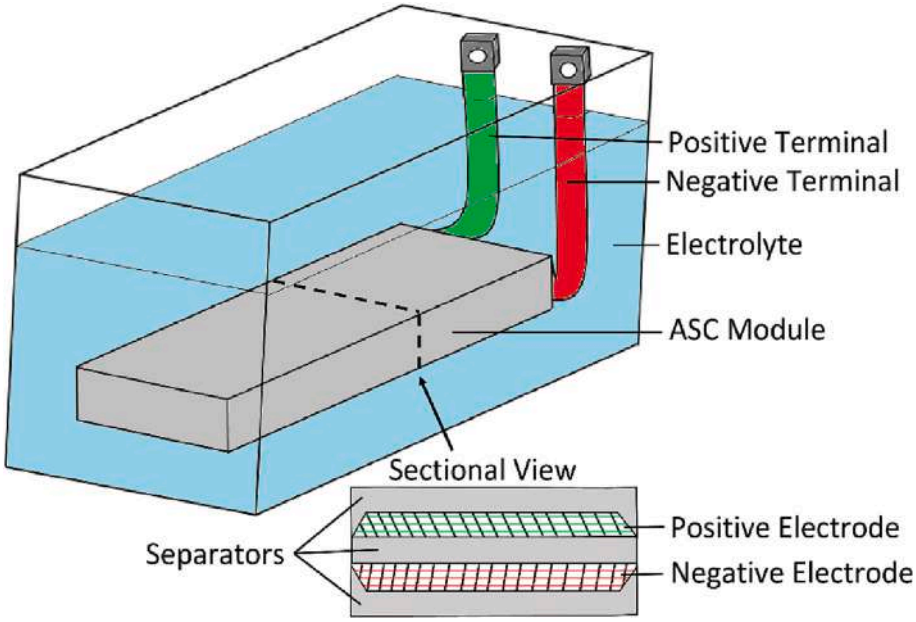

Fig. 1. ASC with horizontally configured electrodes by keeping positive electrode at the top.

engineering and charge matching mechanism has been also reported [7]. Optimization of electrode material using artificial neural network has been successfully demonstrated [8]. Research work entailing use of solar energy to charge asymmetrical supercapacitor has been reported [9]. Lot of research work related to adhesives, binders and current collectors have been reported in recent past [10–13]. Use of various modelling methods such as material-based modelling, circuit based modelling etc. are suitable for analysis of electrical energy storage devices. It is found that statistical modelling method is better than others as it gives insights of the device at electrode and electrolyte level [14]. Carbon based materials are most suitable as base material in electrical energy storage devices. Use of graphene is also found to be good option for electrode material [15]. Work related to hybrid energy storage system using various carbon materials is also found in literature review [16,17]. Use of composite material along with activated-carbon is latest trend in electrochemical devices [18]. Study related to thermal characteristics, ageing and innovative output parameters is also being reported [19,20]. Numerical method-based modelling is also tried by researchers [21]. Carbon nano-sheets, 3D free formable graphene foam related research work is showing promising results [22–24]. Use of nano-sheets with enhanced material properties is also reported be few researchers [25–27]. It is found that materials like graphene composites for anode have exhibited good results [28]. Research has been conducted on synthesis of organic hybrid supercapacitors that are sustainable to the environment and are economical [29]. MXene and manganese dioxide have been used to construct asymmetric supercapacitors with extremely high energy and power densities [30]. Use of scaffold-regulated strategy for secondary-ion batteries is the latest research found in recent literature [31]. ASC with horizontally configured electrodes has been reported with more than 2000 cyclic stability [32]. Use of statistical modelling method is suitable for analysis of ASC like complicated systems [2,33]. After extensive literature survey, it was found that, the research has been carried out on the electrode parameters i.e. material loading of negative electrode, material loading of positive electrode and percentage manganese-dioxide in positive electrode on the ASC with vertically configured electrodes. The results obtained were that loading of positive electrode was a vital parameter, and the loading of activated-carbon on the negative electrode contributed towards nonlinearity. Interaction between the activated-carbon in the negative electrode and percentage of manganese-dioxide in the positive electrode had a strong effect [2]. ASC with horizontally configured electrode is giving better parameters and higher cyclic life [32]. Similar kind of analysis was not found with respect to ASC with horizontally configured electrodes and is the major research gap identified from the literature survey. 3D electrode structure is also rarely investigated but it is out of scope of the presented work. It was decided to analyse effects of electrode parameters of ASC with horizontally configured electrodes. Conventional electrochemical techniques for analysis are not used as they cannot give interaction effects and non-linearity effects. Two level-three parameters full factorial Design of Experiment (DoE) as well as Response Surface Methodology (RSM) modelling method are used and are presented in the following sections.

This paper is divided into following sections: Section 2 is based on the electrode parameters for analysis of ASC with horizontally configured electrodes. The three electrode parameters selected for modelling are discussed in detail in this section. Section 3 is about full factorial DoE modelling with specific-capacitance as an output parameter. This model gives main effect and interaction effect. Section 4 is about the RSM modelling to identify the parameter introducing nonlinearity in the device and it is followed by concluding remarks.

2. Electrode parameters for analysis

Supercapacitors are pulse current devices. They can be broadly classified based on their electrode composition. A symmetrical supercapacitor is one that has both electrodes made of the same material, such as activated carbon or a combination of activated carbon and a suitable metal oxide. ASCs have two electrodes made of different materials, such as activated carbon or a metal oxide mixed in activated carbon. Comparison of symmetrical and asymmetrical supercapacitors was undertaken through experimental trials. Symmetrical supercapacitor was made using activated-carbon on both the electrodes. Then asymmetrical supercapacitor with activated-carbon on negative electrode and metal oxide on the positive electrode was tested. Subsequently, asymmetrical supercapacitor using activated-carbon on the negative electrode and activated-carbon mixed in metal oxide in equal weight proportions on the positive electrode was also tested. Of these three combinations, it was found that the asymmetrical supercapacitor using activated-carbon on the negative electrode and activated-carbon mixed in metal oxide in equal weight proportions on the positive electrode gave 40 % better

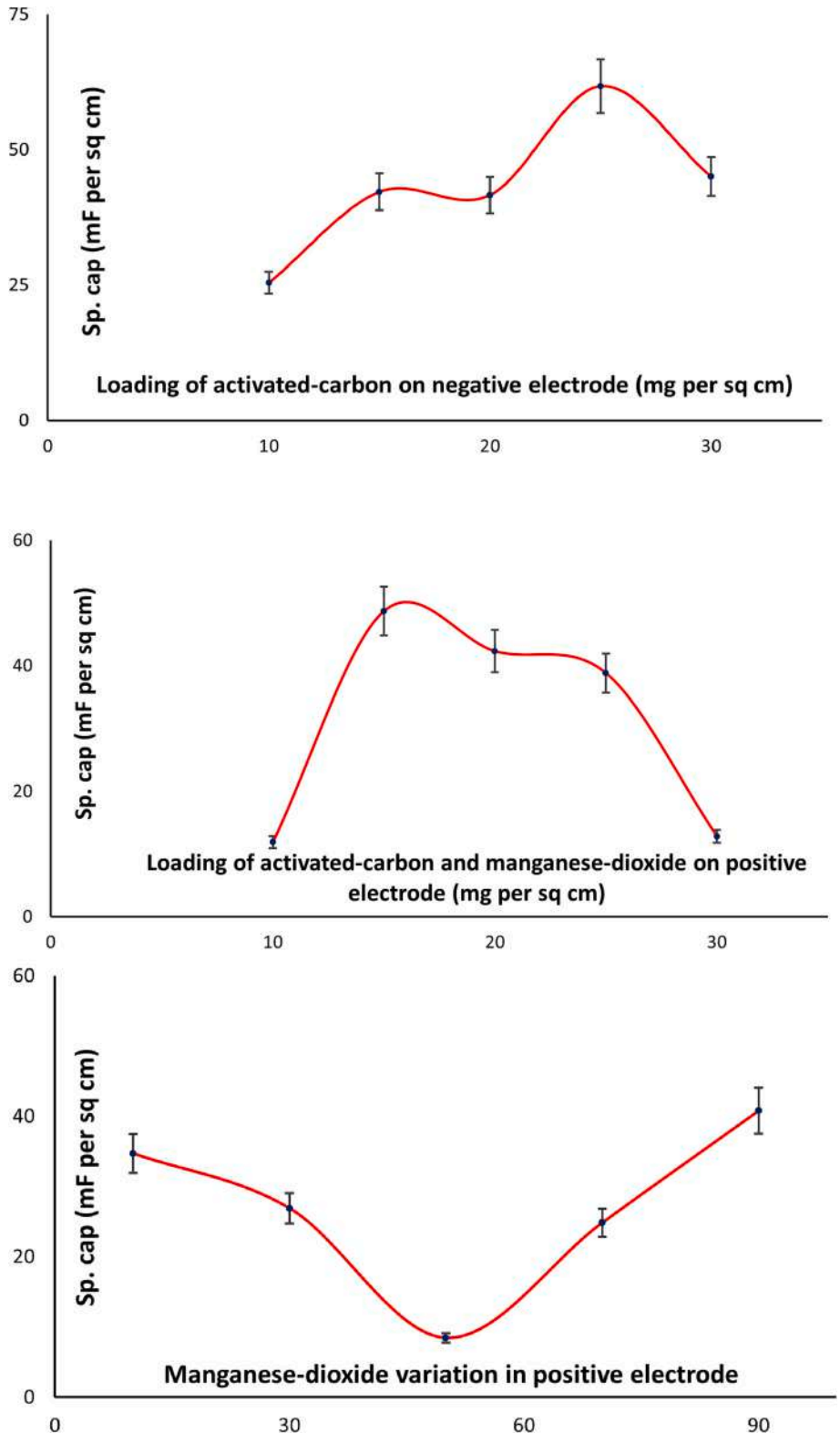

Fig. 2. Variation of specific capacitance against the change in selected parameters for modelling by considering one-parameter at a time.

results in case of capacitance than symmetrical supercapacitor and hence it is used for further analysis [20].

Most energy storage devices have vertical electrode configuration. The other possibility that arises is the fact that energy storage devices can have electrodes in horizontal configuration. The study of specific-capacitance of ASC with horizontally and vertically configured electrodes over a period had been conducted where the ASC with horizontally configured electrodes at the lab level is found to be better. Experimentation or Trials of various combinations with Vulcan XC72-R as the activated-carbon and manganese-dioxide as the metal oxide were loaded on stainless steel current collector without the use of binder material. Potassium sulphate of 0.65 molarity electrolyte which gives

Table 1
Coded and actual values for full-factorial DoE trials.

DoE parameter notation	Name of the parameter	Max value (Actual and coded)	Min value (Actual and coded)
A	Loading of activated-carbon on negative electrode	25 mg per sq. cm coded as +1	10 mg per sq. cm coded as −1
B	Loading of activated-carbon and manganese-dioxide on positive electrode	15 mg per sq. cm coded as +1	10 mg per sq. cm coded as −1
C	Manganese-dioxide variation in positive electrode	90 % coded as +1	50 % coded as −1

Table 2
Coded values of input parameters for trials carried out to develop full factorial DoE model [33].

	Factors		
Sr. No.	A	B	C
1	−1	−1	−1
2	−1	−1	1
3	−1	1	−1
4	−1	1	1
5	1	−1	−1
6	1	−1	1
7	1	1	−1
8	1	1	1

2.2 V as an operating voltage with polythene as separator material has been used for trials [10]. During experimentation, negative electrode is loaded only with activated-carbon, and positive electrode is coated with a mixture of activated-carbon and manganese-dioxide to form ASC. The electrodes are separated by a dielectric and porous separator piece, which is then submerged in an electrolyte. An important step in determining the performance and durability of electrical energy storage devices can be to test the electrodes' structural stability. Some potential methods to test for structural stability are cyclic voltammetry, scanning electron microscopy, X-ray diffraction, electrochemical impedance spectroscopy, In-situ electrochemical atomic force microscopy etc. it is important to select the appropriate method based on specific requirements and the electrode materials being tested. Authors found that the developed ASC modules to be structurally strong. Detailed analysis related to structural stability requires different approach and will be taken up subsequently. Output parameters for ASC are specific-capacitance, power density, energy density, internal resistance and pulse current. Specific-capacitance is taken as an output parameter in this research paper as it is the most important parameter in all the applications of this device. ASC with vertical electrode configuration gave 25 % more specific capacitance as compared to symmetrical supercapacitor with vertical electrode configuration. On comparison of asymmetrical supercapacitor with vertical electrode configuration, ASC with horizontally configured electrodes with negative electrode on top gave 30 % more specific-capacitance and ASC with horizontally configured electrodes with positive electrode on top gave 80 % more specific-capacitance [32]. In the vertical configuration, the electrode material after it has established contact with the electrolyte gets moistened and detaches from the current collector leading to less faradaic reaction taking place to generate and store electrons. In the case of horizontal configuration, the possibility of this effect is very less and hence horizontally configured electrode ASC is better than vertically configured electrode ASC. This leads to stable performance of ASC with horizontally configured electrodes with time. It was noticed that the horizontal configuration with positive electrode at the top and negative electrode at bottom configuration is better and more stable. This is primarily because the active material of electrode i.e., metal oxide is

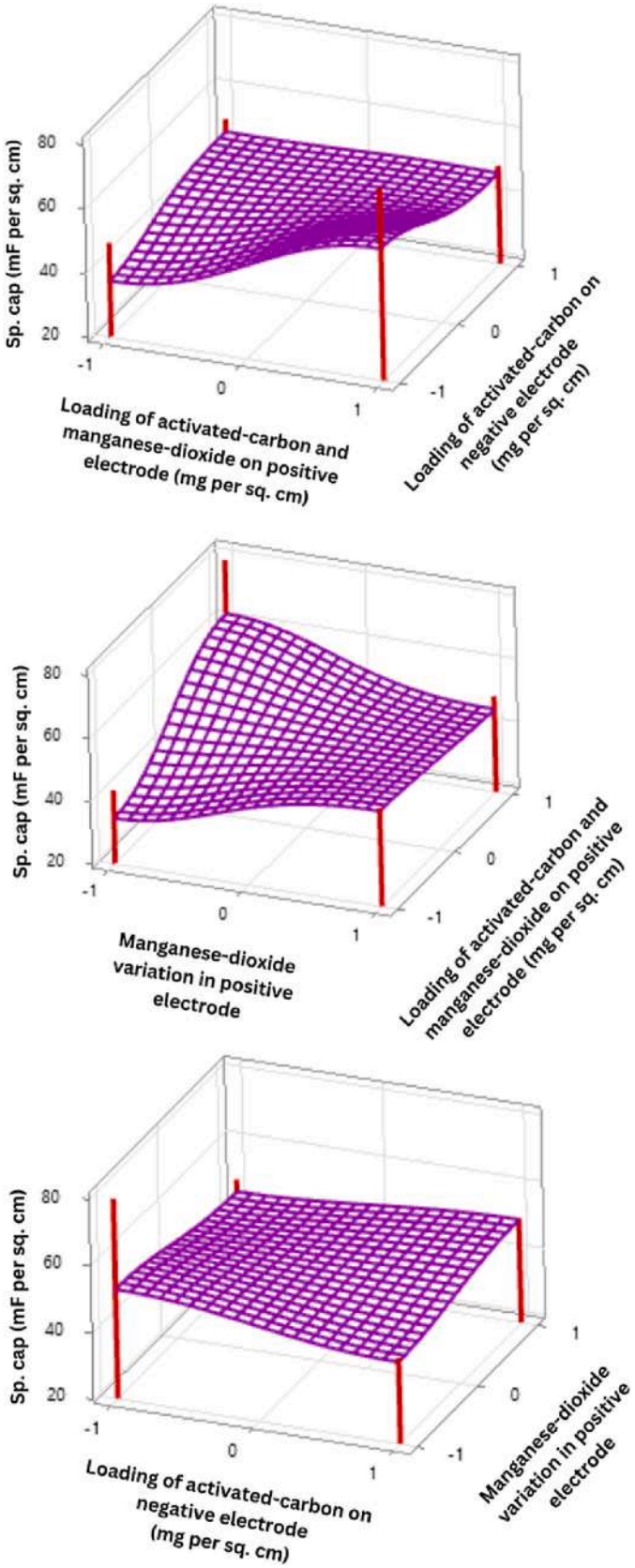

Fig. 3. Surface plots obtained by Minitab software with project lines using full factorial DoE model of various parameters influencing specific-capacitance to indicating interaction effect.

Table 3
Coded and actual values for RSM trials.

RSM Parameter notation	Name of the parameter	Max value (coded: +1.68)	Intermediated min value (coded: +1)	Mid value (coded: 0)	Intermediated max value (coded: −1)	Min Value (coded: 1.68)
A	Loading of activated-carbon on negative electrode	25 mg per sq. cm	22.2 mg per sq. Cm	17.5 mg per sq. cm	12.8 mg per sq. cm	10 mg per sq. cm
B	Loading of activated-carbon and manganese-dioxide on positive electrode	15 mg per sq. cm	14.1 mg per sq. Cm	12.5 mg per sq. cm	10.9 mg per sq. cm	10 mg per sq. cm
C	Manganese-dioxide variation in positive electrode	90 %	82.5 %	70 %	57.5 %	50 %

Table 4
Coded values of input parameters for trials carried out to develop RSM model [33].

	Factors		
Sr. No.	A	B	C
1	−1	−1	−1
2	−1	1	−1
3	0	0	0
4	1	1	1
5	1	−1	−1
6	0	0	0
7	0	0	0
8	1	1	−1
9	0	0	0
10	−1	−1	1
11	1	−1	1
12	−1	1	1
13	0	1.68	0
14	0	0	0
15	0	0	0
16	0	−1.68	0
17	0	0	1.68
18	0	0	−1.68
19	1.68	0	0
20	−1.68	0	0

moving towards the current collector as a result, capacitance stabilizes. ASC with horizontally configured electrodes as shown in Fig. 1 is used for further analysis through modelling approach presented in the following sections.

There are several parameters that influence the specific-capacitance value. Carbon-based material is used to construct the electrode, as it is electrochemically noble, inert and poses more resistance to corrosion action. Also, it is economically viable. Several types of electrolytes can be used in an ASC e.g., sodium sulphate, potassium sulphate, sulphuric acid, etc. [20]. The type of electrolyte decides the operating voltage of the device. Numerous sub-parameters of electrolytes can be considered for modelling. Various parameters of separator can be considered when a mathematical model is to be produced. One can vary and decide the specific capacitance from the composition of the material, electrode shape and size, type of electrolyte and the molarities of the electrolyte. However, electrode parameters are more influential on the value of specific-capacitance. This section is dedicated for the selection of input parameters for the implementation of statistical modelling of ASC with horizontal electrode configuration with positive electrode at the top. Input parameters of ASC model can be related to material or process. Charge storing in ASC is governed mainly by the parameters of electrode materials. Positive and negative electrodes have many parameters such as various properties of activated-carbon and metal oxide [14]. Current-collector materials and its structure also play an important role. This paper has taken the three most significant parameters associated with electrodes that affect the specific-capacitance. These parameters include the loading of activated-carbon i.e., Vulcan XC72-R on the negative electrode (A), loading of activated-carbon and manganese-dioxide on the positive electrode (B), and percentage manganese-dioxide on the positive electrode (C). Loading of electrode material is expressed in actual value and a content of metal oxide is expressed in percentage. The initial experiments focus on varying the composition of activated-carbon on the negative electrode, loading of metal oxide and activated-carbon on the current collector of the positive electrode and changing the percentage of metal oxide on the positive electrode have been considered. Trials which vary single parameter at a time, keeping the others constant, are carried out to confirm that the selected parameters are affecting the output parameter. Effect of selected input parameter for analysis shows a non-linear behaviour as shown in Fig. 2 with an error bar. It is found that specific-capacitance is dependent on all three selected parameters. Variation of specific capacitance with material loading on both positive and negative electrode is maximum. It is clearly indicating that both parameters are contributing in main as well as interaction effect. Statistical modelling approach is used for studying effect of selected input parameters on specific-capacitance of ASC with horizontally configured electrodes with positive electrode at the top. Two level- three parameters, full factorial DoE and RSM modelling are used for analysis of ASC with horizontally configured electrodes. These methods allow user to exactly analyse main and interaction effect in minimum number of trials such as 8 in case of DoE and 20 in case of RSM.

3. Full factorial DoE model

Type or composition of electrode material and the amount of material loading on it are some of the parameters which affect the amount of charge stored. Based on the results of one-parameter variation at a time, it is seen that the loading of electrode material must be varied between 10 mg per sq. cm and 30 mg per sq. cm. Hence, trials are conducted for the same. During experimentation it was found that electrode material is slipping off from the current collector if electrode material loading is done at a rate above 30 mg per sq. cm. It was also observed that sufficient material is not getting loaded to forma usable electrode of ASC when electrode material loading is done at rate below 10 mg per sq. cm. Percentage of manganese-dioxide in the positive electrode is varied between 10 % to 90 % of the total electrode material. With less than 10 %, the device would have been equivalent to a symmetrical supercapacitor. Above 90 %, device would have been of different configuration and capacitance obtained is on the lower side as presented in [20]. Three parameters are chosen for full factorial DoE, which mainly decide the values of specific capacitance (Sp. cap). Table 1 show their actual/coded, min and max values which are chosen from the results of one parameter variation trials as shown in Fig. 2. Standard two level, three parameter, full factorial DoE experimental is run to obtain a DoE model of specific capacitance is shown in Table 2. Using statistical modelling software i.e., Minitab, a mathematical model is obtained and given in Eq. (1).

$$Spcap = 47.5 - 0.7A + 6.1B - 0.2C - 5.7AB + 3.3AC - 8.1BC - 7.3\,ABC \quad (1)$$

As per full factorial DoE model, loading of activated-carbon and manganese-dioxide on the current collector of positive electrode is the most critical parameter. The factors which contribute the least are the loading of activated-carbon on the current collector of negative electrode and percentage variation of manganese-dioxide in positive

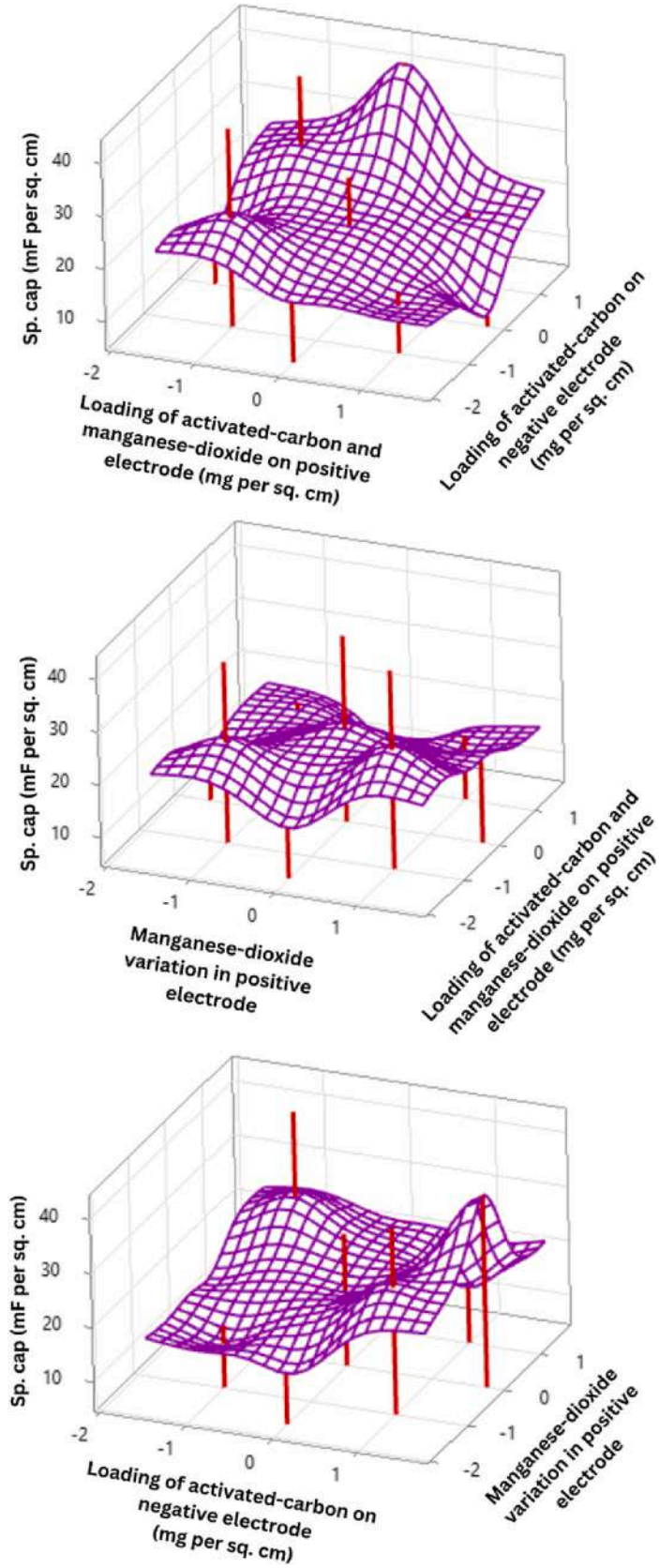

Fig. 4. Surface plots obtained by Minitab software with project lines of various parameters affecting specific capacitance that reflect on non-linearity.

Table 5
Validation of full factorial DoE and RSM model with randomly selected data points.

Input parameters			Specific capacitance in mF per sq. cm			
A	B	C	By Full factorial DoE model	By RSM model	Experimental value	Error Percentage
0.5	−0.5	1	–	21.9	23.4	6.4 %
−1	−0.5	0.75	39.9	–	42.3	5.7 %
0.75	0.25	−1.68	–	29.5	31.1	5.1 %
0.75	−0.75	0	45.6	–	47.6	4.2 %

electrode. Fig. 3 shows the surface plots using full factorial DoE model of various parameters affecting specific-capacitance to show interaction effect between the input parameters under consideration. Surface plot obtained using Minitab software with project lines drawn at intersection of two parameters intersection point with third parameter kept constant. Surface plot between loading of material on positive electrode and percentage of manganese dioxide in positive electrode has highest slope, indicating high level of interaction in them. Surface plot between loading of material on negative plate and percentage of manganese dioxide in positive electrode has least slope, indicating least interaction effect between these two parameters. Interaction effect is strong in parameters associated with loading of activated-carbon and manganese-dioxide on positive electrode.

4. RSM model

The full factorial DoE model gives a linear equation which shows the effect of individual parameters as well as interaction between them. The non-linearity that the experiment poses stays hidden in this model as it is based only on two-level trials. In the RSM model, three levels of each parameter are considered for trials. It is basically an experimental strategy that includes a set of non-linear equations. It is a statistical approach that works best in analysing the non-linearity of the experimental data and its effects. Here the experimental approach consists of a broad five level exploratory design of three levels, which consists of 125 different combinations and involves 20 experiments which are proved to be very efficient and reliable. Table 3 shows the coded and actual values of the three parameters that are selected for RSM trials. Min and max values are considered, which are same as considered in the full factorial DoE model of specific capacitance (Sp. cap). Trials are conducted as coded part shown in Table 4 which is the standard runs required in RSM. Using the Minitab software, the RSM model is obtained as shown in Eq. (2). This model has information about the individual effect, interaction effect and the non-linearity effect.

$$Spcap = 21.1 + 3.5A - 4.1B + 0.9C + 3.1A^2 - 3.5B^2 - 0.95C^2 + 0.78AB - 6.9AC - 1.6BC \quad (2)$$

It is found that the critical parameter in the full factorial DoE is in line with the RSM model. The critical parameter is the loading of activated-carbon and manganese-dioxide on the stainless-steel current collector of the positive electrode. The other two parameters that are taken into consideration are comparatively less significant when considered exclusively. Furthermore, the interaction which is seen in the loading of manganese-dioxide and activated-carbon on the stainless current collector of the positive electrode with the other two input parameters is strong. Equation of the RSM model suggests that there is significant interaction between loading of activated-carbon in the negative electrode and loading of activated carbon and manganese dioxide in the positive electrode with the percentage of manganese-dioxide in the positive electrode. This shows that manganese-dioxide plays an important role in the interaction effect. Fig. 4 shows surface plots using RSM model of the various parameters affecting the value of specific-capacitance and the interaction effect between the input parameters that are taken into consideration. Surface plot obtained using Minitab software with project lines drawn at intersection of two parameters intersection point with third parameter kept constant. As seen in the surface response, there are saddle type planes, which indicate a presence of non-linearity in the system. Surface plots involving material loading on positive plate and percentage manganese dioxide has the highest ups-downs, indicating heavy interaction effect as well as presence of factor contributing to non-linearity in system. Loading of electrode material for both electrodes add to non-linearity. Positive electrode composition and construction should be focussed on manufacturing ASC with horizontally configured electrodes. Data from ref. [2] cannot be used for validation propose as it is for vertical configuration of electrodes. Different set of randomly selected data points have been used to take care of diversity of data which is the key to the validity of mathematical model. It is standard practice in statistical modelling methods used for analysis of manufacturing processes used in the industry. The values of specific-capacitance predicted by these models are fairly close to the actual values as seen in Table 5.

5. Conclusions

Analysis of electrical energy storage devices is generally done with the assumption that they are constructed with vertically configured electrodes. Investigation of ASC with horizontally configured electrodes using statistical modelling methods is the novelty of the presented work. Results obtained through full factorial DoE and RSM methods indicate that electrode material loading on both the positive and negative electrode are critical parameters. These parameters also add to the non-linearity. Electrode material loaded on positive electrode accumulates electrons due to both faradic reactions associated with manganese-dioxide and electrostatic charge storage mechanisms whereas the electrode material on negative electrode accumulates electrons only due to electrostatic charge storage mechanisms. The RSM model indicates that the loading of electrode material on negative electrode is a significant parameter in both main effect and interaction effect. Coefficient of the factor - loading of activated-carbon on current collector of negative electrode is smaller in both the full factorial DoE and RSM models. Increasing the loading of positive electrode will not increase specific-capacitance as the loading of negative electrode is deficit. This is a clear indication for the need of extra sized negative electrode or extra negative electrodes in ASC similar to lead acid battery with horizontally configured electrodes. This is one of the findings of the presented research work. Furthermore, interaction of percentage manganese-dioxide with the material loading on positive and negative electrode loading is strong. This is because the extent of shift of electrode material from current collector is less. Moreover, manganese-dioxide particles, being heavier than activated carbon settle down and move towards the separator. Over a time, they rest on the separator piece, this close proximity leads to interaction effects. Thus, it can be inferred that manganese-dioxide plays an important role in interaction effect. Conclusions drawn are universally applicable so long as input parameters are in the limit set in DoE and RSM trials. This analysis is useful in setting electrode parameter values during the manufacture of this device. Findings of this research work can be used as basis for study of other electrical energy storage devices such as battery, fuel cell etc.

CRediT authorship contribution statement

Sangram Gite: Formal analysis, Visualization, Investigation, Writing – original draft. **R.S. Ambekar:** Formal analysis, Visualization, Investigation, Writing – original draft. **S.B. Abrish Aaditya:** Formal analysis, Visualization, Investigation, Writing – original draft, Writing – review & editing. **Sarang Joshi:** Formal analysis, Investigation, Writing – original draft, Writing – review & editing, Validation. **P.B. Karandikar:**

Conceptualization, Methodology, Project administration, Supervision.

Declaration of competing interest

The authors declare that they have no known competing financial interests or personal relationships that could have appeared to influence the work reported in this paper.

Data availability

Data will be made available on request.

Acknowledgement

The authors would like to thank the management of Army Institute of Technology, Pune, India, for funding support (AIT/R&D Grant-07) and providing research facility of Lt. Col. Suhas Gogate Electric Vehicle Laboratory in its premises.

References

[1] J. Hawke, P. Enjeti, L. Palma, H. Sarma, A modular fuel cell with hybrid energy storage, in: 2011 IEEE Energy Conversion Congress and Exposition, 2011, pp. 2971–2976, https://doi.org/10.1109/ECCE.2011.6064169.

[2] Vispi Neville DeepuJha, P.B. Karandikar Karkaria, R.S. Desai, Statistical modelling of hybrid supercapacitor, J. Energy storage 46 (Feb 2022) 1–9, https://doi.org/10.1016/j.e.2021.103869, 103869, ISSN 2352-152X,.

[3] S. Mathew, P. Kadam, M. Rai, P.B. Karandikar, N.R. Kulkarni, Symmetric and asymmetric supercapacitors derived from banyan tree leaves and rose petals, in: 2016 IEEE Students' Conference on Electrical, Electronics and Computer Science (SCEECS), 2016, pp. 1–4, https://doi.org/10.1109/SCEECS.2016.7509345.

[4] W.A.M. Kethaki, Pabasara Wickramaarachchi, Manickam Minakshi, Xiangpeng Gao, Rukshima Dabare, Kok Wai Wong, Hierarchical porous carbon from mango seed husk for electro-chemical energy storage, Chem. Eng. J. Adv. 8 (Nov 2021) 1–5, https://doi.org/10.1016/j.ceja.2021.100158.

[5] Yue Zhou, Haiping Xu, Lachman No, Mehdi Ghaffari, Shan Wua, Yang Liu, Asli Ugur, Karen K. Gleason, Brian L. Wardlec, Q.M. Zhang, Advanced asymmetric supercapacitor based on conducting polymer and aligned carbon nanotubes with controlled nanomorphology, Nano Energy Rapid Commun. 9 (October 2014) 176–185, https://doi.org/10.1016/j.nanoen.2014.07.007.

[6] Guangmeng Qu, Xixi Zhang, Guotao Xiang, Yunrui Wei, Jiangmei Yin, Zonghua Wang, Xiaoli Zhang, Xijin Xu, ZIF-67 derived hollow Ni-Co-Se nano-polyhedrons for flexible hybrid supercapacitors with remarkable electrochemical performances, Chin. Chem. Lett. 31 (7) (July 2020) 2007–2012, https://doi.org/10.1016/j.cclet.2020.01.040.

[7] Guangmeng Qu, Zonghua Wang, Xixi Zhang, Shunshun Zhao, Chenggang Wang, Gang Zhao, Peiyu Hou, Xijin Xu, Designing flexible asymmetric supercapacitor with high energy density by electrode engineering and charge matching mechanism, Chem. Eng. J. 429 (132406) (Feb 2022) 1–6, https://doi.org/10.1016/j.cej.2021.132406.

[8] S. Mathew, P. Kadam, B. Panda, I. Dwivedi, K. Priya, P.B. Karandikar, An optimization of hybrid capacitor with respect to mass of electrode material, in: 2016 IEEE Students' Conference on Electrical, Electronics and Computer Science (SCEECS), 2016, pp. 1–4, https://doi.org/10.1109/SCEECS.2016.7509269.

[9] K. Hariraman, J. Selvam, M. Alagirisamy, S.S. Sivaraju, Asymmetrical supercapacitor based solar powered automatic emergency light, in: 2022 8th International Conference on Smart Structures and Systems (ICSSS), 2022, pp. 1–5, https://doi.org/10.1109/ICSSS54381.2022.9782231.

[10] B Panda, Indu Dwivedi, K Priya, P B Karandikar and P Mandake, "Analysis of aqueous supercapacitor with various current collectors, binders and adhesives", 2016 Biennial International Conference on Power and Energy Systems: Towards Sustainable Energy (PESTSE), pp1–6, DOI:https://doi.org/10.1109/ICPEICES.2018.8897277.

[11] I. Dwivedi, S. Mathew, K. Priya, B. Panda, P.B. Karandikar, A hybrid capacitor with an innovative double layer electrode, in: 2016 IEEE 1st International Conference on Power Electronics, Intelligent Control and Energy Systems (ICPEICES), Delhi, India, 2016, pp. 1–4, https://doi.org/10.1109/ICPEICES.2016.7853203.

[12] A. Vlad, N. Singh, J. Rolland, et al., Hybrid supercapacitor-battery materials for fast electrochemical charge storage, Sci. Rep. 4 (4315) (2014) 1–9, https://doi.org/10.1038/srep04315.

[13] P. Sharma, Vinod Kumar, Study of electrode and electrolyte material of supercapacitor, Mater. Today Proc. 33 (3) (2020) 1573–1578, https://doi.org/10.1016/j.matpr.2020.04.694.

[14] P. B. Karandikar, D. B. Talange, Uday Mhaskar and R C Bansal, "Investigations for parameter improvement of manganese oxide based aqueous supercapacitor", Mater. Manuf. Process., Volume 27, Issue 11, pp1164–1170, DOI:https://doi.org/10.1080/10426914.2012.663139.

[15] H. Wang, Y. Liang, T. Mirfakhrai, et al., Advanced asymmetrical supercapacitors based on graphene hybrid materials, Nano Res. 4 (2011) 729–736, https://doi.org/10.1007/s12274-011-0129-6.

[16] Muhammad Zahir Iqbal, Umer Aziz, Supercapattery: merging of battery-supercapacitor electrodes for hybrid energy storage devices, J. Energy Storage 46 (103823) (2022) 1–8, https://doi.org/10.1016/j.est.2021.103823.

[17] G. Dotelli, R. Ferrero, P. Gallo Stampino, S. Latorrata, S. Toscani, Supercapacitorsizing for fast power dips in a hybrid supercapacitor—PEM fuel cell system, in: IEEE Transactions on Instrumentation and Measurement 65, Issue 10, Oct. 2016, pp. 2196–2203, https://doi.org/10.1109/TIM.2016.2549658.

[18] Manickam Minakshi, Danielle Meyrick, Dominique Appadoo, Maricite(NaMn1/3Ni1/3Co1/3PO4)/activated carbon: hybrid capacitor, Energy Fuels 27 (06) (April 2013) 3516–3522, https://doi.org/10.1021/ef400333s.

[19] Wanqi Liu, Cong Dong, Bo Zhang, Ruibing Cao, Zhijun Qiao, Yuanjun Tang, Chao Ye, Ke Li, Yanghui Ye, Thermal characteristic and performance influence of a hybrid supercapacitor, J. Energy Storage 53 (105188) (2022) 1–10, https://doi.org/10.1016/j.est.2022.105188.

[20] M. Bhajekar, A. Karandikar, S. Joshi, S. Chapekar, P.B. Karandikar, M.J. Bhalerao, Comparative analysis of symmetrical, asymmetrical and hybrid supercapacitors as a pulse current device, in: 2022 International Conference on Futuristic Technologies (INCOFT), Belgaum, India, 2022, pp. 1–5, https://doi.org/10.1109/INCOFT55651.2022.10094449.

[21] Lip Huat Saw, HiewMun Poon, Wen Tong Chong, Chin-Tsan Wang, Ming Chian Yew, Ming Kun Yew, Tan Ching Ng, Numerical modeling of hybrid supercapacitor battery energy storage system for electric vehicles, Energy Procedia 158 (2019) 2750–2755, https://doi.org/10.1016/j.egypro.2019.02.033.

[22] Jiaqi Cao YonghuiXie, Xinghui Wang, Wangyang Li, Liying Deng, Shun Ma, Hong Zhang, Cao Guan, Wei Huang, MOF-Derived Bifunctional Co0.85Se Nanoparticles Embedded in N-Doped Carbon Nanosheet Arrays as Efficient Sulfur Hosts for Lithium-Sulfur Batteries 21, Issue 20, October 2021, pp. 8579–8586, https://doi.org/10.1021/acs.nanolett.1c02037.

[23] Xu Xi, Cao Guan, Xu Le, Yong Hao Tan, Danwei Zhang, Yanqing Wang, Hong Zhang, Daniel John Blackwood, John Wang, Meng Li, Jun Ding, Three dimensionally free-formable graphene foam with designed structures for energy and environmental applications, ACS Nano 14 (1) (2020) 937–947, https://doi.org/10.1021/acsnano.9b08191.

[24] K. Gopalsamy, J. Balamurugan, T. DuyThanh, N. Hoon Kim, J. Hee Lee, Fabrication of nitrogen and sulphur co-doped graphenenanoribbons with porous architecture for high-performance supercapacitors, Chem. Eng. J. 312 (2017) 180–190, https://doi.org/10.1016/j.cej.2016.11.130.

[25] Jayaraman Balamurugan, Thanh Tuan Nguyen, Vanchiappan Aravindan, Nam Hoon Kim, Joong Hee Lee, Flexible solid-state asymmetric supercapacitors based on nitrogen-doped graphene encapsulated ternary metal-nitrides with ultralong cycle life, Adv. Funct. Mater. 1804663 (2018) 1–14, https://doi.org/10.1002/adfm.201804663.

[26] Jayaraman Balamurugan, Chao Li, Vanchiappan Aravindan, Nam Hoon Kim, Joong Hee Lee, Hierarchical Ni-Mo-S and Ni-Fe-S nanosheets with ultrahigh energy density for flexible all solid-state supercapacitors, Adv. Funct. Mater. 1803287 (2018) 1–9, https://doi.org/10.1002/adfm.201803287.

[27] Jayaraman Balamurugan, Tran Duy Thanh, Nam Hoon Kim, Joong Hee Lee, Facile synthesis of 3D hierarchical N-doped graphenenanosheet/cobalt encapsulated carbon nanotubes for high energy density asymmetric supercapacitors, J. Mater. Chem. A 4 (24) (2016) 9555–9565, https://doi.org/10.1039/c6ta03132c.

[28] Jayaraman Balamurgan, Gopalsamy Karthikeyan, Tran Duy Thanh, Nam Hoon Kim, Joong Hee Lee, Facile synthesis of vanadium nitride/nitrogen-doped graphene composite as stable high performance anode materials for supercapacitors, J. Power Source 308 (March 2016) 149–157, https://doi.org/10.1016/j.jpowsour.2016.01.071.

[29] Martin Karlsmo, Patrik Johansson, "Sustainability and technical performance of an all-organic aqueous Na-ion hybrid supercapacitor", volume 5, November 2022, Batter. Supercaps, DOI:https://doi.org/10.1002/batt.202200306.

[30] Wei Zheng, Joseph Halim, Li Yang, Hussein O. Badr, ZhengMing Sun, Per O. Å. Persson, Johanna Rosén, Michel Barsoum, MXene//MnO2 asymmetric supercapacitors with high voltages and high energy densities, Batter. Supercaps 5 (October 2022), https://doi.org/10.1002/batt.202200390.

[31] Tuzhi Xiong, Xincheng Yao, David Adekoya, Hao Yang, M. -Sadeeq Balogun, Scaffold-regulation buffered MoS2 anode kinetics for high-performance Na-/K-ion storage, J. Mater. Sci. Technol. 145 (2023) 14–24. ISSN 1005-0302, https://doi.org/10.1016/j.jmst.2022.10.051.

[32] M. Bhajekar, S.B.A. Aaditya, S. Chakrabarti, S. Chaphekar, P.B. Karandikar, M. J. Bhalerao, Comparative study of vertical and horizontal asymmetric supercapacitors, in: 2022 International Conference on Computer, Power and Communications (ICCPC), Chennai, India, 2022, pp. 230–235, https://doi.org/10.1109/ICCPC55978.2022.10072257.

[33] Available: https://www.leansigmacorporation.com/full-factorial-doe-with-minitab.

Army Institute Of Technology (AIT), Dighi Camp, Pune - 15.
Director : 7249250115, Joint Director : 7249250117, Principal : 7249250186
Exch : 7249250183, 7249250184, 7249250185
Website : www.aitpune.com Email : ait@aitpune.edu.in
Recognised by AICTE and DTE Maharashtra and affiliated to Savitrabai Phule Pune University

ONWARD TO GLORY

Dr. Umesh V. Awasarmol (Mechanical)

- PhD Certificate
- Publication Copy

महेश काकडे
बी.ई (सिव्हिल), एम.ई. (स्ट्रक्च.),
एफ.आय.ई (इंडिया), एम.आय.एस.टी.ई.
परीक्षा नियंत्रक
Mahesh Kakade
B. E. (Civil), M. E. (Struc.)
FIE (INDIA), MISTE
Controller of Examinations

Estd. 1962
'A' Re-accredited by NAAC (2014)
With CGPA 3.16

शिवाजी विद्यापीठ,
कोल्हापूर-४१६ ००४, महाराष्ट्र
SHIVAJI UNIVERSITY,
KOLHAPUR - 416 004, MAHARASHTRA

दूरध्वनी (थेट) : २६९३१७६,
२६०९०६७, २६०९०६८
फॅक्स : 0091-0231-२६९०६५५
Phone : (Dir.) 26693176,
2609067, 2609068
Fax : 0091-0231-2690655
Website : www.unishivaji.ac.in
E-mail : coe@unishivaji.ac.in

Ref. No. :

Date :

Declaration of Result

It is hereby declared that the thesis entitled,

HEAT TRANSFER ENHANCEMENT USING PERMEABLE FINS

submitted by, **Shri. Umesh Vandeorao Awasarmol** in **Mechanical Engineering** under the **Faculty of Engineering and Technology** is accepted by the University authorities for the award of the Degree of **Doctor of Philosophy in Mechanical Engineering** under the Faculty of **Engineering and Technology** on **28/09/2016**.

Controller of Examinations

No. SU/PG/EXAM/Ph.D./6117
Date: 5 OCT 2016

To,

1. **Shri. Umesh Vandeorao Awasarmol,**
   2 A, Parnakuti Hsg., Soc.,
   Yerwada, Pune. 06
2. **Dr. A. T. Pise, (Guide)**
   Dy. Director & Project Ordinator,
   SPFU, TEQIP (II), Directorate of Technical,
   Education M. S. Mumbai – 400 001.
3. The Librarian, Barr. Balasaheb Khardekar Library, Shivaji University, Kolhapur.
4. The Head, Department of **Technology**, Shivaji University, Kolhapur.
5. Statement of Marks / Certificate Unit.
6. Convocation Unit.
7. Statistics Section.
8. UGC Notification File.

International Communications in Heat and Mass Transfer 147 (2023) 106995

Contents lists available at ScienceDirect

International Communications in Heat and Mass Transfer

journal homepage: www.elsevier.com/locate/ichmt

Experimental investigation of heat transfer enhancement by using perforated fin array having different perforation ratios, angle of inclination and configuration of fins under forced convection condition

Umesh V. Awasarmol [a], Ashok T. Pise [b], Jitendra D. Patil [a,*], Laxmikant D. Jathar [a], Ramshiromani R. Verma [a]

[a] Department of Mechanical Engineering, Army Institute of Technology, Pune, MS 411015, India
[b] Department of Mechanical Engineering, Govt. College of Engineering, Karad, MS 415124, India

ARTICLE INFO

Keywords:
Perforated fin
Enhanced heat transfer
Forced convection
Perforation diameter
Fin array

ABSTRACT

In this research work experimental investigation and comparative study of heat transfer enhancement between solid fins and circular perforated fin array is performed. Current investigation is mainly associated with inline and zigzag configuration of perforations, angle of inclination (0°-90°) and size of perforation (4-12 mm) under forced convection condition. Enhancement of performance is reported at 10 mm diameter size perforation (perforation ratio, $\beta = 21\%$) and 45° angle of inclination. Among the fin arrays used in this study two rows of zigzag perforation (ZC) is found to be superior than two rows of inline perforations (IC) configurations. The highest ratio of Nusselt number of perforated fins to that of solid fins up to 1.73 fold is reported. As against solid fin array 57.27% heat transfer enhancement with 21% saving in fin material is reported. Based on optimized experimental results mathematical correlation is suggested for the range of parameters viz. Reynolds number ($14{,}783 \leq Re \leq 73{,}916$), angle of inclination ($\theta = 45^{\circ}$), perforation ratio ($0 \leq \beta \leq 0.21$) and heat input ($Q = 60$ W).

1. Introduction

The enhancement of heat transfer using fins is an important topic in the field of thermal engineering and heat transfer. Fins are used to increase effective area of heat transfer from a system, which enhances the heat transfer rate from the system to the surroundings or vice versa under a mode of natural convection and/or forced convection. The applications of fins in various fields are extensive. For instance, in heat exchangers, I.C. engines, electronic systems, refrigerators, heat pump, energy storage through phase change material, thermal management of battery etc. Selection of type, size and shape of fins, orientation and configuration of fin array is crucial in designing efficient and cost-effective heat transfer systems. The efficiency of heat transfer depends on various factors, including the size, shape, material, fluid properties and orientation of the fins. Rectangular plate fins are often used in heat transfer applications due to their simplicity in manufacturing and design.

Numerous studies have been conducted on fin modifications that involve removing material from fins in the form of holes and cavities to create additional surface area, adding slots, groves and channels to increase the surface area and fluid mixing to enhance their heat transfer performance. Bassam [1,2] numerically investigated heat transfer performance of permeable fins over solid fins with multiple combinations of equally spaced number of fins and fin heights under laminar and forced convection condition. They observed enhancement of Nusselt by 8.4 fold over solid fins at *Ra* of 106 under natural convection and 4.35 at *Re* of 150 in forced convection. Ridouane and Campo [3] numerically investigated two dimensional parallel plate channel having different channel height, number of groves and grove depth for different *Re*. They observed peak enhancement in local heat transfer in grooved channel at optimal depth of groove. Jamin and Mohamad [4] experimentally studied steady state heat transfer rate in vertical heated pipe filled with carbon foam type porous material. They observed 2.5 fold improvements in *Nu* as against vertical pipe without foam. Povel and Mohamad [5] numerically and experimentally investigated potential of heat transfer enhancement in porous insert in vertically heated pipe under constant heat flux condition. Porous insert with small porosity and high conductivity found to be a potential candidate. Experimental study of

* Corresponding author.
E-mail address: jdpatilaitp@gmail.com (J.D. Patil).

https://doi.org/10.1016/j.icheatmasstransfer.2023.106995

Ahn et al. [6] shows that elongated holes blockage in rectangular channel found more heat transfer enhancement than that of round blockage.

Layeghi [7] performed numerical study of heat transfer from staggered tube bundle with porous media insert of different porosity and conductivity under forced convection condition. Enhancement of heat transfer of more than 50% is reported. High conductivity material is good for enhancement of thermal performance and high porosity material for lower pressure drop penalty. Zhnegguo et al. [8] experimentally studied thermo-hydrodynamic performance of helically baffled shell and tube heat exchanger for oil cooling application. The maximum shell side heat transfer coefficient of 2265 W/m^2K with pressure drop penalty of 91 kPa. Detail analysis of solid rectangular fins is presented in Cengel [9].

Pise and Awasarmol [10] performed comparative study of heat transfer enhancement with solid and permeable fins on cylinder block under natural convection condition. They found enhancement of average heat rate and heat transfer coefficient by 5.63% and 42.3% respectively with 30% reduction of material cost with use of perforated fins. Pise and Awasarmol [11] experimentally and numerically investigated comparative study of heat transfer enhancement between solid fins array and perforated fin array having different orientation and geometry under natural convection condition. They observed peak performance of 32% enhancement with 30% saving in material at 12 mm perforation diameter and 45^o inclination. Ibrahim et al. [12] experimentally studied the effect of the shape of perforations on the performance of vertical fins under forced convection condition. In terms of highest temperature difference they observed circular shaped perforations are better than rectangular and triangular shape. As against conventional solid fins, perforated fins showed enhancement of heat transfer coefficient by 35.82–51.29%. Experimental study of laterally perforated fins heat sink under forced convection conditions done by Chingulpitak et al. [13] shows a 10.6% improvement in thermal performance and 28% reduction in volume than solid fin heat sink. They also observed that the diameter and number of perforations play significant role in performance improvement of heat sink. Dastbelaraki et al. [14] numerically studied heat transfer analysis of various configurations of perforated fin arrays using the turbulence RNG k-e model in RANS and DSM model with LES method. They observed that with perforated fins significant improvement in heat transfer rate with a 44% weight reduction.

In the recent years due to increase in energy demand and over-utilization of conventional fuels, motivated researchers in developing green and sustainable energy. The energy efficient use of solar thermal energy depends on the design of solar thermal collector and development of energy storage system. Karami and Kamkari [15] experimentally studied the use of perforated fins in heat exchanger designed for energy storage through phase change material. They observe enhance of the Nusselt number by 30% and 7% reduction in melting point as compared to solid fin heat exchanger. Hongyang Li et al. [16] studied the perforated fin structure for latent heat thermal storage purpose, the numerical result shows that as compared to solid fins reduction in melting point and increase in heat storage capacity of 5.49% and 0.21% respectively. Fan et al. [17] experimentally investigated effect of perforated spiral fines on the performance of latent heat thermal storage device. They observed considerable improvement in the thermal performance even with the reduced heat transfer area. The considerable enhancement in the thermal performance is observed for a same perforated area with a higher perforated diameter. The highest value of the Nusselt number, thermal efficiency and heat flux reported are 44%, 63.4% and 1370.7 W/m^2 respectively.

Guoming Wu et al. [18] experimentally studied the performance of perforated fin type evaporator used in heat pump type air conditioning system. They observed that the perforated fin type evaporator has potential to enhance performance in both frosting and non frosting condition. Karim Egab et al. [19] explored the use of perforated fins in thermal management of Li-ion battery. In the analysis they investigated significant reduction in heat sink temperature due to reduction in thermal resistance caused by an increase in heat dissipation.

AlEssa and his team [20,21] studied heat transfer enhancement by triangular and rectangular perforated fin under natural convection condition for different thickness of fin and thermal conductivity. They observed considerably enhancement in heat transfer with increase in thickness and thermal conductivity. Shaeri with his team [22,23] numerically studied three dimensional analysis of lateral fin with square perforation using finite volume method over the wide range of *Re*. Based on fin efficiency calculations perforated fins found to be superior over solid fins in terms of heat transfer and weight reduction parameter.

Kundu and Lee [24] and Kundu et al. [25] analytically studied heat transfer performance of porous fin and significant heat transfer enhancement is observed in comparison with solid with fins. Kiwan and Zeitoun [26] numerically investigated heat transfer between two horizontal concentric cylinder through porous fin under natural convection condition. They reported enhancement of heat transfer by two fold with bare annulus fin. Kiwan Suhil [27] investigated radiative heat transfer from porous fin attached to vertical isothermal surface. They observed that radiation effect increases with increase in surface temperature and with increase in Rayleigh number radiation effect becomes less significant. Gorla and Bakier [28] studied radiation and convection heat transfer in porous fins. They reported heat transfer by radiation is higher that of without radiation.

Shaeri and Bonner [29,30] experimentally studied thermo-hydrodynamic performance of laterally perforated fin heat sink. They observed more uniform temperature distribution with reduced thermal resistance. Laterally perforated fin heat sink found to be excellent in weight sensitive applications. Saadat et al. [31] experimentally and numerically studied new type of perforations i.e. fin with one longitudinal perforation with either one, two or three vertical perforations having circular or square cross section under forced convection condition. They observed that fin with one longitudinal and three vertical circular perforations gives best thermo-hydrodynamic performance with a 30% weight reduction. Maji et al. [32] numerically studied heat transfer performance of perforated pin fins having inline and staggered configurations. The best results are obtained for staggered fin configurations having elliptical perforations. Ibrahim et al. [33] numerically and experimentally studied performance of fins with and without perforation under forced convection condition over wide range of *Re*, different number and size of perforations. They observed considerable reduction in fin temperature (up to 8.5 °C), fluid friction factor and pumping power. Habet et al. [34] experimentally and numerically studded thermo-hydrodynamic performance of baffled rectangular channels with inline and staggered perforations. They observed that at higher perforation ratio staggered arrangement observed to be better than inline arrangement. Whereas, at smaller perforation ratio inline configuration found to be superior over staggered configuration.

Rauber et al. [35] experimentally and numerically studied effect of diamond and circular shaped perforation on the performance of plate fin heat exchanger. They observed that perforations with large characteristics size give a performance improvement in terms of performance evaluation criterion and mass thermal efficiency of the plate finned heat exchanger. Ibrahim et al. [36] studied experimentally and numerically the effect of square shape perforated fin on heat transfer enhancement. The study was conducted over a range of parameters such as number of perforations 4–15, heat supplied 1730–3150 W and flow velocity of 0.4 to 1.8 m/s. The results of this study show that with the increase in number of perforations there is a reduction in fin temperature to 16 °C with increased heat transfer rate and reduction in pumping power due to drop in friction factor. Experiential study on effect of different geometry of perforation under forced convection condition showed an increase in heat transfer coefficient from 33.04 to 78.98% and 41.42 to 78.98% for 100 W and 150 W respectively for velocity the range of 1.9 to 3.4 m/s [37]. Noori and Saeed [38] performed experimental investigation of

perforated rectangular fin arrays of different shapes (rectangular, circular and V-shape) and pattern (inline and staggered) with three different materials (Stainless steel, aluminum and brass) over the range of parameters $6200 \leq Re \leq 18{,}700$, $20 \leq Q \leq 70$ W in steps of 10 W and $Pr = 0.71$ at constant inlet temperature of 17 °C. They suggested a general correlation (Eq. (9)) for Nusselt number applicable over the wide range of operating parameters with a maximum error of ±9.8%.

Literature review confirms that heat transfer is enhanced by increasing effective area of heat transfer by using perforations; thereby decreasing flow resistance. Heat transfer enhancement from perforated fins under natural convection condition is studied by numbers of researchers as mentioned above where as study of transfer enhancement from perforated fins under forced convection condition is observed to be limited in open literature. The study of circular perforations on rectangular fin in forced convection environment is found to be done only by Dhanawade [39]. The range of perforation dimension used in this study is fixed or limited. Dhanawade et al. [40] performed optimization of design parameters of laterally perforated fin under forced convection condition. The results of this study show that the most important influencing parameter affecting the thermal performance is *Re* followed by the porosity and thickness of the fin. It indicates that for 5 mm thickness of fin having porosities 0.08, 0.14 and 0.22, percentage enhancement of heat rate over solid fin is 10.93%, 15.55% and 19.06% respectively. They suggested imperical correlation (Eq. (10)) for Nusselt number related by Reynolds number and porosity applicable over the range of operating parameters $21{,}000 \leq Re \leq 87{,}000$, $0 \leq \beta \leq 0.21$, $3 \leq t \leq 5$, Heat input of 200 W and $Pr = 0.7$.

Literature shows that perforation dimensions play important role (than number of perforations) in heat transfer enhancement, but very few attempts have been seen to be made in the direction of optimizing the perforation dimensions (or perforation diameter in case of circular perforations) to enhance forced convection heat transfer. Study about different arrangement of perforation is also lacking. Orientation of the fin also plays important role in heat transfer characteristics of the fin array. In majority of the studies discussed in this literature review are limited to only two orientations of fin array (vertical and horizontal prime surface). The study of wide (whole) range of angle of inclination is missing in the literature.

This paper is extension of research work done in enhancement of heat transfer using perforated fins under forced convection condition [41]. The main objective of this study is experimental investigation of heat transfer enhancement using perforated aluminum fin array under different operating conditions in forced convection condition environment with different perforation diameter and configurations. The main aim is to compare heat transfer performance of perforated fins to that of solid fins and to evaluate the impact of perforation configuration and its suitability in different industrial applications.

2. Perforated fins

The perforated fin array is made by drilling the holes of different size and configurations in the rectangular shape solid fin array composed of 10 fins of 25 mm × 75 mm with 2 mm thickness as shown in Fig. 1. Apart from solid fins these configurations are referred as.

i) Inline configuration (IC),
ii) Zigzag inline configuration (ZC),

Fig. 2 shows photo image of different types of perforation size with Zigzag perforation configurations [41]. Dimensional details of fin array and the range of operating parameters considered for this study are presented at Table 1.

Here, this study is presented in two parts. In first part, fin array with 4 mm perforation diameter is investigated for best perforation configuration out of IC and ZC configurations as stated above. Whereas, in second part optimized perforation diameter is investigated for best perforation configuration.

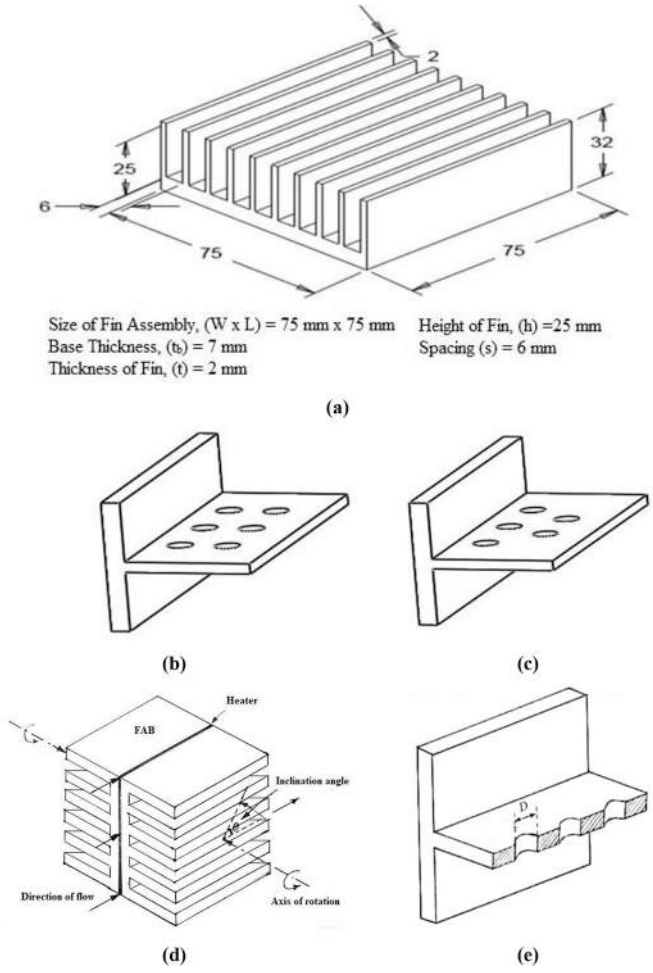

Fig. 1. Schematic diagram of rectangular fin array and perforation configurations.
(a) Dimensional details of rectangular fin array (b) Inline configuration (IC) (c) Zigzag configuration (ZC) (d) Orientation of FAB in test section (e) Cut-section shown at maximum conduction thermal resistance section or maximum convective thermal resistance section in IC and ZC fin configuration.

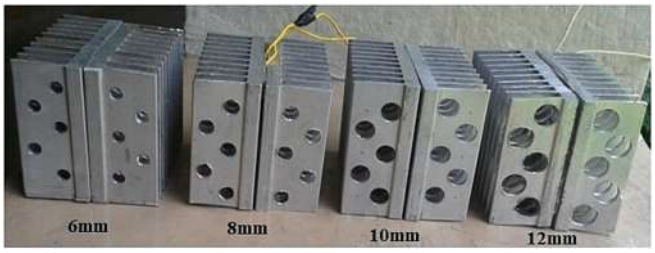

Fig. 2. Photo image of different types of perforation size with zigzag perforation configurations [41].

In rectangular fin array holes of 4 mm diameter are drilled to make perforation in the fin array. The 4 mm diameter size is intentionally decided because after removing two plane surfaces by drilling operation there is an addition of new curved surface of same surface area as that of two plane surface removed. This special case maintains effective surface area of solid fin and perforated fins exactly equal for the case of 4 mm diameter perforation as shown in Table 2.

Table 1
Details of dimensions of fin array and operating parameters.

Particulars /Fin Type	*W*, mm	*L*, mm	*t*, mm	*s*, mm	*n*	*D* (*β*%), mm	*θ* °	*Q*, W	*V*, m/s	*Re*
Solid	75	25	2	6	0	0	0,30, 45,60 &90	50–70	1,2,3,4 & 5	14,000–74,000
IC	75	25	2	6	6	4(4%), 6(9%), 8(16.1%),10(25.1%) & 12 (36.2%)				
ZC	75	25	2	6	4	4(3.4%), 6(7.5%), 8(13.4%),10(21%) & 12 (30.2%)				

Table 2
Details of dimensions of perforations, area and material removed.

D, mm	t, mm	Area removed, mm^2	Surface area increased, mm^2	Area removed/Area increased	Decrease in effective area per perforation, mm^2	% Decrease in area per perforation	Mass of material removed in gram per perforation, g
4.00	2.00	**25.14**	**25.14**	**1.00**	0.00	0.00	0.39
6.00	2.00	56.57	37.71	1.50	−18.86	−33.33	0.89
8.00	2.00	100.57	50.29	2.00	−50.29	−50.00	1.58
10.00	2.00	157.14	62.86	2.50	−94.29	**−60.00**	**2.47**
12.00	2.00	226.29	75.43	3.00	−150.86	−66.67	3.55

3. Experimental setup

Fig. 3 shows schematic of experimental setup used for this investigation. Test setup consists of forced draft blower followed by diverging section, main duct with honeycomb section and at the end test section. Test section is rectangular in cross section of size 275 mm × 248 mm with arrangement to hold the fin array at desired angle of inclination with respect to the direction of flow of fluid in the test section. Honeycomb rectifier placed before the test section ensures uniform velocity profile over the test section.

In order to avoid flow fluctuation in the test section under forced convection condition, hydrodynamic entrance length is decided on the ratio of length of entrance region (x) to hydraulic diameter (D). This ratio is observed to be the different in literature. Its values as observed in literature are 0.8, 1, 3.7 and 4 reported in [39,42–44] respectively. The more the value of this ratio, the more is the degree of confirmation of fully developed flow. In view of this, for the selected dimensions of the duct channel (Fig. 3) in the present study, the above ratio used is on safer/harmless side and equal to 6.38, which ensures the fully developed flow.

In order to ensure equal heat flow in fin array configuration, two identical fin arrays are bolted together back to back with centrally placed 300 W heater. Thermal grease is applied at the interface between heater and base plate to obtain good thermal contact. Hereafter this set of two back-to-back fin arrays will be referred to as Fin Array Block (FAB).

Equal heat flow in two directions of FAB was considered because of symmetry of operating parameter, material, geometry and surroundings to which the FAB was exposed. Moreover, in preliminary work, the temperatures on both the sides were found to be equal for a given heat input.

The FABs were fixed on the wooden rod which was press fitted into the duct. This wooden rod could be rotated to change angle of orientation of FABs. Under constant heat flux condition, the temperature at different location in the test section within the duct and temperature at different locations on the base and tip of fins are recorded using T-type thermocouples (diameter = 0.18 mm and accuracy of ±0.25%). Temperatures reading are recorded using digital multichannel temperature indicator.

The variation in *Re* was achieved by varying the velocity of flow by adjusting the position of damper placed at the inlet of centrifugal blower. Flow velocity was measured using a digital anemometer. Tests were carried out for all three types of fin arrays, at different mass flow rates of air (velocity, $V = 1$–5 m/s), at different angular positions of the fin arrays and for the different power inputs such as $Q = 50$, 55, 60, 65 and 70 W. A dimmer-stat was used for varying the power input to the heater. Fluctuations in voltage were avoided by the use of Constant Voltage Transformer (CVT). CVT (rated 150 W) is a voltage control device with very low response time. Output voltage is always maintained at a constant value of 220 V with a variation of approximately ±0.5%. This would not pass any spike or surge voltage through it. As a result of constant power output, heat flux supplied to the fin array remains steady. Under steady state condition reading are taken for different heat inputs (50–70 W) and angle of inclination ($\theta = 0$–90°) by keeping base surface vertical.

Main focus of this study was to investigate heat transfer

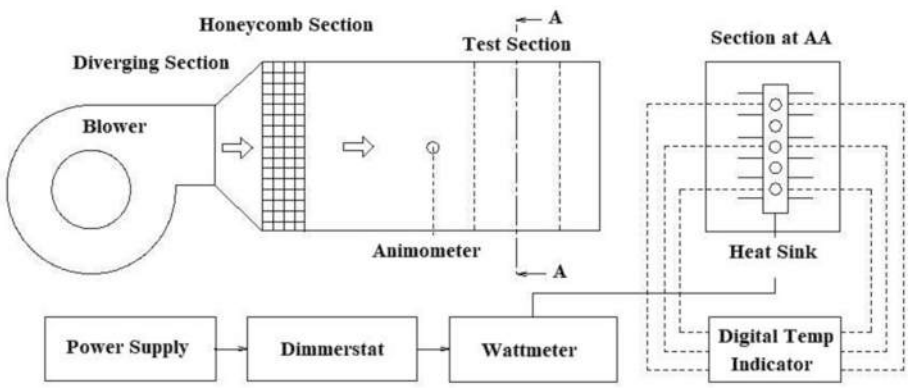

Fig. 3. Experimental setup.

enhancements. Therefore, pressure drop measurements were not conducted in this study. Moreover and importantly, from the literature it was ensured that due to relatively open flow geometry, the pressure drop penalty will be less and hence neglected [8,22,23,45].

4. Test procedure

The fin block is set at an angular position of 0° (air flows parallel to the fin surface and base of the array) in the test section. A constant heat input is supplied to the heater. Inlet velocity of 1 m/s corresponding to the *Re* of 14,000 is set with the help of adjustable dampers. Readings are taken after every 15 min of duration. Usually 2–3 h are required to reach steady state condition. When the temperatures indicated by two conjugative reading of the thermocouples did not vary with more than ±1 °C steady state condition is confirmed and final set of reading are noted. The same procedure is repeated for taking readings at different angle of inclination 0° to 90° and thereafter for different *Re* by gradually increasing flow velocities from 1 m/s to 5 m/s respectively.

The entire procedure as discussed above was then repeated by increasing the power inputs in the range 50-70 W. Overall ranges of geometrical and operational parameters were varied are listed in Table 1.

5. Data reduction

Heat transferred from the fin array is calculated by

$$Q = hA_s(T_s\text{-}T_a) \tag{1}$$

where, h is average convective heat transfer coefficient, T_s and T_a are temperature of base of the fin and ambient air temperature respectively.

$$Surface\ area\ of\ solid\ fin, A_s = n(2W{\cdot}L + 2L{\cdot}t + W{\cdot}t) + n{\cdot}s{\cdot}W - A_p$$

$$Q = h\left[A_b + \eta_f\left(A_f n\right)\right](T_s\text{-}T_a) \tag{2}$$

where, A_b is bare surface area of base of the fin, A_p is effective area of perforation, η_f and n are efficiency and number of fins respectively.

$$Reynolds\ number, Re = \frac{Vd}{\nu} \tag{3}$$

$$Nusselt\ number, Nu = \frac{h_{avg}d}{k_a} \tag{4}$$

where, d is hydraulic diameter of test section and thermal conductivity (k_a) and kinematic viscosity (ν) are properties of air at mean temperature.

$$Fin\ efficiency, \eta_f = \frac{tanh(mL)}{mL}\ where, m = \sqrt{\frac{hP_{pf}}{KA_{pf}}} \tag{5}$$

In order to refine the results of performance parameters, efficiencies of all the configurations of perforated fin are also calculated. These efficiencies were calculated by considering the effect of removing material from the fin (i.e. perforated fins). Therefore, the cross section area of the perforated fin in the direction perpendicular to heat flow, i.e. hatched area shown in Fig. 1 (e) is calculated as;

$$A_{pf} = [W\text{-}(D \times 3)]t \tag{6}$$

Similarly, we can see that the perimeter of the perforated fin (P_1) at perforated section (at maximum conduction thermal resistance section or maximum convective thermal resistance section) is smaller than the perimeter (P_2) at the non perforated section (at minimum convective thermal resistance). Therefore, the average of the perimeters (P_{pf}) is considered, which is calculated as;

$$P_{pf} = \frac{P_1 + P_2}{2} \tag{7}$$

$$where, P_1 = \{[W\text{-}(D \times 3)] + t\} \times 2 \quad and \quad P_2 = (W + t) \times 2 Perforation\ ratio, \beta = \frac{Perforated\ Area\ (A_o)}{Total\ Area\ of\ Fin\ (A_s)}. \tag{8}$$

Noori's correlation [38] for circular perforated fins with staggered configuration

$$Nu = 0.985Re^{0.443} \tag{9}$$

Dhanawade's correlation [40] for perforated fins having different porosity

$$Nu = 0.044Re^{0.730} + 98.65\beta^{1.025} \tag{10}$$

6. Uncertainty analysis

In this study uncertainty analysis is performed for estimating uncertainty propagated in values of the average heat transfer coefficient. The magnitude of uncertainty depends on errors in the measurement due to the accuracy of different instruments used in this experiment. The accuracy of measurement of wattmeter is ±1%, temperature is 0.25% and error in measurement of dimensions is ±0.7 mm. Therefore, error in the measurement of heat input ±1%, temperature difference is 0.35% and area is 1.32%. By substituting these values in Eq. (11) uncertainty in calculations of h is observed to be ±1.69% (≈2%) [46].

$$\frac{\Delta h}{h} = \sqrt{\left(\frac{\Delta Q}{Q}\right)^2 + \left(\frac{\Delta A}{A}\right)^2 + \left(\frac{\Delta(\Delta T)}{T}\right)^2} \tag{11}$$

7. Results and discussion

Result of comparative study of solid and perforated fins in terms of performance parameters such as maximum base temperature, h, θ and Nu for the range of operating parameters such as different flow velocities, perforation diameter, heat input and orientation is presented in this section. Following observations are reported based on experimental data collected through 63 sets of readings.

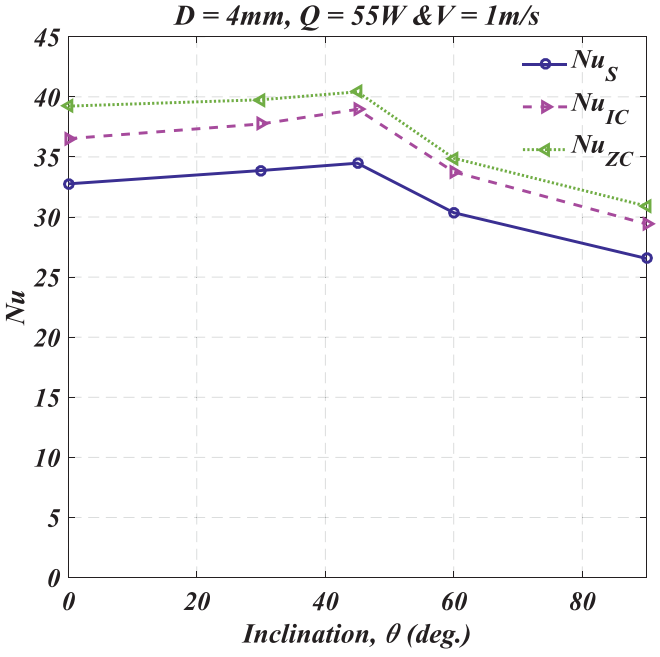

Fig. 4. Variation in the average Nu as a function of different angular positions of fin array at D = 4 mm, Q = 55 W and V = 1.0 m/s.

7.1. Effect of angle of fin inclination/orientation

Fig. 4 shows variation of Nusselt number with different angle of inclination for different fin configurations at perforation diameter (D) of 4 mm, heat input (Q) of 55 W and flow velocity (V) of 1 m/s. It is observed that performance of perforated fins superset the solid fins (Nu_S) whereas performance of perforated fins with zigzag configuration (Nu_{ZC}) superset the inline configuration (Nu_{IC}) under same flow condition. It is also reported that the enhancement in heat transfer behaves differently at different angular positions. For inclination from 0° to 45° it increases with increase in angle and becomes significantly high at 45° but thereafter decreases from 45° to 90°. Similar trend is observed for solid and perforated (both inline and zigzag) fin arrays for different values of selected Reynolds numbers. The cause of this can be explained as under.

When angle is increased from 0° to 45° flow passage is partially obstructed and a recirculation zone is created due to flow obstruction which is expected to be more prominent at $\theta = 45^{\circ}$ along the fin surface. This recirculation zone produces high turbulence in the air flow and formation of eddies along the fin surface. This results in heat transfer enhancement in case of both solid and perforated fins. In case of perforated fins with inline holes the enhancement caused by recirculation zone and eddies, are further assisted by the holes which replace the hot air trapped between the fin array by relatively cold and fresh air. In case of zigzag hole fin arrays, air passing through and coming out of the holes of one particular fin flows over the flat surface of the adjacent fin. The direction of this air flow is normal to the adjacent fin surface, at the same time the fresh air stream entering the fin array is parallel to the fin surface. These two air streams are perpendicular to each other and are having different velocities. Due to this cross flow of two streams at different velocities flow becomes rotational and high turbulence is created and eddies are formed which helps to increase the convection heat transfer rates. For angles of 60° to 90° flow passage of air reduces and it struggles to flow between the fins of the array resulting in reduction of heat transfer rates. For solid fins, at angle of 90°, flow passage is completely blocked and air cannot flow between the fins of the array. This causes an excessive reduction in heat transfer rates of solid fins. At $\theta = 90^{\circ}$, for perforated fins with inline holes air passes through holes of the fins from one end to other end of the array contributing a little to increase heat transfer as compared with solid fins. In case of zigzag holes fin array a little turbulence is also created resulting a little more heat transfer compared with inline holes fin array.

As the thermal performance of perforated fine with ZC, $\beta = 3.4\%$ is observed to be best among IC, $\beta = 4\%$, and solid fins, $\beta = 0\%$, therefore, hereafter fine array with ZC are selected for further investigation.

7.2. Effect of orientation

Fig. 5 shows variation in ΔT as a function of different angular positions at $Q = 60$ W at different flow velocities and perforation diameter. It is observed that among all cases presented in this graph, maximum base temperature (ΔT) of solid fins is highest. This is because even though thermal conduction resistance of solid fins is lowest, thermal boundary layer is uninterrupted and thicker than that of perforated fins which results in reduction of heat dissipation from the fin surface.

Perforations remove material from the fins and hence increase thermal conduction resistance along the length of fin. At the same time removal of material from fin surface leads to increase in ventilation of air and disruption of thermal boundary layer.

It is observed from Fig. 5 that maximum base temperature (ΔT) decrease with increase in angle of inclination up to 45° and start increasing. This is because due to increase in angle of inclination there is increase in ventilation of air and disruption of thermal boundary layer thickness due to flow separation. At the same time, with increase in angle of inclination beyond 45°, there is obstruction in the way of air (at higher angle of inclination) which results into reduction of heat transfer rate. Slight deviation in the trend is reported at 8 and 10 mm perforation diameter that may be due to experimental errors. It is therefore advised to select 45° fins orientation with 10 mm perforation diameter ($\beta = 21\%$) for best thermal performance.

The enhancement in heat can be attributed to the following reasons. In case of perforated fins, at all inclinations flow has two components, one which is responsible for flow through perforations (along t) and the other which is responsible for flow through inter-fin spacing (along W). As inclination increases from 0 to 90°, former component increases from minimum to maximum and the later decreases from maximum to minimum. The mixing of two streams (i.e. components) improves as the angles increases from 0 to 45°. Mixing is superior at 45° due to cross flow and there after it deteriorates up to 90°.

In case of perforated fins, at 45° inclination, air enters through perforations and also through inter-fin spacing. Flow of air has two components, one is responsible for flow through perforations (along t) and other is responsible for flow through inter-fin spacing (along w). At this inclination (i.e. 45°), these two components are in such a way that the fin array experiences intensive cross flow condition which leads to enhanced heat transfer. The perforated fin array becomes utterly permeable to the flow of air. Strong vortices and recirculating zones are observed at many locations on both upstream and downstream side of each perforated fin of the array. The intense vortices are developed in the vicinity of perforations. The turbulence and vortices created due to the presence of perforations are similar to those described in the literature [22,23].

7.3. Effect of perforations diameter

Fig. 6 shows effect of size of perforation on convective heat transfer coefficient at heat input of 50 W, angle of inclination of 45° and at different flow velocities. It is observed from the figure that h increases gradually with increase in diameter of perforation and reaches to maximum at optimum size ($D = 10$ mm, $\beta = 21\%$) and then start to decrease.

The same trend is observed for different flow velocity. Thus from these figures it is clear that 10 mm ($\beta = 21\%$) is observed to be optimum diameter of perforation for horizontal fins, at which more heat transfer coefficient is obtained in comparison with all other diameters.

With increase in diameter of perforation, thermal conduction resistance increases whereas with perforated fins thermal boundary layer get interrupted and air passes along the fins with creation of whirl and turbulence. Interruption of thermal boundary and creation of swirl and turbulence increase convective heat transfer from the surface of fin. The rate of increase of convective heat transfer is higher than that of increase in thermal conduction resistance; therefore there is net increase in heat transfer rate. With increase in size of perforation above optimum value, magnitude of thermal conduction resistance becomes higher than that of increase in convective heat transfer rate, which results in decrease in net heat transfer rate.

The slight deviation is observed at flow velocity of 5 m/s which may be due to experimental error. Thus, the enhancement in heat transfer coefficient is attributed to improved flow, strong vortices, cross flow of air in case of perforated fins as opposed to its solid counterpart.

7.4. Effect of Re

Fig. 7 shows variation of Nu with Re at different angular position and size of perforation at 60 W heat supplied condition. It is observed from the figure that with increase in Re, Nu increases gradually for all angle of inclination (0°-90°). In addition to this significant enhancement in heat transfer rate is observed in perforated fins than that of solid fins over the range of parameters investigated. Optimum size of perforation and angle of inclination reported to be 10 mm diameter ($\beta = 21\%$) and 45° respectively for the reason as discussed in the previous sections.

Although a slight reduction in heat transfer area is caused by creating

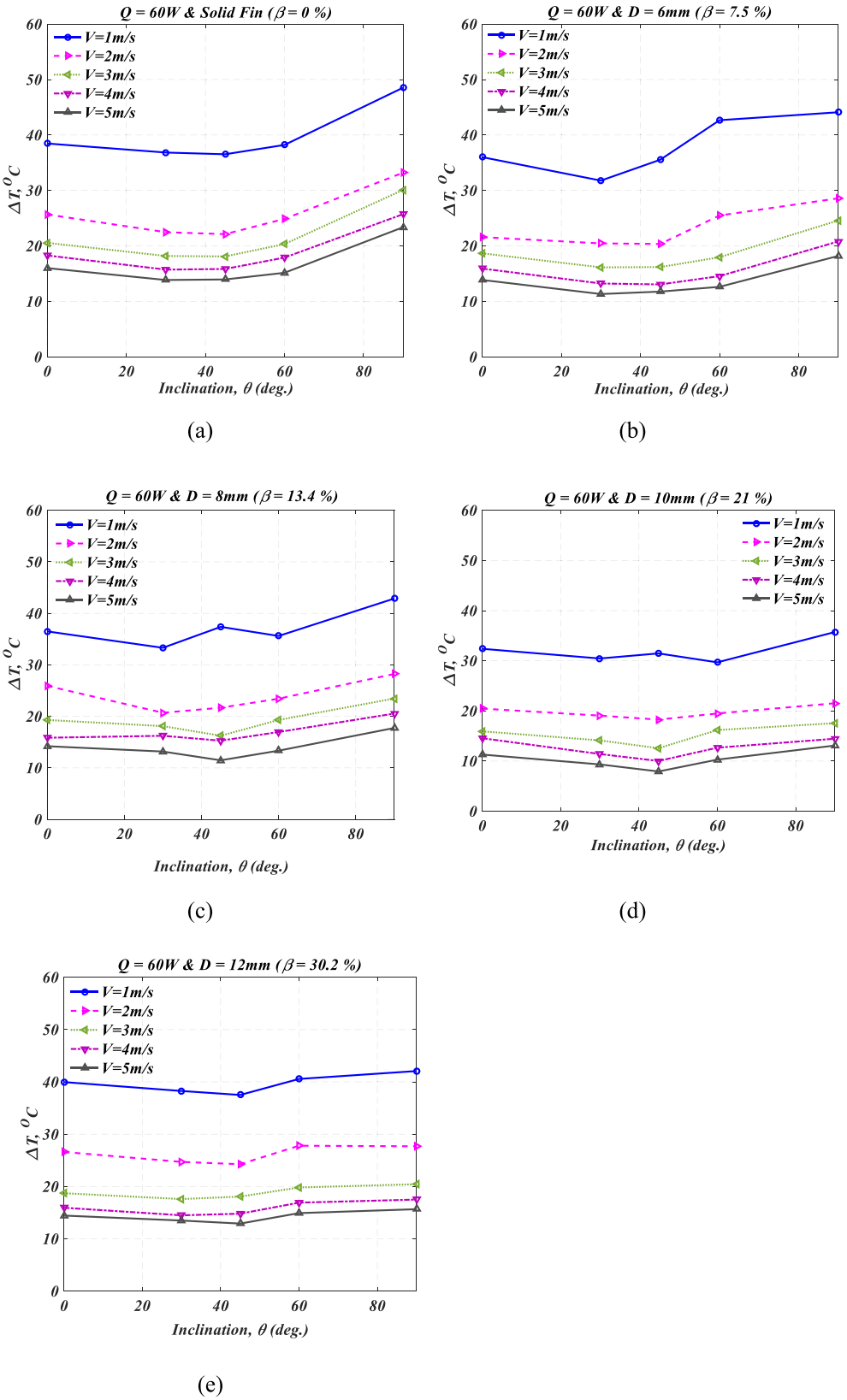

Fig. 5. Variation in ΔT as a function of different angular positions at $Q = 60$ W.
(a) Solid Fin ($\beta = 0\%$) (b) $D = 6$ mm ($\beta = 7.5\%$) (c) $D = 8$ mm ($\beta = 13.4\%$) (d) $D = 10$ mm ($\beta = 21\%$) (e) $D = 12$ mm ($\beta = 30.2\%$)

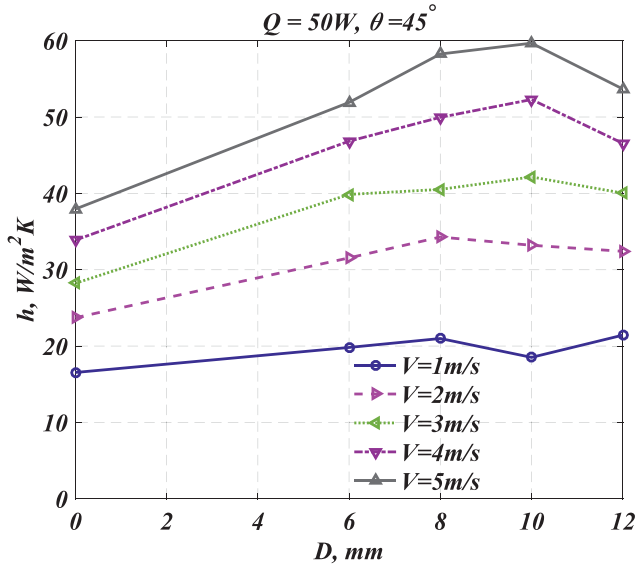

Fig. 6. Variation of h with size of perforation at $\theta = 45^{\circ}$ and $Q = 50$ W.

holes in the fins, it increases the flow of air through them compensating the effect of reduced area. At high velocities the difference in Nusselt number between perforated fin array and with solid fins array is 1.73 fold. That is in case of solid fin array slope of *Nu* vs *Re* curve decreases.

Fig. 8 shows performance of perforated fin array in terms of increase in *Nu* relative to that of solid fin array at 60 W heat input and 45° angle of inclination for all the perforation diameters against Reynolds number. Graph for sold fin is horizontal line which is considered as reference line for comparison for enhancement of heat transfer due to perforation. Performance of perforated fins is observed to be superior than that of solid fins over the range of parameters investigated. The highest value of 1.73 is obtained for 10 mm perforation diameter (β = 21%) for the reason as discussed in the previous sections.

7.5. Weight reduction

Fig. 9 shows enhancement of heat transfer coefficient with solid fins and perforated fins having different perforation diameters. As compared to solid fins enhancement of convective heat transfer gradually increases with increase in diameter of perforation, reaches to peak and thereafter start decreasing. Peak performance is observed at 10 mm perforation diameter.

Summary of enhancement of convective heat transfer coefficient and percentage reduction in mass in perforated fins for different operating parameters are presented in Table 3. It is observed that at 10 mm size perforations 57.27% enhancement in h is reported with 21% reduction in fin material. It is therefore concluded that use of permeable fins not only enhance heat transfer rate but also make heat sink light weight, compact and economical.

8. Empirical correlations

Based on optimized experimental results following mathematical correlation [Eq. (12)] for three different parameters viz. Reynolds number $14783 \leq Re \leq 73{,}916$, $0 \leq \beta \leq 0.21$ and heat input ($Q = 60$ W) for zigzag configuration with angle of inclination of,$\theta = 45^{\circ}$, is suggested.

$$Nu = 0.063Re^{0.7134} + 125.11\ \phi^{1.473} \tag{12}$$

The value of R^2 is 0.98 for this correlation.

Proposed correlation is compared with previously published correlations viz. Nooris correlation [38] and Dhanawade's correlation [40] to verify the methodology and assumptions used to simplify the calculations. The results are presented in Fig. 10. Even though there is considerable deviation in the range of operating parameters, dimensions and orientation, good agreement between the results are observed. It is observed that proposed correlation, over predicts the values of *Nu* for the same *Re* in comparison with previously published correlations. This is because both these correlations are derived for horizontal orientation of the fin i.e. fluid flow parallel to the length of the fin. In the present study, in addition to the perforation ratio effect of inclination of fin array is also studied. It is observed that at $\theta = 45^{\circ}$ inclination considerable enhancement is observed due to increase in ventilation of air and disruption of thermal boundary layer thickness due to separation of flow.

9. Conclusions

In this paper, experimental investigation of effect of different fin configurations in perforated fins arrays under forced convection condition are presented. Key findings of this study are:

a) Base temperature of the perforated fin array is smaller by 3.7–12.8° C as compared to the solid fins over the range of parameters studied.
b) It is reported that with increase in the angle of inclination, *Nu* increases gradually, reaches to maximum at $\theta = 45^{\circ}$ and thereafter decreases. Similar results are obtained for different configuration viz. RC and ZC. Among these configuration ZC configurations gives the best results.
c) It is observed that for a particular values of flow velocities with increase in the size of perforation, h increases gradually, reaches to maximum at $D = 10$ mm ($\beta = 21\%$) and thereafter decreases. Same pattern is observed for different flow velocities. Enhancement of h improves with increase in flow velocity. At flow velocity of 5 m/s, enhancement of h is observed to be increased by 57.27% than that at $D = 6$ mm.
d) For the case of $D = 10$ mm ($\beta = 21\%$), $\theta = 45^{\circ}$, heat input of 60 W and over the range of *Re* between 14,783–73,916, the highest ratio of Nusselt number of perforated fins to that of solid fins up to 1.73 times is reported. It is also observed that at 10 mm size perforation (β = 21%), 57.27% enhancement in h is reported with 21% reduction in fin material which makes fin array light and economical.
e) Based on optimized experimental results, mathematical correlation is suggested for the range of parameters viz. $14{,}783 \leq Re \leq 73{,}916$), $0 \leq \beta \leq 0.21$, $\theta = 45^{\circ}$ and $Q = 60$ W.

The findings of this investigation will be useful in designing heat sink under forced convection condition, suitable for applications such as I.C. engines, electronic systems, refrigerators, heat pump, energy storage through phase change material, thermal management of battery etc. There is more scope for further improvement in enhancement of thermal performance of rectangular fin array with different size of perforation with zigzag configuration and angle of inclination under natural and forced convection condition.

CRediT authorship contribution statement

Umesh V. Awasarmol: Conceptualization, Methodology, Writing – original draft, Formal analysis. **Ashok T. Pise:** Supervision. **Jitendra D. Patil:** Data curation, Visualization, Writing – review & editing. **Laxmikant D. Jathar:** Resources, Investigation, Formal analysis. **Ramshiromani R. Verma:** Resources, Validation.

Declaration of Competing Interest

The authors declare that they have no known competing financial interests or personal relationships that could have appeared to influence the work reported in this paper. There is no funding agency associated

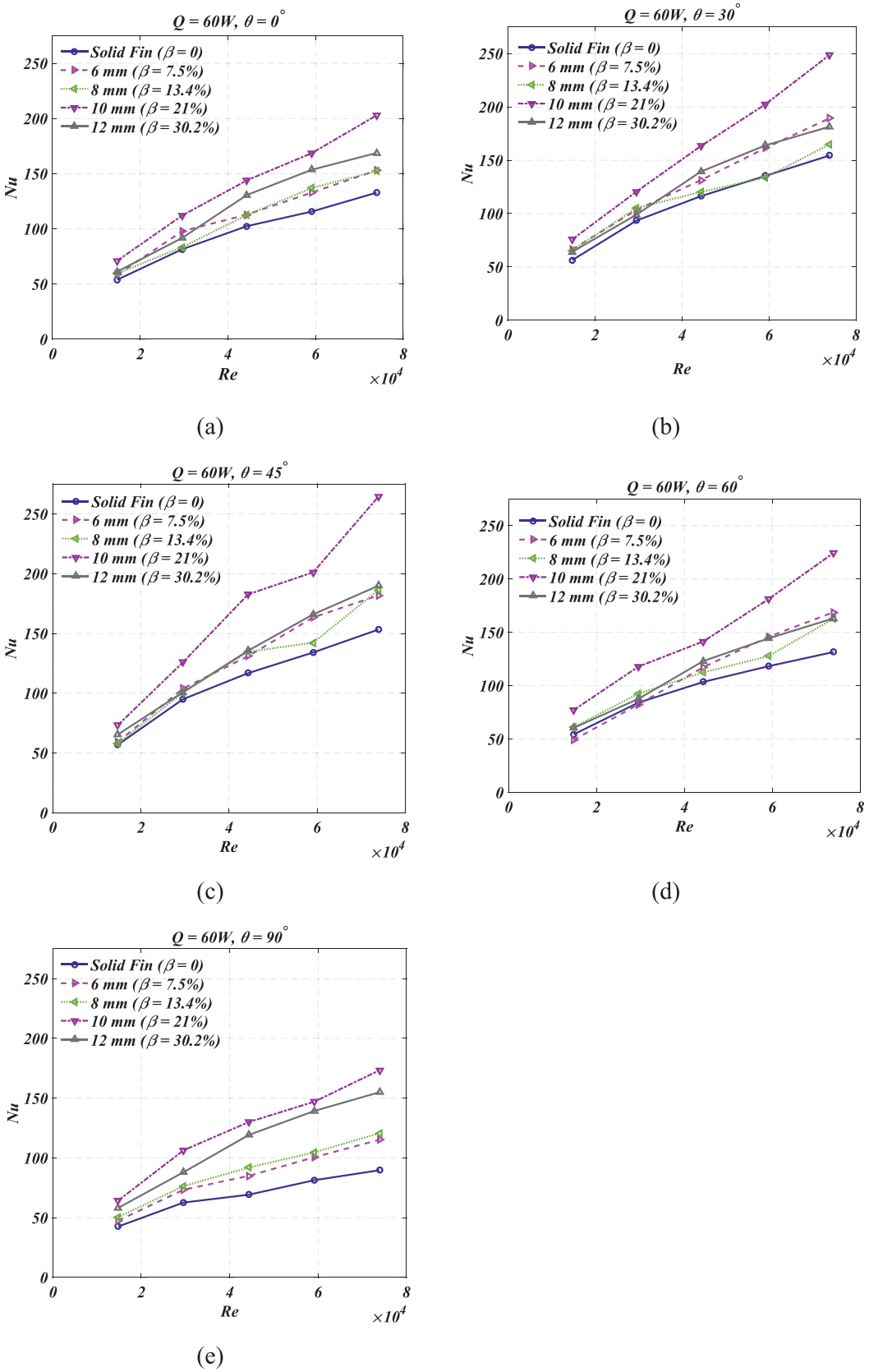

Fig. 7. Variation of *Nu* with *Re* at different angular position and size of perforation at 60 W heat input (a) $\theta = 0^{\circ}$ (b) $\theta = 30^{\circ}$ (c) $\theta = 45^{\circ}$ (d) $\theta = 60^{\circ}$ (e) $\theta = 90^{\circ}$.

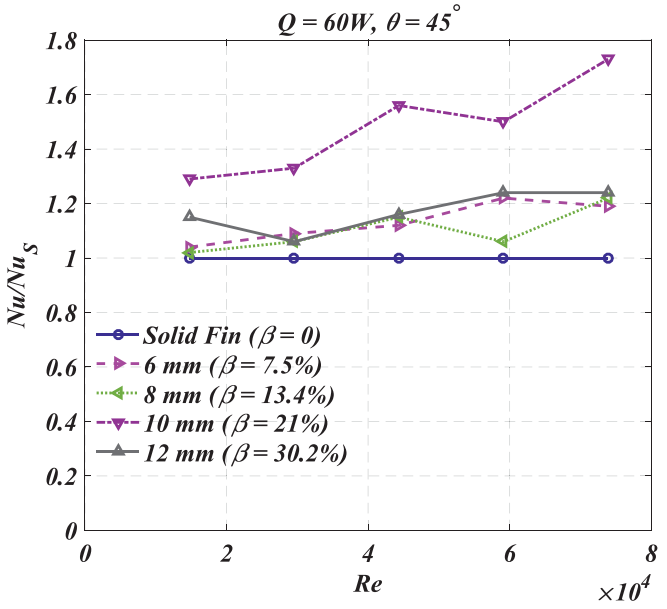

Fig. 8. Performance of perforated fins in terms of *Nu* enhancement for different perforation diameters and $Q = 60$ W & $\theta = 45^{o}$.

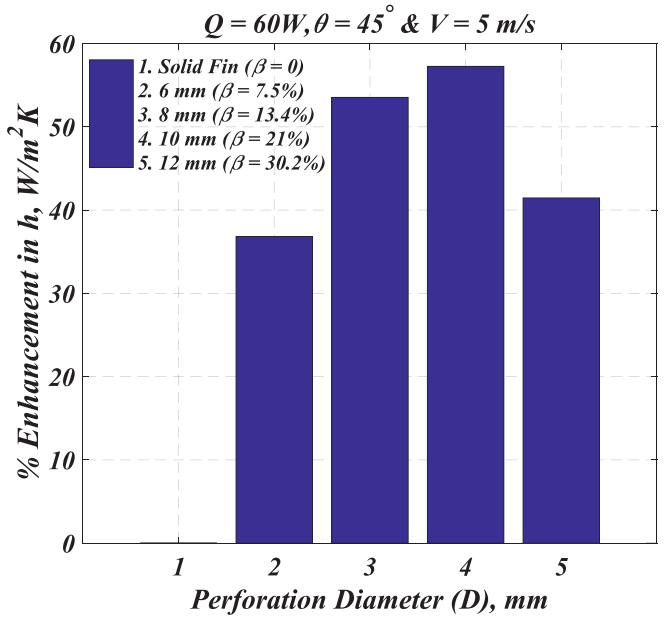

Fig. 9. Enhancement in h for different perforation diameter at $Q = 60$ W, $\theta = 45^{\circ}$ & $V = 5$ m/s.

Table 3
Summary of enhancement of convective heat transfer coefficient and percentage reduction in mass in perforated fins for different operating parameters.

Particulars /Fin Type	Operating Parameters	*D*, mm	Number of Perforations, *n*	% mass removed	% Enhancement in, *h*
Solid	$\theta = 45^{\circ}$, $Q = 60$ W & $V = 5$ m/s.	0	0	0	0
IC or ZC		6	5	7.53	36.83
		8	5	13.39	53.54
		10	**5**	**20.93**	**57.27**
		12	5	30.14	41.46

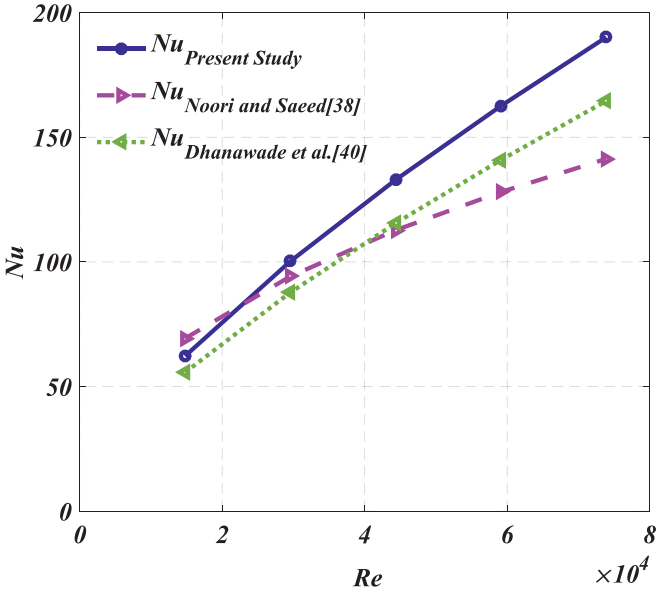

Fig. 10. Comparative study of proposed correlation with previously published correlations.

with this research work.

Data availability

The data that has been used is confidential.

References

[1] Bassam A. Abu-Hijleh, Natural convection heat transfer from a cylinder with high conductivity permeable fins, J. Heat Transf. 125 (2003) 282–288, https://doi.org/10.1115/1.1532013.

[2] Bassam A.K. Abu-Hijleh, Enhanced forced convection heat transfer from a cylinder using permeable fins, J. Heat Transf. 125 (2003) 804–811, https://doi.org/10.1115/1.1599371.

[3] E.H. Ridouane, A. Campo, Heat transfer enhancement of air flowing across grooved channels: joint effects of channel height and groove depth, J. Heat Transf. 130 (2008), https://doi.org/10.1115/1.2790022.

[4] Y.L. Jamin, A.A. Mohamad, Natural convection heat transfer enhancements from a cylinder using porous carbon foam: experimental study, J. Heat Transf. 130 (2008), https://doi.org/10.1115/1.2977606.

[5] B.I. Pavel, A.A. Mohamad, An experimental and numerical study on heat transfer enhancement for gas heat exchangers fitted with porous media, Int. J. Heat Mass Transf. 47 (2004) 4939–4952, https://doi.org/10.1016/j.ijheatmasstransfer.2004.06.014.

[6] H.S. Ahn, S.W. Lee, S.C. Lau, Heat transfer enhancement for turbulent flow through blockages with round and elongated holes in a rectangular channel, J. Heat Transf. 129 (2007) 1611–1615, https://doi.org/10.1115/1.2764091.

[7] M. Layeghi, Numerical analysis of wooden porous media effects on heat transfer from a staggered tube bundle, J. Heat Transf. 130 (2008), https://doi.org/10.1115/1.2780184.

[8] Z. Zhnegguo, X. Tao, F. Xiaoming, Experimental study on heat transfer enhancement of a helically baffled heat exchanger combined with three-dimensional finned tubes, Appl. Therm. Eng. 24 (2004) 2293–2300, https://doi.org/10.1016/j.applthermaleng.2004.01.012.

[9] Y.A. Cengel, Heat Transfer: A Practical Approach, Tata McGraw Hill Publishing Company Ltd, 2005.

[10] U.V. Awasarmol, A.T. Pise, Investigation of enhancement of natural convection heat transfer from engine cylinder with permeable fins, Int. J. Mech. Eng. Technol. 1 (2010) 238–247.

[11] A.T. Pise, U.V. Awasarmol, Experimental study of effect of angle of inclination of fins on natural convection heat transfer through permeable fins, in: Int. Conf. Therm. Energy Environ. 2011, 2011.

[12] T.K. Ibrahim, M.N. Mohammed, M. Kamil Mohammed, G. Najafi, N. Azwadi Che Sidik, F. Basrawi, A.N. Abdalla, S.S. Hoseini, Experimental study on the effect of perforations shapes on vertical heated fins performance under forced convection heat transfer, Int. J. Heat Mass Transf. 118 (2018) 832–846, https://doi.org/10.1016/j.ijheatmasstransfer.2017.11.047.

[13] S. Chingulpitak, H.S. Ahn, L.G. Asirvatham, S. Wongwises, Fluid flow and heat transfer characteristics of heat sinks with laterally perforated plate fins, Int. J. Heat Mass Transf. 138 (2019) 293–303, https://doi.org/10.1016/j.ijheatmasstransfer.2019.04.027.

[14] A.H. Dastbelaraki, M. Yaghoubi, M.M. Tavakol, A. Rahmatmand, Numerical analysis of convection heat transfer from an array of perforated fins using the Reynolds averaged Navier–Stokes equations and large-eddy simulation method, Appl. Math. Model. 63 (2018) 660–687, https://doi.org/10.1016/j.apm.2018.06.005.
[15] R. Karami, B. Kamkari, Experimental investigation of the effect of perforated fins on thermal performance enhancement of vertical shell and tube latent heat energy storage systems, Energy Convers. Manag. 210 (2020), 112679, https://doi.org/10.1016/j.enconman.2020.112679.
[16] C. Hu Hongyang Li, Y. He, D. Tang, K. Wang, W. Huang, Effect of perforated fins on the heat-transfer performance of vertical shell-and-tube latent heat energy storage unit, J. Energy Storage. 39 (2021), 102647, https://doi.org/10.1016/j.est.2021.102647.
[17] B. Fan He, J. Yan, C. Zou, X. Hu, W. Gao Meng, Experimental evaluation of the effect of perforated spiral fins on the thermal performance of latent heat storage units, J. Energy Storage. 58 (2023), 106359, https://doi.org/10.1016/j.est.2022.106359.
[18] Wu Guoming, B. Yu, T. Ren, G. Ding, Modeling and experimental investigation on comprehensive performance of perforated wavy fins for heat pump type air conditioners at frosting and non-frosting conditions, Energy Build. 225 (2020), 110342, https://doi.org/10.1016/j.enbuild.2020.110342.
[19] S.K. Oudah Karim Egab, Thermal management analysis of li-ion battery-based on cooling system using dimples with air fins and perforated fins, Int. J. Therm. Sci. 171 (2022), 107200, https://doi.org/10.1016/j.ijthermalsci.2021.107200.
[20] A.H. AlEssa, M.I. Al-Widyan, Enhancement of natural convection heat transfer from a fin by triangular perforation of bases parallel and toward its tip, Appl. Math. Mech. 29 (2008) 1033–1044, https://doi.org/10.1007/s10483-008-0807-x.
[21] S. Abdullah, H. AlEssa, Ayman M. Maqableh, Enhancement of natural convection heat transfer from a fin by rectangular perforations with aspect ratio of two, Int. J. Phys. Sci. 4 (2009) 540–547.
[22] M.R. Shaeri, M. Yaghoubi, K. Jafarpur, Heat transfer analysis of lateral perforated fin heat sinks, Appl. Energy 86 (2009) 2019–2029, https://doi.org/10.1016/j.apenergy.2008.12.029.
[23] M.R. Shaeri, M. Yaghoubi, Numerical analysis of turbulent convection heat transfer from an array of perforated fins, Int. J. Heat Fluid Flow 30 (2009) 218–228, https://doi.org/10.1016/j.ijheatfluidflow.2008.12.011.
[24] B. Kundu, K.-S. Lee, Exact analysis for minimum shape of porous fins under convection and radiation heat exchange with surrounding, Int. J. Heat Mass Transf. 81 (2015) 439–448, https://doi.org/10.1016/j.ijheatmasstransfer.2014.10.044.
[25] B. Kundu, D. Bhanja, K.-S. Lee, A model on the basis of analytics for computing maximum heat transfer in porous fins, Int. J. Heat Mass Transf. 55 (2012) 7611–7622, https://doi.org/10.1016/j.ijheatmasstransfer.2012.07.069.
[26] S. Kiwan, O. Zeitoun, Natural convection in a horizontal cylindrical annulus using porous fins, Int. J. Numer. Methods Heat Fluid Flow. 18 (2008) 618–634, https://doi.org/10.1108/09615530810879747.
[27] S. Kiwan, Effect of radiative losses on the heat transfer from porous fins, Int. J. Therm. Sci. 46 (2007) 1046–1055, https://doi.org/10.1016/j.ijthermalsci.2006.11.013.
[28] R.S.R. Gorla, A.Y. Bakier, Thermal analysis of natural convection and radiation in porous fins, Int. Commun. Heat Mass Transf. 38 (2011) 638–645, https://doi.org/10.1016/j.icheatmasstransfer.2010.12.024.
[29] M.R. Shaeri, R. Bonner, Laminar forced convection heat transfer from laterally perforated-finned heat sinks, Appl. Therm. Eng. 116 (2017) 406–418, https://doi.org/10.1016/j.applthermaleng.2016.12.103.
[30] M.R. Shaeri, R. Bonner, Heat transfer and pressure drop in laterally perforated-finned heat sinks across different flow regimes, Int. Commun. Heat Mass Transf. 87 (2017) 220–227, https://doi.org/10.1016/j.icheatmasstransfer.2017.07.022.
[31] H. Saadat, M.M. Tavakol, M. Yaghoubi, Experimental and numerical study of forced convection heat transfer from array of fins with various cross perforations, Thermophys. Aeromechan. 26 (2019) 531–546, https://doi.org/10.1134/S0869864319040061.
[32] A. Maji, D. Bhanja, P.K. Patowari, Numerical investigation on heat transfer enhancement of heat sink using perforated pin fins with inline and staggered arrangement, Appl. Therm. Eng. 125 (2017) 596–616, https://doi.org/10.1016/j.applthermaleng.2017.07.053.
[33] T.K. Ibrahim, A.T. Al-Sammarraie, W.H. Al-Taha, M.R. Salimpour, M. Al-Jethelah, A.N. Abdalla, H. Tao, Experimental and numerical investigation of heat transfer augmentation in heat sinks using perforation technique, Appl. Therm. Eng. 160 (2019), 113974, https://doi.org/10.1016/j.applthermaleng.2019.113974.
[34] M.A. El Habet, S.A. Ahmed, M.A. Saleh, Thermal/hydraulic characteristics of a rectangular channel with inline/staggered perforated baffles, Int. Commun. Heat Mass Transf. 128 (2021), 105591, https://doi.org/10.1016/j.icheatmasstransfer.2021.105591.
[35] W.K. Rauber, U.F. Silva, M. Vaz, M.V.C. Alves, P.S.B. Zdanski, Investigation of the effects of fin perforations on the thermal-hydraulic performance of plate-finned heat exchangers, Int. J. Heat Mass Transf. 187 (2022), 122561, https://doi.org/10.1016/j.ijheatmasstransfer.2022.122561.
[36] T.K. Ibrahim, A.T. Al-Sammarraie, M.S.M. Al-Jethelah, W.H. Al-Doori, M. R. Salimpour, H. Tao, The impact of square shape perforations on the enhanced heat transfer from fins: experimental and numerical study, Int. J. Therm. Sci. 149 (2020), 106144, https://doi.org/10.1016/j.ijthermalsci.2019.106144.
[37] M. Mohammad, M.P. Hossain Talukder, K. Rahman, M. Hridoy, Experimental Investigation on the Effect of Different Perforation Geometry of Vertical Fins under Forced Convection Heat Transfer, 2019.
[38] N. Raad Noori, A. Fawzi Saeed, A study of finding empirical correlation for the Nusselt number and the factors influencing it for perforated fin array of different shapes, Ain Shams Eng. J. (2023), 102320, https://doi.org/10.1016/j.asej.2023.102320.
[39] K.H. Dhanawade, H.S. Dhanawade, Enhancement of forced convection heat transfer from fin arrays with circular perforation, in: Front. Automob. Mech. Eng. 2010, 2010, pp. 192–196, https://doi.org/10.1109/FAME.2010.5714845.
[40] K.H. Dhanawade, V.K. Sunnapwar, H.S. Dhanawade, Optimization of design parameters for lateral circular perforated fin arrays under forced convection, Heat Transf. Res. 45 (2016) 30–45, https://doi.org/10.1002/htj.21150.
[41] U.V. Awasarmol, A.T. Pise, An experimental investigation of natural convection heat transfer enhancement from perforated rectangular fins array at different inclinations, Exp. Thermal Fluid Sci. 68 (2015) 145–154, https://doi.org/10.1016/j.expthermflusci.2015.04.008.
[42] V.K. Maudgal, J.E. Sunderland, An experimental study of forced convection heat transfer from in-line pin fin arrays, in: Thirteen. Annu. IEEE. Semicond. Therm. Meas. Manag. Symp., 1997, pp. 149–157, https://doi.org/10.1109/STHERM.1997.566792.
[43] T. Igarashi, Y. Mayumi, Fluid flow and heat transfer around a rectangular cylinder with small inclined angle (the case of a width/height ratio of a section of 5), Int. J. Heat Fluid Flow 22 (2001) 279–286, https://doi.org/10.1016/S0142-727X(01)00089-3.
[44] I.M. Didarul, O. Kenyu, Y. Minoru, S. Izuru, Study on heat transfer and fluid flow characteristics with short rectangular plate fin of different pattern, Exp. Thermal Fluid Sci. 31 (2007) 367–379, https://doi.org/10.1016/j.expthermflusci.2006.05.009.
[45] K.R. Yakar, Effects of holes placed on perforated finned heat exchangers at different angles on the Nusselt and Re, Sci. Res. Essay 5 (2010) 224–234.
[46] J.R. Taylor, An Introduction to Error Analysis—The Study of Uncertainties in Physical Measurements, University Science Books, Mill Valley, CA, 1980.

Army Institute Of Technology (AIT), Dighi Camp, Pune - 15.
Director : 7249250115, Joint Director : 7249250117, Principal : 7249250186
Exch : 7249250183, 7249250184, 7249250185
Website : www.aitpune.com Email : ait@aitpune.edu.in
Recognised by AICTE and DTE Maharashtra and affiliated to Savitrabai Phule Pune University

ONWARD TO GLORY

Dr. Ashwini T. Sankpal (IT)

- Course Work
- PhD Certificate
- Publication Copy

Shri Guru Gobind Singhji
Institute of Engineering and Technology, Nanded
An Autonomous Institute cent-percent funded by Govt. of Maharashtra
Vishnupuri, NANDED (Maharashtra State) PIN 431606 INDIA
STD: 02462, EPABX: 229307, 229235, FAX: 229236 Email: director@sggs.ac.in, Web: http://www.sggs.ac.in
Vision of SGGSIE&T, Nanded "Education of human power for technological excellence"

Date: 02.07.2013

To Whomsoever It May Concern

This is to certify that Mr./Mrs/Miss Ashvini T. Gapkal of AIT, Pune has attended the Summer Coursework (June/July 2013) held during 24/06/2013 to 02/07/2013 in the subjects of "Research Methodology (Paper 1)" and "Computer Applications (Paper 2)".

Dr. Suhas S. Gajre
(Coordinator for coursework)
Associate Professor
Department of Electronics & Telecom.
SGGS College of Engineering & Technology
Vishnupuri, Nanded - 431606 (MS)

Sr. No. Q1- 0001088

Swami Ramanand Teerth Marathwada University, Nanded

We, the Chancellor, the Vice-Chancellor, Members of the Management Council and the Academic Council of the Swami Ramanand Teerth Marathwada University, certify that the degree of

Doctor of Philosophy

In the faculty of Science & Technology (Computer Science & Engineering)

has been conferred on Sapkal Askwini Tukaram

on Twenty Eight September Two Thousand Nineteen

who has been found duly qualified for the same. In testimony whereof is set the seal of the said University.

स्वामी रामानंद तीर्थ मराठवाडा विद्यापीठ, नांदेड

सपकाळ आश्वीनी तुकाराम हे/ह्या

विद्यावाचस्पती या पदवीस पात्र ठरल्यामुळे त्यांना स्वामी रामानंद तीर्थ मराठवाडा विद्यापीठाचे कुलपती, कुलगुरू, व्यवस्थापन परिषद आणि विद्या परिषद सदस्य यांच्या अनुमतीने

विद्याशाखांतर्गत

विज्ञान व तंत्रज्ञान (संगणक शास्त्र व अभियांत्रिकी)

विद्यावाचस्पती

ही पदवी दिनांक अठ्ठावीस सप्टेंबर दोन हजार एकोणीस रोजी प्रदान करण्यात येत आहे. याची साक्ष म्हणून विद्यापीठाची अधिकृत मुद्रा येथे अंकित करण्यात येत आहे.

Dr. Uddhav V. Bhosle
Vice-Chancellor

Date : 28th September, 2019
Place: Nanded, Maharashtra State, India.

Multimedia Tools and Applications (2023) 82:33983–34004
https://doi.org/10.1007/s11042-023-14446-6

Lane detection techniques for self-driving vehicle: comprehensive review

Ashwini Sapkal[1] · Arti[1] · Dishant Pawar[1] · Prashant Singh[1]

Received: 6 August 2021 / Revised: 14 August 2022 / Accepted: 31 January 2023 /
Published online: 10 March 2023

Abstract
According to WHO, 1.35 million people, every year are cut short in road accidents, most of them caused due to human misconduct and ignorance. To improve safety over the roads, road perception and lane detection play a crucial part in avoiding accidents. Lane Detection is a constitution for various Advanced Driver Assisting System (ADAS) like Lane Keeping Assisting System (LKAS) and Lane Departure Warning System (LDWS). It also enables fully assistive and autonomous navigation in self-driving vehicles. Therefore, it has been an effective field of research for the past few decades, but various milestones are yet to be achieved. The problem has encountered various challenging scenarios due to the past limitations of resources and technologies. In this paper, we reviewed the different approaches based on image processing and computer vision that have revolutionized the lane detection problem. This paper also summarizes the different benchmark data sets for lane detection, evaluation criteria. We implemented Lane detection system using Unet and Segnet model and applied it on Tusimple dataset. The Unet performance is better as compared to Segnet model. We also compare the detection performance and running time of various methods, and conclude with some current challenges and future trends for deep learning-based lane marking detection algorithm. Finally, we compare various researcher's approaches with their performances. This paper concluded with the challenges to predict accurate lanes under different scenarios.

Keywords Autonomous driving · Lane detection · Deep learning · Advanced driver assisting system · Lane keeping assisting system · Lane departure warning system

1 Introduction

Advanced driver assisting systems (ADASs) are developed to reduce road accidents by assisting the driver. Lane detection is an essential module of ADAS that provides navigational assistance to the driver. A lane departure warning (LDW) system alerts a driver

Arti, Dishant Pawar and Prashant Singh are contributed equally to this work.

✉ Ashwini Sapkal
asapkal@aitpune.edu.in

Extended author information available on the last page of the article.

if the vehicle diverges from a lane or a narrow road on arterial roads and freeways. The LDW system assists the driver to reduce vehicle crashes that careless drivers cause. As the safety and comfort of passengers is the primary for developing ADAS, this has led to the creation of fully autonomous self-driving vehicles. Many automotive enterprises such as Tesla, Google, Lyft, Uber, etc. have developed their own lane detection models used in assistive autonomous navigation in driver-less cars that have achieved significant importance in research and the real world. Normally, highways are more structured and predictable, with road surfaces well-maintained and lanes well-marked. Contrary, residential or urban driving surrounding features are highly unpredictable with many generic objects, different kinds of lane markings, and complex traffic flow patterns. The comparative consistency and predictability of highways have encouraged some first real-life applications of automation in driving technology. Various automotive enterprises are pursuing highway auto-pilot methods to alleviate driver stress and enable more safety features for vehicles and passengers.

With the recent developments in high computing devices, sensors, computer vision techniques and machine learning theories, real-time lane detection problems are solved more realistically. There are many sensing modalities used for road and lane perception such as monocular vision (i.e. one video camera), stereo, LIDAR, real-time vehicle information secured from car odometry, inertial measurement unit (IMU) alongside global positioning information acquired from global positioning system (GPS) and digital maps. Computer vision is the leading research area in road and lane detection since markings are built for human vision, whereas GPS and LIDAR are prime supplements.

With automaticity, there comes an elevated risk therefore, reliability and robustness are the most essential properties of the system. The high-class automation vehicles should constantly observe their surroundings and must deal with low-accuracy detection problems. Therefore, the assessment of lane detection systems becomes more severe with an increase in automation at each level.

An advanced lane detection model should be robust enough to perform even in critical and diverse conditions such as:

- Poor visibility due to heavy shadows or wet roads.
- A curve or steep roads
- Change in road color or material
- Different slopes
- Continuous or broken lines.
- Environmental conditions such as fog, snow, or heavy rainfall
- Road mark degradation

Due to different environmental conditions and lane variations, gradual degradation of lane marking perfectly accomplished lane detection is very difficult. Therefore, many researchers have been attracted to this field. In the past decade, many sophisticated detection models have been introduced. Some of these were based on conventional geometric modeling techniques and some used machine learning-based approaches. The research efforts in this domain are made since 2005 in DARPA Grand Challenge (2005) and Urban Challenge (2007) and, yet more need to be achieved [11].

The detailed review of existing techniques used for lane detection is described in this paper. This paper covers several insights into recent research toward the goal of enabling secure and robust lane detection. It presents different techniques of lane detection including

conventional geometry modelling and deep learning models. It also explores the commonly used benchmark datasets, evaluation metrics and performance evaluation of different techniques. There are many research challenges and limitations that needs to be addressed for accurate lane detection. Some of these challenges are listed in this paper. These challenges opens up the further research in this direction for providing effective driver assistance systems.

This paper specifically discusses the problem of lane detection in order to determine the correct lane position from the markings on the road. The appropriate information of the environment is extracted using a camera mounted on the vehicle. The lane location is then obtained from the image. The pipeline of lane detection model consists of the feature extraction from the road images followed by the classification of each pixel from the image as the lane or not. We have also implemented Lane detection system using Unet and Segnet model and applied it on Tusimple dataset. It is found that the Unet model outperforms as compared to Segnet model when applied on Tusimple Dataset.

The paper is oriented as follows: Section 2 provides the literature survey for the existing lane detection models. The section is subdivided into conventional and machine learning-based models. Section 3 is the discussion portion to analyze and interpret the Literature Survey and research existing gaps that need to be bridged. Finally, we conclude our work in Section 4.

2 Survey on existing models

Researchers faces many problems and challenges in implementing the automatic lane detection system. In Table 1 the critical parameters are listed which makes the lane detection task challenging

2.1 Conventional geometry modelling using lane detection algorithms

This approach particularly uses gradient, texture, boundaries, color, etc., for extracting information about lane markings from the image, followed by line detection and line fitting. Therefore, the pipeline of traditional lane detection models is mainly divided into three stages Image Preprocessing, Feature extraction and model fitting, and detected lane tracking as given in Fig. 1.

Table 1 Factors affecting lane detection

Factors	Its impact on Lane Detection
Lane and road	lane color, inconsistent road texture, Crossway, curve roads, degraded lane markings
Urban Roads	complex painted road surface markings, utility poles, and buildings
Town Roads	road markings, pedestrian sidewalk, and guardrails
Hardware	camera type, camera calibration correctness,camera mounting and positions, different sensor
Traffic	vehicles, shadows, lighting conditions, guardrail
Weather	rain, snow, fog

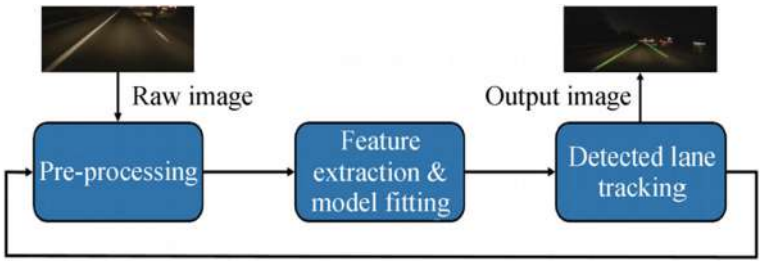

Fig. 1 General architecture of lane detection system

2.1.1 Image pre-processing

The advantage of pre-processing is to enhance image data, and certain features and remove noises that interfere with the accuracy of subsequent recognition of lane lines. In pre-processing the most commonly used methodologies are camera calibration correction, Color space transformation, noise removal, blurring, inverse perspective mapping (IPM) (birds-eye view), region of interest (ROI) selection, etc.

Camera calibration correction While developing a robust computer vision algorithm, various possible errors need to be addressed. Every camera inherits the lens distortion and occlusions properties during an object's 3D to 2D transformation and the camera image undergoes Radial Distortion and Tangential Distortion.

In Radial Distortion, the straight lines in the image are slightly curved or bent at the corners. In Tangential Distortion, the lens is not parallel configured to the image plane and generates a little extended or tilted image, making the objects look closer or further away.

These distortions degrade the quality of data, henceforth the detection. Therefore, camera calibration is an important procedure.

Inverse perspective mapping (IPM) The camera has a perspective view as the human eye due to this property the lane lines seem to merge at a point called the vanishing point. Certain features when perceived from distinct viewpoints, they are identified with better precision. The road curvature lane marking is one such feature. Applying perspective transform would transform the perspective image captured by the camera to a "bird's eye view" of the road, which are mainly focused on the lane markings and present them relatively parallel to each other [1, 2, 7, 20, 46, 47]. This will further make it easier to fit polynomial and measure the curvature of the lane lines. Ju Han Yoo et al. [57] used vanishing point estimation for lane detection; they used inverse perspective transformation rather than IPM. Yingping et al. [26] set a simple trapezoidal transformation from the rectangular region obtained after ROI selection to produce the bird's eye view image (Figs. 2, 3, 4).

ROI selection Another method [19, 32, 33, 40] to remove noise from the image is by defining Regions of Interest (ROI) on the image plane. ROI selected from the probability of locating the lanes is highest and the remaining region is treated as noise and it is masked. This averts from locating unwanted features from the image. Zhang et al. [60] and Yingmao et al. [26] define the image's lower half as ROI in a simplified way. In [9, 44] the ROI was selected based on the calculated depths.

Fig. 2 Inverse perspective transformation

Color space transformation(CST) The significant intensity edges and heavy shades on the road surfaces are a primary source of clutter. To get rid of this illumination researchers [1, 15, 30] performed various Color Space Transformation (CST) such as HSL(Hue, Saturation and Lightness), LAB (L for lightness and A and B for the color dimensions), YCbCr, YIQ, and others [27, 54]. Illumination invariant images is obtained by combining different colors. This results in the same intensity over a surface in both the illuminated and shadowed areas. Further, to isolate lane marking different threshold masking is applied for both yellow and white color lane lines.

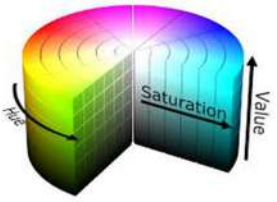

[HSL]

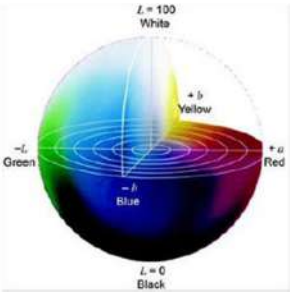

[LAB color space]

2.1.2 Lane feature extraction

In various lane detection systems, image gradient and boundary information are the frequently used image features for image segmentation. This lane feature extraction needs some computation and it finds details depending on the change of image pixel intensities. Well-painted lane markings contrast highly with the road surface, enabling the detection of lanes lines. In literature various authors evaluated the most commonly used feature extractors, such as edge detectors [53], top hat filters [5], steerable filters [37], global threshold [12], local threshold [8] and SLT [51].

The lane features ought not to be intense or degraded by shadow or external influential factors due to the environmental conditions. Therefore a strong and dominant edge detector is required. In contrast to other edge detection algorithms, the Canny edge detection algorithm is widely used to achieve the best feature extraction of the edges from the image [35, 45].

Canny detection The Canny Detector is a multi-stage algorithm for fast real-time edge detection [4, 32, 35, 45]. To detect edge from the given set of thresholds the algorithm detects intense changes in illumination in the image, like a shift from white to black. In

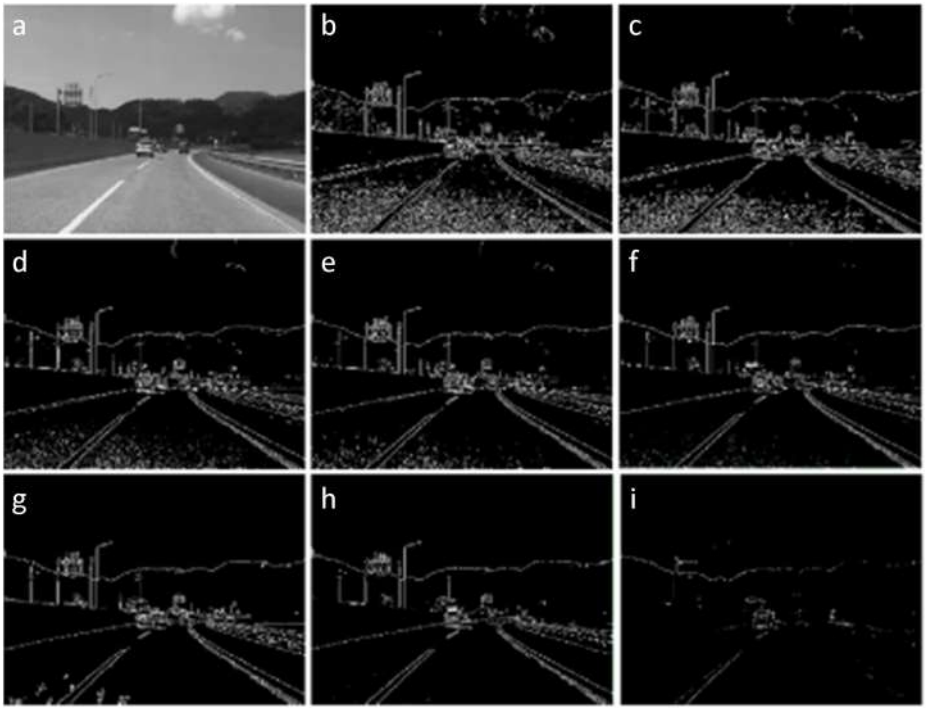

Fig. 3 Canny edge detection with different thresholds

lane feature extraction, the contrast of pixel intensity between the road surface and lane line defines the lane lines. The Gaussian filter is commonly used to remove and mask the noise and then lane features are extracted by Canny edge detection afterward, the lines are recognized from these edges. Figure 3 shows the output of canny detection at different thresholds (th1 and th2)(x is the grey scale image from a source b) th1=40, th2=40; c) th1=90, th2=40; d) th1=90, th2=90; e) th1=140, th2=90; f) th1=140, th24=140; g) th1=40, th2=240; h) th1=240, th2=40; i) th1=450, th2=50. The enigma for this technique is: higher the threshold value lower noises are detected. The crucial point is to apply the appropriate thresholds on the image to locate the correct position of the lane with the lane detection technique.

2.1.3 Line fitting

A simple lane model cannot illustrate lane shape precisely as the lines differ from straight segment to sharp curve. Whereas a complex lane model requires heavy computational power, thereby, making it inefficient in real-time and also, increasing the error detection rate. Therefore, lower computation and robustness are the essential properties to enable realistic lane detection. Various algorithms such as Least Squares Fitting, Random Sample Consensus (RANSAC), Spline Models, and Hough Transformation are used for line fitting.

Kalman filters The Kalman filter is considered as a solution to various tracking and data prediction tasks [7, 39, 45]. After lane marking detection, Kalman filter is commonly used

to predict the lane in the next frame. To predict the future frame, the algorithm makes the noise estimation of the system over time to calculate the parameters of the system (which are unnoticed) and remembers the formerly detected lanes from the former video frame. At every stage, it makes a prediction, draws measurement, and modify itself. To add stability to lane markings, the variant of detected lines are averaged by adding up the measurement errors and previous state by the Kalman filter.

Least squares fitting Least-squares fitting (or least squares estimation) is a method to locate the best fit curve or line from a given set of points [45]. In this technique, instead of the absolute values of the residuals (offsets), the sum of squares of the residuals is used to determine the best-fit curve or line. But the disadvantage of this technique is the outlier's unbalanced effect that influences the line or curve equation. The reason behind this is the residuals squares are used rather than the absolute value of the residuals and the large outliers will influence the curve or line detection more than the points closer. Therefore, this approach cannot guarantee accurate lane findings.

RANSAC RANSAC algorithm is a robust algorithm that has generally been used in numerous computer-vision problems. Researchers have used RANSAC in the Lane Detection model to estimate lane model parameters. The lane features extracted in the previous stage are not distributed evenly and contain too much noise that hinders accurate line prediction. Thus, it is a computationally heavy task to accurately compute the model parameters on feature points with too much noise. RANSAC does not require a training process contrary to other algorithms such as Hough Transformation (HT) or template matching and it can even adjust to the challenging scenarios in model parameters estimation.

Vanishing point Due to the perspective effect of the camera in the process of 3D to 2D transformation images seem to converse to a point called vanishing Point, this property could be exploited to filter out false lane detection. For Lane detection, the intersection point of pair of line segments is computed as the vanishing point for lanes [27, 40, 54]. Liu et al. [34] use maximum intersection points of pairs of line segments detected from Line Segment Detector (LSD) [52] to identify vanishing points of lanes. Yuan et al. [58] estimated vanishing point with a probabilistic framework. The estimated vanishing point in the image space is converted into the approximate line parameters in the parametric space. Ju Ham et al. [57] In order to detect lanes from the input image, firstly the line segment is obtained by the LSD method [52], and for each line segment, the strength is calculated. Then, with the computed line segments strength the vanishing point is obtained using a probabilistic voting procedure.

Spline model Splines are piece wise polynomial functions used to draw curves from the given points. Usually, there is a sequence of the feature points and a curve is designed to smoothly transit (or pass-over) them. Discrete spline models with discrete functions and methodologies were used to identify lane boundaries. To ensure energy-based optimization Wang et al. [53] used the B-Splines model and M Aly et al. [3] used Active Contours (Snakes). Kim [29] uses the Cubic Splines model as the curve comprises the control points. The [18] Catmull Rom spline model is used to find a broader range of lane structure tracking. In most of these models, the curve is represented in parameters from the set of control points. In [26] 100 "seed" is chosen at a closer distance(in Perspective view) as they generally have lower noise points. The resulting spline is evaluated to expose every next point by

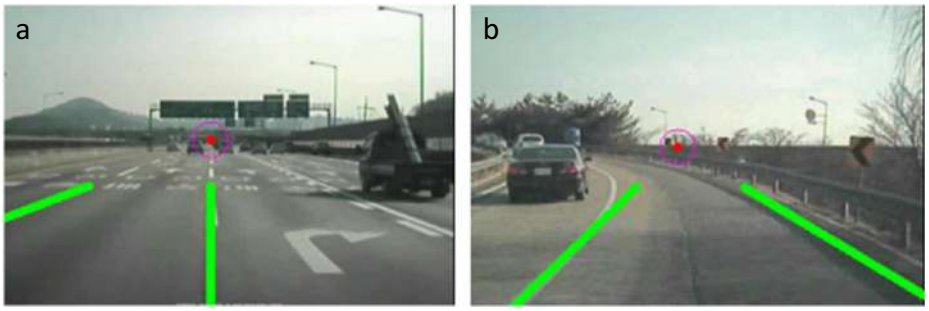

Fig. 4 Hough transformation outputs

a "greedy" search. At each stage evenly spaced control points are generated from the points ranging at 50 pixels from the previous point.

Hough transformation(HT) The HT is commonly used to isolate features of any shape within an image that can be written in a mathematical formula. A typical HT often identifies regular shapes such as lines, ellipses, circles, etc. The advantage of this technique is that it is more tolerant to noise. This technique identifies a line passing through collinear points by detecting the crossing of correspondent curves on the parametric plane in Hough Space. The unique equation for every possible line through the point of an image is counted, and then the dominant lines in an image are computed. Although the points are practically barely collinear and dispersed about the line, curves do not absolutely converge at a point.

Generally, to solve lane detection problems, the image first converted into a binary image using some thresholds then HT is applied to find the dominant lines [28, 45]. This technique is widely used as it also detects false positives in the presence of noise and occlusion.

2.2 Deep learning-based lane detection models

The Deep learning evolution has revolutionized the research on Lane detection. It has gained tremendous popularity as they outrun conventional computationally intensive image-processing-based models, especially in object detection, speech recognition, natural language processing, and image classification. Deep learning-based models do not require additional preprocessing and implicitly learn the features while training the model.

2.2.1 Encoder and decoder model based on CNN

The Convolutional Neural Network (CNN) is one of the most approved and used methods for lane detection. To inhabit more accurate detection, many researchers have integrated CNN and other deep learning techniques [19, 33]. CNN is computationally efficient and excellent in handling extensive unstructured data and has high detection accuracy and automatic feature learning. It was reported that compared to conventional methods CNN, improves the accuracy from 80% to 90% [21]. Therefore, numerous deep learning-based models were proposed. Here we present some of the models.

Lane detection using SegNet Rama Sai et al. [36] present an unique approach using CNN's SegNet architectural model. As shown in Fig. 5 the encoder consists of convolutional layers, activation function (rectified linear unit/ ReLu), and a pooling layer. It generates

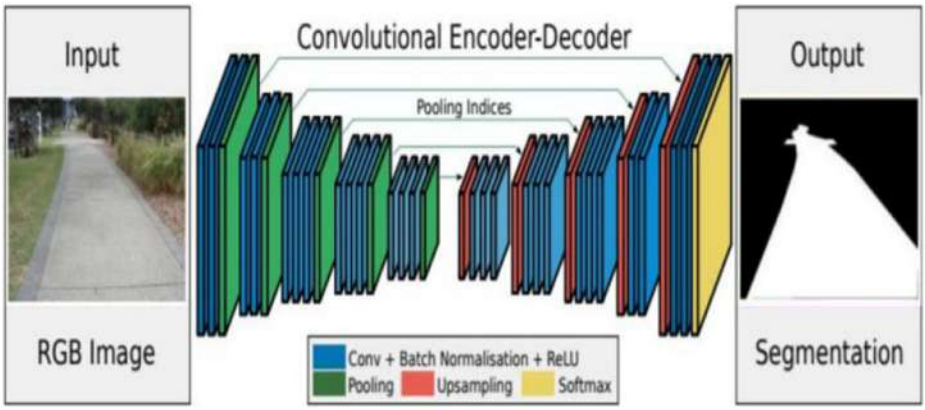

Fig. 5 Illustrating SegNet architecture

low-resolution feature maps from the input image. The output from the encoder is fed to the decoder that consists of deconvolutional layers to compute pixel-wise classification. To enable dynamic navigation, the model's prediction is interfaced with Google APIs such as Google geo-locate, Google maps, and Google street-view APIs. These APIs provide real–time information of the street. Google APIs allow to interface to Google cloud in order to make the applications powerful through the services like computing, storage, networking, etc. Google Cloud APIs are programmatic interfaces to Google Cloud Platform services. They are a key part of Google Cloud Platform, allowing you to easily add the power of everything from computing to networking to storage to machine-learning-based data analysis to your applications. The Encoder-Decoder Seg-net architecture (fully convolutional neural network) and Unet architecture is implemented.

Lane detection using Segnet The encoder-decoder framework model consists of a sequence of nonlinear processing layers (encoders) and a corresponding set of decoders followed by a pixel wise classifier to detect lane in a semantic pixel-wise segmentation manner. The Segnet model contain 13 convolutional layers in the VGG16 network and 5 pooling layers. The model takes single 128*256*3(where 3 is no. of channels) image size and outputs the single channel image which is combined with original image to generate the image of same size. The Encoder consist of convolutional layer with batch normalisation, a ReLU non-linearity and maxpooling layer of 2*2 with stride 2. It takes the input image and construct the feature map. Decoder consist of deconvolutional layers and upsampling layers, the output feature map from encoder is fed to decoder to map the low resolution encoder feature maps to full input resolution feature maps for pixel-wise classification. Specifically, the decoder uses pooling indices computed in the maxpooling step of the corresponding encoder to perform non-linear upsampling. This eliminates the need for learning to upsample. The upsampled maps are sparse and are then convolved with trainable filters to produce dense feature maps.

Lane detection using Unet In Unet, the contraction and expansion part gives the U shaped architecture. The contraction path is actually the encoder part of the model. The VGG network is used as the backbone. There are 10 convolutinal layer with rectifier linear (ReLu) is used. The Kernal size is 2*2, downconvolutional has 3*3 dimension. The Contraction

path is convolutional network that consist of repeated application of convolutions. During contraction the saptial information is reduced while feature information has increased. The Expansion part is the decoder part of the model. It combines the feature and spatial information through a sequence of up-convolutions and concatenations with feature maps from the encoder part. The up-convolutions has 2*2 dimension and stride is 2 (Figs. 6 and 7).

The Lane detection system is implemented using Segnet and Unet Architecture. The dataset used in the implementation is Tusimple [49] which is explained in detail further. As shown in Table 2 the Unet performance is better than the Segnet.

2.2.2 GAN model

The generative adversarial network(GAN) [17] model is used for lane detection. The model comprises a generator and a discriminator for semantically separate out lanes from the image. Mohsen et al [17] use an embedding-loss GAN (EL-GAN). The generator produces a semantic segmentation map to predict the lanes from the input image, and the discriminator is used to differentiate produced data from ground truth labels based on weights. The GAN model is primary used to resolve the aforementioned issues with the per-pixel loss. The model avoids soft boundaries generally produced in CNN models, the final predicted lane is thin and accurate.

2.2.3 Dual-view convolutional neutral network (DVCNN)

Bei et al. [22] proposed a DVCNN framework where both perspective-view and the bird eye view images are optimized together for correct lane prediction. The lane detection problem is solved in three folds, initially from perspective-view image all obstacles like vehicles, barriers are excluded to avoid false detection, while in bird eye view generated by

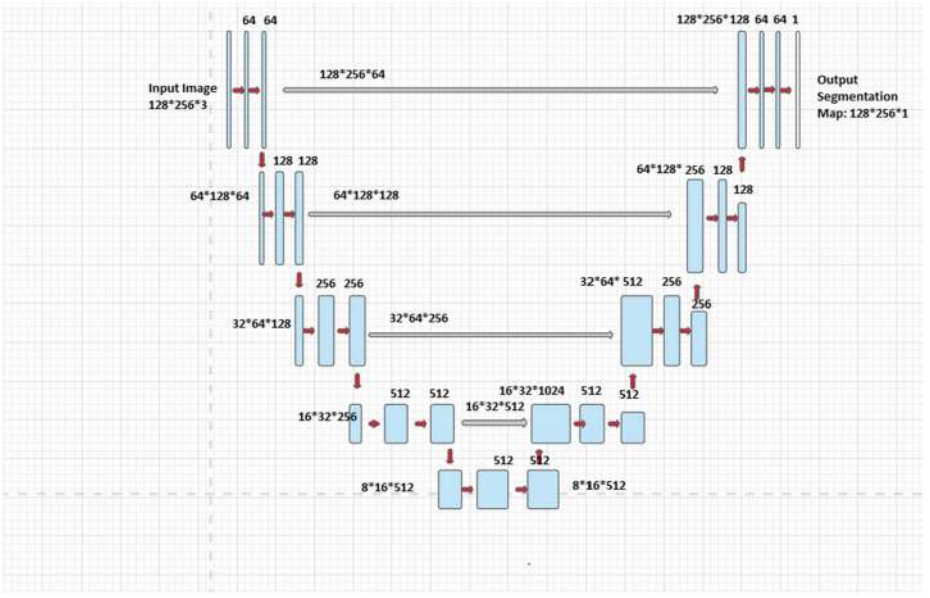

Fig. 6 Illustrating UNet architecture

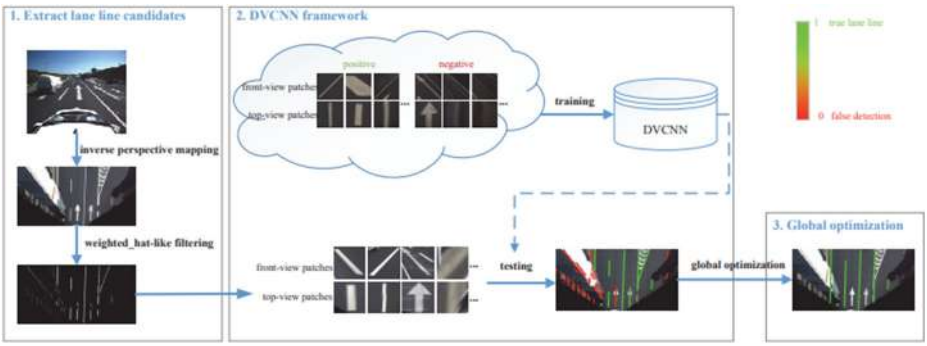

Fig. 7 Methodology for Lane Detection 1) lane line extraction 2) the DVCNN framework 3) the global optimization

perspective transformation mapping from perspective-view image non-club-shaped constructions such as ground arrows, words, etc. are removed. Secondly to extract lane candidate lines a weighted hat-like filter is created. This filter relieves the interference of gradual texture and reduces false detection. Afterward, the front-view and top-view images are the inputs to the DVCNN framework. Thirdly, a global optimization function is constructed to refine the final output using lane probability, lane geometry like length and width. After the optimization, the optimal fusion comprising correct lane lines is detected.

The average, recall, and precision ratios are 92.80% and 95.49% respectively. However, the algorithm fails when the lane lines are over-imposed by obstacles or vehicles.

2.2.4 Cloud point and CNN framework

Bei He et al. [23] suggested lane detection technique using CNN from the point cloud. CNN framework is designed to identify lane lines from point clouds. The road features are extracted using orthogonal projection and a top-view reflectivity image is obtained. The CNN architecture is proposed to distinguish candidate lane markings from reflective images. For accurate detection, the gradual up-sampling is applied to CNN. CNN cannot deploy the global information and domain knowledge, but the lane layout must be evaluated and classified into different groups. To reduce false alarms or detection ground arrows and texts are eliminated by mathematical and geometrical position or length restrictions (Figs. 8 and 9).

2.2.5 Fully connected layer

Alexandru [39] use two laterally-mounted cameras to the input image to fully convolutional deep learning model. They state that the front camera configuration does not furnish an

Table 2 Comparative analysis of lane detection models implemented using Segnet and Unet on tusimple dataset

Model Implemented	Training Accuracy	Validation Accuracy	Testing Accuracy
Segnet	95.81	95.19	95.176
Unet	97.93	97.44	97.527

Fig. 8 The schematic of framework

optimal lane marking sight, as it also records the entire front-facing driving scene, counting all vehicles or clusters. They produced 40,000 artificial image data that provide data augmentation, allows class distribution. The dataset contains images generated in diverse scenarios such as scattered, parallel, and partially interrupted lane markers. A few basic image processing transformations induced variance in the dataset by varying lighting conditions and shadows. Also, the pixel intensities are reduced by constant value in parts of an image to have imitated shadows cast on the lane markings. The network consists of convolutional layers, fully connected layers, and soft-max classification that operates on laterally mounted camera images. The network can predict the lane marking from the image with 97.85 accuracy%

3 Discussion on dataset and evaluation metrics

The Computer vision-based models have dominated the market and will continue due to low-cost hardware and substantial knowledge of image processing and machine learning techniques. Even though its wide range of applications in lane detection, vision-based models suffers from critical, challenging scenarios discussed previously. Many advanced machine learning and deep learning-based models were designed to obtain more reliability and robustness in real-time lane detection. Therefore, robustness is important to assess the system's maturity level and determine the loss ends.

Below Table 3 shows the different methods and its limitation. This table also justifies the significance of using deep learning-based model.

Researchers use various methodologies and assessment criteria to evaluate and benchmark the algorithms. As explained before, a lane detection problem is be broken down

Fig. 9 Sideways cameras focusing on lane lines

Table 3 Analysis of lane detection models

Techniques	Models	Merits	Demerits
Traditional	Geometric modeling with edge detection, line fitting	Works fine with simple lane detection	Does not work for challenging scenarios
Non Deep Learning Based	Uses perspective transformation, camera calibration, ROI	Better for curved roads	Computationally expensive, fail to detect the steep lanes
Deep Learning based	Encoder-decoder CNN Model, SegNet, U-Net	shows better results in challenging situations	Computationally expensive

into preprocessing, lane detection, and tracking. Correspondingly, assessment could be carried out in all 3 phases. Here we have divided the evaluation methods into two categories: Evaluation based on Dataset and evaluation metric.

3.1 Evaluation dataset

The evaluation of the model is broadly categorised in two section based on dataset used is offline or online.

3.1.1 Offline evaluation dataset

The designed lane detection model is generally evaluated offline by image dataset or continuous image frames (videos). There are various public datasets available such as TuSimple, Kitti, Caltech, Camvid (Cambridge-driving Labelled Video Database), Culane, BDD100k, VPGNet, and CurveLanes dataset. The below table describes different dataset used in image segmentation and object detection task

- TuSimple Dataset [49] collected from American Highway contains 7,000 one-second-long video clips of 20 frames. The Training set contains 3626 video clips, 3626 annotated frames, and the Testing set has 2782 video clips and the Testing set has 2782 video clips.
- There are 600 images in Kitti Dataset containing 290 training images and 300 testing images divided into three categories, representing challenging road scenarios. For both training and testing set in each category, there are 100 annotated images. The data is collected from GPS information and Velodyne laser scans. There are 3 categories of dataset urban unmarked (UU), urban marked (UMM), and urban multiple marked lanes (URBAN) [16]
- There are 1225 frames in the Caltech lane dataset, distributed in four clips recorded from the street in Pasadena, CA at distinct daytime. Caltech-lanes Dataset [13]
- CamVid Dataset [10] is road/driving scene video dataset which is captured by the car-mounted camera with a resolution 960×720. The dataset consists of 367 training set, 101 validation set and 233 test sets
- Culane datasetbd6This dataset is collected by mounting cameras on six different vehicles using six different drivers on Beijing roads. The dataset is crested by recording videos for more than 55 hours. Total 133235 frames were extracted. The dataset is

divided into 88880 training set, 9675 validation set and 34860 testing dataset. This dataset contains normal and 8 different challenging categories.

- BDD100k [24] dataset is a diverse driving dataset for Heterogeneous Multitask Learning
- VPGNet [31] was associated with the methods proposed to use the vanishing point to predict the lane marking. In addition to vanishing point labels, various types of lane markings and road signs are marked in detail. This dataset includes varying degrees of rainfall and nighttime images, which is challenging due to severe weather and extreme lighting conditions.
- CurveLanes [2] has more images with curved lines. So it fulfills the requirement of curved scenes.

3.1.2 Online evaluation dataset

To compute detection correctness and confidence the online evaluation techniques integrates roadway and lane configuration stats and combine them with other sensors like GPS or LIDAR. The road and lane geometric configurations are discovered after the camera calibration. The lane configuration restriction such as slope, intercept, the position of the vanishing point, etc. is used as an authentic metric for determining the model robustness. The lane parameters are analyzed to evaluate the correctness of lane detection. If the parameters exceed the constraints, re-estimation is proposed. LLAMAS dataset [6] is unsupervised annotated dataset by creating high definition maps for automated driving including lane markers based on Lidar.

The above Table 4 describes data acquisition details of each dataset.

3.1.3 Evaluation metrics

Recently, Visual Assessment or Simple Detection Rates(SDR) are used as evaluation metrics for lane detection models. The most regular metrics used for performance evaluating of

Table 4 Data acquisition details of datasets

Datasets	Data Acquisition Devices	Image Resolution	Annotation
TuSimple	Color Camera	1280*720	Key point coordinates
Kitti	Grey Scale Camera,Color Camera,Laser Scanner	1242*375	Pixel level,Rectangle Coordinates
Caltech	Color Camera	640*780	Key point coordinates
Camvid	Color Camera	960*720	Pixel level
Culane	Color Camera	1640*590	Key point coordinates
BDD100k	Color Camera	1280*720	Computationally expensive
VPGNet	Color Camera	640*780	Key point coordinates
CurveLanes	Dynamic Color Cameras,Sensor	2560*1440	Key point coordinates
LLAMAS	Color Camera, LiDAR Maps	1276*717	Pixel level

lane detection algorithms are Receiver Operating Characteristic (ROC) curves, Accuracy, Precision, Recall, F-score, and Dice Similarity Coefficient (DSC) [50].

$$Accuracy = (TrP + TrN) \div (m) \tag{1}$$

$$Recall = TrP \div (TrP + FaN) \tag{2}$$

$$Precision = TrP \div ((TrP + FaP) \tag{3}$$

$$F\−measure = 2 * Precision * Recall \div (Precision + Recall) \tag{4}$$

$$DSC = 2 * TrP \div (TrP + FaP + m) \tag{5}$$

Here, TrP is True Positive, TrN is True Negative, FaP is False Positive, FaN is False Negative, n is Total Lanes, m = Total Pixels (Table 5).

Below Table 6 shows the performance comparison of different deep learning based techniques.

3.2 Current limitation & challenges

Significant advancements are being made in road perception and lane finding. It is practically used in ADAS systems such as LDWS and LKAS. Most of these models used camera-vision based techniques due to low-cost device that gives extensive knowledge of surrounding to enable lane detection. Still, the vision-based models suffer from illumination variation, shadow, bad weather, etc. Due to the inevitable limitations of the camera, building a high-reliability vision-based model requires lots of development efforts. Therefore, various milestones are to be achieved.

The complexity of the ADAS system varies from simple (LWS) to the hardest problem (autonomous navigation), which led to different approaches by researchers. The most important properties of a system are accuracy and robustness which determine if the model

Table 5 Performance comparison of different technique

Techniques	Accuracy	FaP	FaN	F1-Score
Ripple-GAN [59]	97.82	0.0048	0.0289	97.67
Keep Eye on Lane [48]	95.63	0.0353	0.0292	96.77
Salmnet [55]	96.91	0.0263	0.0252	93.44
EndToEnd-LaneMarker [56]	96.22	0.0308	0.0376	92.28
EL-GAN [17]	96.39	0.0412	0.0336	90.56
PointLaneNet [14]	96.34	0.0467	0.0518	89.61
Lightweight Lane [25]	96.64	0.0602	0.0205	87.56
Spatial as Deep [41]	96.53	0.0617	0.0180	87.27
Agnostic lane detection [24]	96.29	0.0722	0.0218	85.52
Towards end-to-end lane detection [38]	96.40	0.0780	0.0244	84.71
FastDraw [42]	95.20	0.0760	0.0450	84.39
Cascaded CNN [43]	95.24	0.197	0.0620	78.35

Table 6 Synopsis for various lane detection models

Ref	Preprocessing	Lane detection	Tracking	Evaluation	Comments
Wu et al [54]	YIQ color space transform, vanishing point detection	Fan-scanning line detection	None	Visual Examination and Correct Detection Rate	The highway lane departure warning and front collision system is built with straight lane model
Niu et al [39]	Temporal blur, IPM, adaptive threshold	RANSAC	Kalman filter	Camera Quantitative analysis and visual assessment	ALD 2.0 is used for labeling video ground truth systematically
Jung and Kelber [28]	Edge detection, Gaussian filter	Gradient Weighted Hough transformation	a lane boundary model	Camera Frame images and visual assessment	proposed linear-parabolic model requires low computational power and memory requirements and showed better predictions in noise, shadows, lack of lane painting and change of illumination conditions.
Wang et al [53]	Vanishing point detection and canny detection	Control point detection	None	Camera Frame images and visual assessment	The B-snake model is powerful in shadows and lighting discrepancy
Aly [2]	IPM, Gaussian kernel filter	RANSAC	Hough transform	Evaluated on Caltech dataset and Quantitative analysis	This method is robust on curve lanes and shadows but affected by road painting and crossways
Borkar et al [7]	IPM, temporal blur	RANSAC	Kalman filter	Visual assessment and detection metrics	The model is created mainly for night vision.
Haloi and Jayagopi [20]	IPM, steerable filter	RANSAC	None	Evaluated on public KITTI dataset	optical flow was employed to built LDWS and the model is robust to shadows
Gurghian et al [19]	ROI, artificial image generation	CNN	None	Pixel level distance evaluation	end-to-end lane recognition method is applied in real time
Rose et al [45]	Dynamic thresholds, Canny detector	Least Squares fitting , Hough Transform	Kalman filter	Real time assessment for spatial and slope criterion and MAE with ground truth position	A reliable lane detection model and lateral offset measurement using sensors like camera and Lidar

Table 6 (continued)

Ref	Preprocessing	Lane detection	Tracking	Evaluation	Comments
Sehestedt et al [46]	IPM	Markov model	Clustered Particle Filters	Tested on dataset from testbed vehicle CRUISE and Evaluation using Matlab	Robust in challenging illumination scenario and reliable for urban straight and curved roads
Li et al [33]	ROI, IPM	CNN, RNN	None	Quantitative analysis with receiver operating characteristic curve	The model uses long-short-term memory(LSTM) that record lane's geometrical structures for a timespan in the video sequences
Assidiq et al [4]	Canny edge detector	Hough transform	Hyperbola Fitting	Visual assessment and correct detection rate	Robust in shadows and lighting discrepancy situations, Suitable for color coated curved or linear roads
Liu et al [35]	Gaussian filter	Canny Edge detection	Hough transform	Evaluation using Performance Metric	Computationally expensive and poor at curve lane detection
Guo et al [18]	IPM	Cascade lane feature detector	Catmull Rom splines	Analysis using 6121 images sequences	the model use weighted graph particle filter. Robust in various lighting and weather conditions.
Ozgunalp and Dahnoun [40]	Symmetrical Local Threshold	Hough accumulator	ROI,vanishing point	Camera Frame images and visual assessment	Robust in shadows and night Suitable for both straight and curved roads
Li et al [32]	Camera Calibration, Noise Cancellation filer	ROI, Canny edge detector	Kalman filter	Evaluated using manually labeled frames with multiple metrics	Suitable simple straight lane detection but has inadequate performance in challenging scenarios like heavy traffic, complex road textures and poor illumination
Mamidala et al [36]	Reduce Resolution	SegNet	None	Performance Evaluation using multiple metrics	dynamic data is collected from Google street-view api that gives quality information about roads and lane.
He et al [22]	IPM and weighted hat-like filter	DVCNN framework	Google Optimization	Visual and Quantitative Evaluation	Fails when the lanes in the image is occluded by the vehicle.

can be used in real-time. Various lane detection models implemented using machine learning techniques have achieved significantly better processing and lane prediction results. But generally, the detection fails as the camera moves out of the region of interest (ROI) and in various challenging scenarios. Also, there is a considerable research gap in the road perception issues: perception of multi-lane and stochastic typologies of road and lane, this is known as middle-complexity. The analysis carried out on full autonomy does not answer the middle-complexity problem. In fact, as the full autonomous problem is very difficult to solve, ad-hoc solutions are created to avoid extensive onboard understanding and focus on finite problem aspects only. Therefore, the biggest challenge to future models in the next decade is extending the scope of lane perception and support secure and reliable lane prediction under challenging scenarios.

To build a secure and reliable model, various functional blocks and diverse conditions, assumptions need to be recognized. Additional validation tasks must be performed, as many failure cases are infrequent and tough to recognize. Hence, significant research and development efforts are required to achieve satisfying results. One of the solutions to overcome camera limitations is combining other modalities. Considering the scenario following are few ways that may be helpful:

3.2.1 Fusion or integration technique

If Single vision-based techniques gives less performance due to camera limitations, fusion of other perception models is helpful. To enhance the lane prediction, multiple backup models are integrated, this is known as algorithm level integration. The algorithms are parallel or serially integrated and weighted. The system should be able to infer the corner cases where the algorithm fails to weigh them accordingly or transit among these.

3.2.2 Public benchmark evaluation

All the researchers follow different evaluation metrics to assess the system performance in terms of accuracy and robustness as there is no standard benchmark to evaluate the model and it becomes very difficult to compare across publications. A public video benchmark solves this problem.

4 Conclusion

In this review, various conventional and recent lane detection techniques based on deep learning are discussed. We compared various methodologies to give an overview of preprocessing, detection, and tracking techniques used by various researchers. Many evaluation metrics and data-sets used for Lane detection systems are also presented here. The Lane detection system is implemented using Unet and Segnet architecture using Tusimple dataset. As compared to the Segnet, Unet performs better and gives an accuracy 97.52%. Based on in depth survey on deep learning based techniques used for lane detection system, we conclude that the performance of the GAN model and Encoder Decoder based deep learning techniques is quite better as compared to the other deep learning based techniques. Finally, we discuss current gaps or limitations in lane detection and the future challenges, furthermore we provide approaches to bridge these gaps.

Nature Portfolio journals: https://www.nature.com/nature-research/editorial-policies
Scientific Reports: https://www.nature.com/srep/journal-policies/editorial-policies
BMC journals: https://www.biomedcentral.com/getpublished/editorial-policies

Acknowledgements We thank Dr Swati Shinde, Professor, Pimpari Chinchwad College of Engineering, Pune for her assistance in the revision of this paper. Her comments and suggestions has greatly improved the manuscript.

Author Contributions All authors have equally contributed to the design and implementation of the research, to the analysis of the results and to the writing of the manuscript.

Funding Not applicable

Data Availability Not applicable

Code Availability Not applicable

Declarations

Data sharing not applicable to this article as no datasets were generated or analyzed during the current study.

Conflict of Interests We certify that there is no actual or potential conflict of interest in relation to this article.

Ethics approval The submitted work is original and not have been published elsewhere in any form or language

Consent to participate Not applicable

Consent for Publication Not applicable

References

1. Alvarez JM, Salzmann M, Barnes N (2014) Large-scale semantic co-labeling of image sets. In: IEEE winter conference on applications of computer vision. IEEE, pp 501–508
2. Aly M (2008) Real time detection of lane markers in urban streets. In: 2008 IEEE intelligent vehicles symposium. IEEE, pp 7–12
3. Aly M (2008) Real time detection of lane markers in urban streets. In: 2008 IEEE intelligent vehicles symposium. IEEE, pp 7–12
4. Assidiq AA, Khalifa OO, Islam MR, Khan S (2008) Real time lane detection for autonomous vehicles. In: 2008 International conference on computer and communication engineering. IEEE, pp 82–88
5. Aubert D, Kluge KC, Thorpe CE (1991) Autonomous navigation of structured city roads. In: Mobile Robots V. SPIE, vol 1388, pp 141–151
6. Behrendt K, Soussan R (2019) Unsupervised labeled lane markers using maps. In: Proceedings of the IEEE/CVF international conference on computer vision workshops, pp 0–0
7. Borkar A, Hayes M, Smith MT (2009) Robust lane detection and tracking with ransac and kalman filter. In: 2009 16th IEEE international conference on image processing (ICIP). IEEE, pp 3261–3264
8. Broggi A, Cappalunga A, Caraffi C, Cattani S, Ghidoni S, Grisleri P, Porta PP, Posterli M, Zani P (2010) Terramax vision at the urban challenge 2007. IEEE Trans Intell Transp Syst 11(1):194–205
9. Broggi A, Cattani S (2006) An agent based evolutionary approach to path detection for off-road vehicle guidance. Pattern Recogn Lett 27(11):1164–1173
10. Brostow GJ, Fauqueur J, Cipolla R (2009) Semantic object classes in video: a high-definition ground truth database. Pattern Recogn Lett 30(2):88–97
11. Buehler M, Iagnemma K, Singh S (2007) The 2005 DARPA grand challenge: the great robot race. Springer, vol 36
12. Burrow M, Evdorides H, Snaith M (2003) Segmentation algorithms for road marking digital image analysis. In: Proceedings of the institution of civil engineers-transport. Thomas telford ltd, vol 156, pp 17–28

13. Caltech-lanes Dataset (2022) https://www.vision.caltech.edu/malaa/datasets/caltech-lanes/. Accessed April 2021
14. Chen Z, Liu Q, Lian C (2019) Pointlanenet: efficient end-to-end cnns for accurate real-time lane detection. In: 2019 IEEE intelligent vehicles symposium (IV). IEEE, pp 2563–2568
15. Cheng H-Y, Jeng B-S, Tseng P-T, Fan K-C (2006) Lane detection with moving vehicles in the traffic scenes. IEEE Trans Intell Trans Syst 7(4):571–582
16. Fritsch J, Kuehnl T, Geiger A (2013) A new performance measure and evaluation benchmark for road detection algorithms. In: 16th International IEEE conference on intelligent transportation systems (ITSC 2013). IEEE, pp 1693–1700
17. Ghafoorian M, Nugteren C, Baka N, Booij O, Hofmann M (2018) Elgan: embedding loss driven generative adversarial networks for lane detection. In: Proceedings of the European conference on computer vision (ECCV) workshops, pp 0–0
18. Guo C, Mita S, McAllester D (2010) Lane detection and tracking in challenging environments based on a weighted graph and integrated cues. In: 2010 IEEE/RSJ international conference on intelligent robots and systems. IEEE, pp 5543–5550
19. Gurghian A, Koduri T, Bailur SV, Carey KJ, Murali VN (2016) Deeplanes: End-to-end lane position estimation using deep neural networksa. In: Proceedings of the IEEE conference on computer vision and pattern recognition workshops, pp 38–45
20. Haloi M, Jayagopi DB (2015) A robust lane detection and departure warning system. In: 2015 IEEE intelligent vehicles symposium (IV). IEEE, pp 126–131
21. He B, Ai R, Yan Y, Lang X (2016) Lane marking detection based on convolution neural network from point clouds. In: 2016 IEEE 19th international conference on intelligent transportation systems (ITSC). IEEE, pp 2475–2480
22. He B, Ai R, Yan Y, Lang X (2016) Accurate and robust lane detection based on dual-view convolutional neutral network. In: 2016 IEEE intelligent vehicles symposium (IV). IEEE, pp 1041–1046
23. He B, Ai R, Yan Y, Lang X (2016) Lane marking detection based on convolution neural network from point clouds. In: 2016 IEEE 19th international conference on intelligent transportation systems (ITSC). IEEE, pp 2475–2480
24. Hou Y (2019) Agnostic lane detection. arXiv:1905.03704
25. Hou Y, Ma Z, Liu C, Loy CC (2019) Learning lightweight lane detection cnns by self attention distillation. In: 2019 IEEE/CVF international conference on computer vision (ICCV), pp 1013–1021. https://doi.org/10.1109/ICCV.2019.00110
26. Huang Y, Li Y, Hu X, Ci W (2018) Lane detection based on inverse perspective transformation and kalman filter. KSII Trans Internet Inf Syst (TIIS) 12(2):643–661
27. Huang AS, Moore D, Antone M, Olson E, Teller S (2009) Finding multiple lanes in urban road networks with vision and lidar. Auton Robot 26(2):103–122
28. Jung CR, Kelber CR (2004) A robust linear-parabolic model for lane following. In: Proceedings. 17th Brazilian symposium on computer graphics and image processing. IEEE, pp 72–79
29. Kim Z (2008) Robust lane detection and tracking in challenging scenarios. IEEE Trans Intell Trans Syst 9(1):16–26
30. Kuderer M, Kretzschmar H, Burgard W (2013) Teaching mobile robots to cooperatively navigate in populated environments. In: 2013 IEEE/RSJ Int Conf Intell Robots Syst. IEEE, pp 3138–3143
31. Lee S, Kim J, Shin Yoon J, Shin S, Bailo O, Kim N, Lee T-H, Seok Hong H, Han S-H, So Kweon I (2017) Vpgnet: vanishing point guided network for lane and road marking detection and recognition. In: Proceedings of the IEEE international conference on computer vision, pp 1947–1955
32. Li Y, Iqbal A, Gans NR (2014) Multiple lane boundary detection using a combination of low-level image features. In: 17th International IEEE conference on intelligent transportation systems (ITSC). IEEE, pp 1682–1687
33. Li J, Mei X, Prokhorov D, Tao D (2016) Deep neural network for structural prediction and lane detection in traffic scene. IEEE Trans Neural Netw Learn Syst 28(3):690–703
34. Liu W, Li S, Huang X (2014) Extraction of lane markings using orientation and vanishing point constraints in structured road scenes. Int J Comput Math 91(11):2359–2373
35. Liu G, Wörgötter F, Markelić I (2010) Combining statistical hough transform and particle filter for robust lane detection and tracking. In: 2010 IEEE intelligent vehicles symposium. IEEE, pp 993–997
36. Mamidala RS, Uthkota U, Shankar MB, Antony AJ, Narasimhadhan A (2019) Dynamic 0approach for lane detection using google street view and cnn. In: TENCON 2019-2019 IEEE region 10 conference (TENCON). IEEE, pp 2454–2459

37. McCall JC, Trivedi MM (2004) An integrated, robust approach to lane marking detection and lane tracking. In: IEEE Intelligent vehicles symposium. IEEE, 2004, pp 533–537
38. Neven D, Brabandere B, Georgoulis S, Proesmans M, Van Gool L (2018) Towards end-to-end lane detection: an instance segmentation approach, pp 286–291. https://doi.org/10.1109/IVS.2018.8500547
39. Niu J, Lu J, Xu M, Lv P, Zhao X (2016) Robust lane detection using two-stage feature extraction with curve fitting. Pattern Recogn 59:225–233
40. Ozgunalp U, Dahnoun N (2014) Robust lane detection & tracking based on novel feature extraction and lane categorization. In: 2014 Ieee international conference on acoustics, speech and signal processing (icassp). IEEE, pp 8129–8133
41. Pan X, Shi J, Luo P, Wang X, Tang X (2018) Spatial as deep: spatial cnn for traffic scene understanding. In: AAAI
42. Philion J (2019) Fastdraw: addressing the long tail of lane detection by adapting a sequential prediction network, pp 11574–11583. https://doi.org/10.1109/CVPR.2019.01185
43. Pizzati F, Allodi M, Barrera A, García F (2019) Lane detection and classification using cascaded cnns
44. Pomerleau D (1995) Ralph: rapidly adapting lateral position handler. In: Proceedings of the intelligent vehicles' 95. Symposium. IEEE, pp 506–511
45. Rose C, Britt J, Allen J, Bevly D (2014) An integrated vehicle navigation system utilizing lane-detection and lateral position estimation systems in difficult environments for gps. IEEE Trans Intell Transp Syst 15(6):2615–2629
46. Sehestedt S, Kodagoda S, Alempijevic A, Dissanayake G (2007) Robust lane detection in urban environments. In: 2007 IEEE/RSJ international conference on intelligent robots and systems. IEEE, pp 123–128
47. Sivaraman S, Trivedi MM (2013) Integrated lane and vehicle detection, localization, and tracking: a synergistic approach. IEEE Trans Intell Transp Syst 14(2):906–917
48. Tabelini L, Berriel R, Paixao TM, Badue C, De Souza AF, Oliveira-Santos T (2021) Keep your eyes on the lane: real-time attention-guided lane detection. In: Proceedings of the IEEE/CVF conference on computer vision and pattern recognition, pp 294–302
49. Tusimple Dataset (2017). https://github.com/TuSimple/tusimple-benchmark. Accessed April 2021
50. Veit T, Tarel J-P, Nicolle P, Charbonnier P (2008) Evaluation of road marking feature extraction. In: 2008 11th International IEEE conference on intelligent transportation systems. IEEE, pp 174–181
51. Veit T, Tarel J-P, Nicolle P, Charbonnier P (2008) Evaluation of road marking feature extraction. In: 2008 11th International IEEE conference on intelligent transportation systems. IEEE, pp 174–181
52. Von Gioi RG, Jakubowicz J, Morel J-M, Randall G (2008) Lsd: a fast line segment detector with a false detection control. IEEE Trans Pattern Anal Mach Intell 32(4):722–732
53. Wang Y, Teoh EK, Shen D (2004) Lane detection and tracking using b-snake. Image Vis Comput 22(4):269–280
54. Wu C-F, Lin C-J, Lee C-Y (2011) Applying a functional neurofuzzy network to real-time lane detection and front-vehicle distance measurement. IEEE Trans Syst Man Cybern Part C (Appl Rev) 42(4):577–589
55. Xu X, Yu T, Hu X, Ng WW, Heng P-A (2020) Salmnet: a structure-aware lane marking detection network. IEEE Trans Intell Transp Syst 22(8):4986–4997
56. Yoo S, Lee HS, Myeong H, Yun S, Park H, Cho J, Kim DH (2020) End-to-end lane marker detection via row-wise classification. In: Proceedings of the IEEE/CVF conference on computer vision and pattern recognition workshops, pp 1006–1007
57. Yoo JH, Lee S-W, Park S-K, Kim DH (2017) A robust lane detection method based on vanishing point estimation using the relevance of line segments. IEEE Trans Intell Transp Syst 18(12):3254–3266
58. Yuan J, Tang S, Pan X, Zhang H (2014) A robust vanishing point estimation method for lane detection. In: Proceedings of the 33rd chinese control conference. IEEE, pp 4887–4892
59. Zhang Y, Lu Z, Ma D, Xue J-H, Liao Q (2020) Ripple-gan: lane line detection with ripple lane line detection network and wasserstein gan. IEEE Trans Intell Transp Syst 22(3):1532–1542
60. Zhang G, Zheng N, Cui C, Yan Y, Yuan Z (2009) An efficient road detection method in noisy urban environment. In: 2009 IEEE intelligent vehicles symposium. IEEE, pp 556–561

Affiliations

Ashwini Sapkal[1] · Arti[1] · Dishant Pawar[1] · Prashant Singh[1]

Arti
artisaradhna12@gmail.com

Dishant Pawar
dishantpawar_17343@aitpune.edu.in

Prashant Singh
prashantsingh_17459@aitpune.edu.in

[1] Department of Information Technology, Pune, Army Institute of Technology, Dighi, Pune, 411015, Maharashtra, India

Army Institute Of Technology (AIT), Dighi Camp, Pune - 15.
Director : 7249250115, Joint Director : 7249250117, Principal : 7249250186
Exch : 7249250183, 7249250184, 7249250185
Website : www.aitpune.com Email : ait@aitpune.edu.in
Recognised by AICTE and DTE Maharashtra and affiliated to Savitrabai Phule Pune University

ONWARD TO GLORY

Dr. Sagar R. Rane (CE)

- Course Work
- PhD Certificate
- Publication Copy

NO.: 15 - 0002473

SAVITRIBAI PHULE PUNE UNIVERSITY

(Formerly University of Pune)

GANESHKHIND, PUNE 411 007.

DEPARTMENT OF TECHNOLOGY

(ACADEMIC AUTONOMY)

GRADE SHEET

PRN NO : **CI13MP04** EXAMINATION : **June2015**

NAME : **Rane Sagar Ramesh** MOTHER's NAME : **Sangita**

COURSE : **M.Tech - Ph.D (Integrated) (COMPUTER & INFORMATION TECHNOLOGY)**

Semester	Subject Code	Subject Name	Credits	Grade	Grade Points
Semester-I	CIC1	Parallel and Distributed Computing	5	A	05
	CIC2	Advanced Algorithms and Advanced Statistics	5	E	01
	CIC3	Advanced Database Management System	5	D	02
	CIC6	Cyber Security	2	E	01
	CIE1	Privacy and Security in Cloud Computing	5	O	06
	CIO2	Mashups	5	O	06
	CISM1	Seminar 1	5	D	02
Semester-II	CIC4	Network System Design	5	E	01
	CIC5	Advanced Software Engineering	5	O	06
	CIC7	Human Rights	2	O	06
	CIE4	Advanced Operating System	5	A	05
	CIE7	Machine Learning	5	A	05
	CIE9	Semantic Web	5	A	05
	CISM2	Seminar 2	5	O	06
Semester-III	CIMaths	Advanced Mathematics	5	E	01
	CIRM	Research Methodology	5	A	05
	CIE38	Knowledge Management & Applications	5	B	04
	CISM3	Seminar 3	5	B	04

Final Grade and Grade Point Average (GPA) awarded for **M.Tech - Ph.D (Integrated)**

MAXIMUM GPA=06 GPA = Grade =

CONTROLLER OF EXAMINATIONS HEAD OF THE DEPARTMENT DATE : 4 MAR 2016

Savitribai Phule Pune University

(formerly University of Pune)

We, the Chancellor, the Vice Chancellor and the Members of the Management Council and the Academic Council of the Savitribai Phule Pune University certify that

Rane Sagar Ramesh, Mother's Name : Sangita

having been examined and found duly qualified for the degree of

M.Tech (Integrated) - Doctor of Philosophy

(Computer and Information Technology)

The said degree has been conferred on him. In testimony where of is set the seal of the said University.

सावित्रीबाई फुले पुणे विद्यापीठ

(पूर्वीचे पुणे विद्यापीठ)

आम्ही, सावित्रीबाई फुले पुणे विद्यापीठाचे कुलपती, कुलगुरु आणि व्यवस्थापन परिषद व विद्या परिषद सदस्य, प्रमाणित करितो की,

राणे सागर रमेश , आईचे नाव: संगिता

तंत्रविद्या पारंगत (एकत्रित) - विद्यावाचस्पती

(संगणक व माहिती तंत्रज्ञान)

पदवीस पात्र झाल्याबद्दल त्यांना ही पदवी प्रदान करण्यात येत आहे. याची साक्ष म्हणून विद्यापीठाची अधिकृत मुद्रा येथे अंकित करण्यात येत आहे.

Vice Chancellor

122th Convocation (Summer)

TE22-00006

International Journal of Computing and Digital Systems
ISSN (2210-142X)
Int. J. Com. Dig. Sys. 11, No.1 (Jun-2022)

http://dx.doi.org/10.12785/ijcds/1101117

Blockchain Driven Secure and Efficient Logging for Cloud Forensics

Sagar Rane[1], Sanjeev Wagh[1, 2] and Arati Dixit[1, 3]

[1] Department of Technology, Savitribai Phule Pune University, Pune, MH, India
[2]Government College of Engineering, Shivaji University, Karad, Maharashtra, India
[3]Applied Research Associates Inc., Raleigh, North Carolina, USA

Received 16 Feb. 2021, Revised 11 Apr. 2022, Accepted 18 Apr. 2022, Published 15 Jun. 2022

Abstract: Cloud computing is one of the most holistically used technology nowadays. To do the forensics in the cloud, it is essential to accumulate as well as safeguard the justifiable facts of different events to find out the culprit. However, logging the events that take place in the cloud and securing them while preserving the privacy of cloud consumers is a big challenge. Currently, cloud consumers are relying on cloud service providers to get the logs of events that take place on their data despite multi-stakeholder collusion. Thus, there is a strong requirement of publicly verifiable secure logging which will play a vital role in criminal investigations without depending on a third party. In this paper, we developed a Blockchain-driven Secure Logging-as-a-Service (BlockSLaaS) scheme that supports, privacy-preserving secure logging and eclectic verification. To make a serene forensic investigation, the proposed scheme guarantees the trustworthiness and reclamation of logs in case of tampering. The scheme proposes integrating the Interplanetary File System (IPFS), a decentralized off-chain data storage platform with blockchain for efficient logging and its visualization. The extensive experiments on the number of transactions, storage requirement, uploading, reading, and downloading of log files for varying node count and file size are performed. The proposed method is compared with nine existing methods based on 9 security and performance features. The response, proof insertion, and proof-verification times of the proposed BlockSLaaS are 38.3, 29.7, and 26.3 milliseconds respectively which outperform the existing methods.

Keywords: Blockchain, Cloud Computing, Cloud Forensics, Secure and Efficent Logging, Forensic Investigation.

1. INTRODUCTION

Today, cloud computing services are widely used in various industries due to a tremendous efficiency of cost over conventional storage services [1] [2]. Currently, the market of cloud-based data storage is on the upsurge due to the successful espousal of cloud facilities in almost all companies. In India, cloud computing market will be valued at seven billion dollars by 2022 and expected to cross 1 trillion dollars by 2025 globally as per the NASSCOM report [3] [4]. However, the shift from onsite storage techniques to cloud storage services is a big challenge due to the rise in the issues of data security [5-11]. Certain malevolent cloud consumers can utilize the cloud storage to stock illegitimate information including but not limited to stolen Intellectual Property Rights (IPR) documents, pornographic content, and contraband documents or can target other cloud consumers by hosting the malware injection attacks, denial of service attacks, wrapping attacks, structured query language injection attacks, abuse and hijacking of services on cloud computing environment [12]. Once the attackers accomplish the unethical goal, they can smoothly wipe out the hints, traces, and remain unidentified [13] [14]. Therefore, there is a strong requirement of procedures and scientific methods to ensure trustworthiness and confidentiality of data in cloud computing environment for effective forensic investigations [2] [15]. Consequently, a new branch of forensics came into existence i. e. Cloud Forensics. Federal Bureau of Investigation (FBI) report of 2017 on internet crime statistics depicted that, over 3 lakh online misconduct complaints have been registered which amounted to around fifteen thousand-million-dollar loss in the year of 2017 itself [12]. The count of digital forensic belongings is on the upsurge [16]. The existing forensic methods and techniques cannot be applied to the cloud directly due to the nature of the cloud. Also, they require to be modernized to be competent and suitable for the cloud environment [6] [15]. In cloud computing, virtual

E-mail: scholarsaggy@gmail.com

machines (VMs) may be located out of the jurisdiction and they may consist of volatile data which could be lost once the VM turns off. Thus, forensic investigations of virtual machines' volatile data pose a grave challenge from the technical, organizational, and legal perspective [17].

The behavior of cloud consumers which is captured into the activity logs has the ability to report as to what events happened in the cloud [13]. Hence, logs are a crucial element to gain insight into any malicious activity. As of today, once the malevolent action got reported law enforcement agency has to depend on the activity logs that are given through the Cloud Service Provider (CSP) [18]. The most experienced crime perpetrators majorly focus and destroy the logging facilities and service stations to do away with the hints and traces of their nasty actions [7]. Therefore, integrity and confidentiality of responsible log marks is a leading worry to conduct forensic investigations in the cloud environment. Some invader may utilize the cloud environment to do the denial of service attack on the collocated apps successively on cloud system & can also lay off their virtual machines or attempt to fabricate the logs to remain untraceable. Figure 1. shows some advantages of using blockchain in secure logging.

Researchers have proposed various techniques to increase reciprocal trust among stakeholders of cloud systems i.e. Cloud Service Provider (CSP), Cloud Service Consumer (CSC), and Cloud Forensic Investigator (CFI). Few are in the field of secure logging [12] [19] but, using probabilistic data structures. Cloud data auditing schemes was presented like dynamic [18] [20] [21], shared [18] [22] [23] and privacy protected [24] [25] in existing work. Unlike the above-mentioned techniques and schemes whose focus was to protect cloud users' data, we aim to develop a privacy-preserving secure logging scheme for cloud users' activity logs. Extending SecLaaS [12] and CLASS [19], we develop blockchain-driven secure logging-as-a-service scheme (BlockSLaaS), a two-step privacy preservation scheme which certifies (a) CSP is putting correct information into the log file for associated cloud consumer event and (b) eclectic verification of logs without having actual logs. This paper is an extended version of our previous work [26] [27].

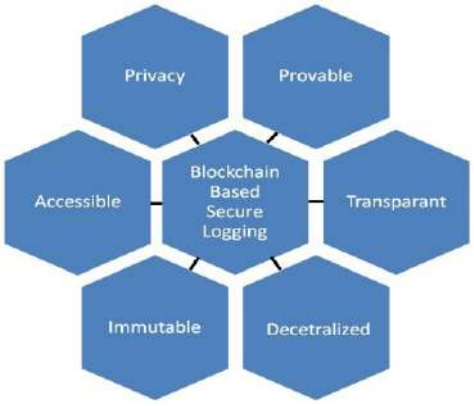

Figure 1. Advantages of blockchain in Secure Logging

According to the authors' knowledge, there is no work carried out on privacy-preserving secure logging for cloud forensics. The privacy of cloud consumers' is a very important aspect while considering the cost of a logging system. Thus, we propose an integration of blockchain and IPFS for efficient and cost-effective logging while maintaining the privacy, integrity, and confidentiality of cloud consumers' data. Our proposed scheme is publicly verifiable which means any authorized peer can verify the eclectic logs, unlike existing methods. Further, BlockSLaaS provides original logs via IPFS in case of tampering. This research work gives better access control to the cloud consumers on their data. Previous works have not comprehensively considered the multi-stakeholder collusion problem in the context of cloud forensics. There is no published analysis of the factors affecting the performance of secure logging. The extensive experiments on the number of transactions, storage requirement, uploading, reading, and downloading of log files for varying node count and file size are performed. Log visualization mechanism has been developed on top of IPFS for a better understanding of the process of cloud forensics. The following hypothesis describes the precise concern and apprehensive research problem which we planned to solve.

Hypothesis: Imagine Sagar is the proprietor of an international firm that provides cloud services. He has set up a cloud in different continents to manage the data for finance and insurance applications. He has demanded from the technical team a backup of every second for all the applications for financial and insurance data. A technical team of the firm configured the system to take the backup which guarantees that there is adequate space available to save the dealings.

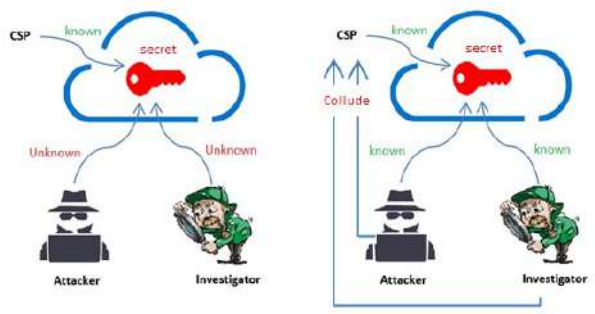

Figure 2. Collusion of Multiple Parties in Cloud

After few days, due to hardware failure, the firm's main storage got affected. A technical team discovers that the physical backup arrangement not working properly for the last few days and had sent many alerts to the technical team that no one observed. The technical team has the responsibility for this work. Thus, the technical team may be motivated to fabricate the firm's logs to be away from the issue.

The firm's consumers' operations, transactions data, personal data, and all relevant finance and insurance statistics are entirely managed by Sagar. Manasi is one of the consumers of cloud services offered by Sagar doesn't have direct access to the logs of their activity which is unfair. She has to be dependent on Sagar who is the service provider. As it is financial data, Manasi initially asked the cloud provider to update the security services on the cloud. Amol who is the competitor of Manasi did a DDOS attack on her application for his personal gains. Imagine that due to non-updated security services Manasi receives complaints related to their transactions for which Amol is responsible. Sagar knows that he has not updated the security patches. Hence, Sagar can collude with the technical team or Amol or forensic investigator to cover up the tracks and be motivated to change the logs before sending them to Manasi. As shown in Figure 2. At first, the lone CSP acquainted with the initial covert, as he is supervising all the cloud activities. However, the hypothesis talks about the untrusted system and CSP can be motivated to conspire through the malevolent invader or forensic investigator en route for tamper with data. To solve this type of problem we did some contributions which are listed in the next section.

Our Contributions: Following are the main contributions of our paper:

a) We developed an access control mechanism for different parties of the cloud while preserving data integrity and confidentiality.
b) We developed a forensic-enabled secure logging scheme in cloud despite multiple-party collusion.
c) We implemented a proof publication method for publishing cloud users' data for forensic investigations in a distributed environment where every authorized peer can check the signs of tampering and verify the eclectic logs in terms of better accuracy and performance.
d) We designed an efficient and cost effective decentralized off-chain log storage mechanism by engaging IPFS to reduce the data packing load of blockchain.

Organization: We have presented the background and the challenges of cloud log forensics in Section 2. Section 3 presents the literature review. The threat model & security properties are deliberated in Section 4. Our proposed technique is presented in Section 5. System setup, security analysis, evaluation results are discussed in Sections 6 and 7 respectively. The conclusion and future scope are provided in Section 8.

2. BACKGROUND

In this segment, we introduce a succinct background and overview of the forensic field, components, and characteristics of the blockchain. In section 3(A), (B), (C), we acquaint the branches of forensics i.e. digital forensics, cloud forensics, and cloud log forensics. In section 3(D), (E) we provide the overview of block chain, IPFS, and their usage to devise a solution to the cloud collusion problem.

A. Digital Forensics (DF)

As per the National Institute of Standards and Technology (NIST) document, DF is a systematic procedure of discovering & interpreting computing information using detection, assembling, investigation, and analysis. The penultimate objective is to maintain the data in some specific way that will be beneficial for the reintegration of old actions chronologically [5]. The information which is existent on machines in the form of images, audios, etc. can act as pieces of potential evidence. This information can help us to investigate the crimes, by providing supportive shreds of evidence. To procure, stock, and examine digital information, robust methods are required in the cloud [1].

B. Cloud Forensics (CF)

The CF is a subdivision of DF. It is firstly presented by author Keyun [28] as an inter-discipline of two popular fields i.e. cloud computing and digital forensics. It deals with and applicable to digital forensics, but the working atmosphere is different. However, this can lead to several defiances for pursuing forensics inside the cloud

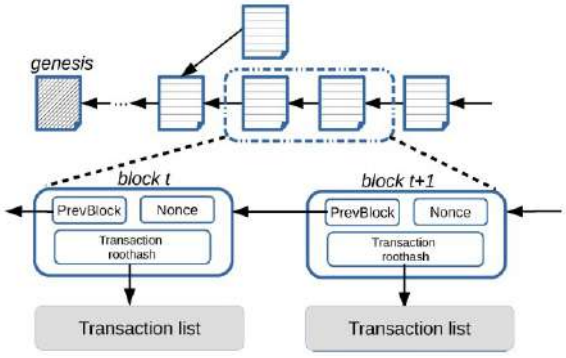

Figure 3. Structure of Blockchain

computing environment [16] [29]. The final aim remains unchanged, reintegration and ensuring the safety of ancient chronological actions [12] [30].

C. Cloud Log Forensics (CLF)

The third branch of forensics is quite challenging to implement since of the distributed nature and less control of consumers over the cloud. This can lead to a conundrum while accessing cloud logs and maintaining the integrity of consumers' behavior logs. In anticipation of getting multiple logs generated within the system [1], all stakeholders of the system are dependent on the CSP to get the logs and as previously pointed out in our proposition, there is no assurance that the cloud provider will make available justifiable and correct logs. Espousal of cloud computing is rising day by day consequences the assaults on the cloud have also been on the rise and there is a dire urgency of implementing log forensics in the cloud [31].

D. Blockchain

In the blockchain, there are three components as shown in Figure 3. The genesis block is the first component of any blockchain. This block states the start of the blockchain. The second component of blockchain is the data block which consists of transaction data, a hash of transaction data, a hash of the previous block, nonce, and timestamp. A hash is a unique value generated from hashing algorithm, e.g. SHA-256. A nonce is a random number that is used to verify the hash. The timestamp is a time of block creation in UTC. The genesis block is also a data block as it stores the above-mentioned information. Miners are some specific nodes that plays important role in the block verification process. The third core component of blockchain is chain i.e. sequence of blocks in a specific order. With the hash and chain of blocks, data is promised immutable. The linking of the data blocks with the previous hash creates a blockchain that assures data integrity [32]. Algorithm-1 from the appendix shows the creation of a single block in the blockchain.

E. IPFS

The Interplanetary File System (IPFS) is a decentralized network that is developed to style the internet faster without harm. In the IPFS system, if one machine goes down, other machines in the network can provide the required data. If we add any document on the IPFS network, it creates a hash value of the document. Other machines in the network can access this document through hash value which is published on the network. IPFS is a versioned file system like Git, it can stock records and track changes by checking versions of those records for any prescribed chronological period. IPFS is essentially a scattered organization that stocks and shares the documents based on content addressing [33].

3. RELATED WORK

The overall goal of this extensive literature survey was to understand the current related work going on cloud forensics field. This section clearly describes the previous work and its limitations and the need for new techniques and methods for cloud forensics. We tried to address secure logging and related problems of the cloud computing domain. Both centralized and decentralized types of systems have been studied. This work was inspired by [12] [19] as they tried to solve the same problem using different methods and techniques. Several research efforts have been undertaken to various extents for doing forensics in the cloud by a multitude of people [31]. The early work [34] encapsulates questions to answers on application logging ranging from enabling logging on to possible sources, setting up safe log transference, and fine-tuning logging formations. With the help of these pieces of advice, logging responsibilities can be completed successfully. A trustworthy and protected transference layer is essential in logging cloud applications. To obtain pieces of prospective evidence, a virtual contract of reliance amongst diverse cloud computing layers is a requisite. However, only guidelines have been given in the present research for how what, and when to do logging. Forensic tools and methods for doing forensics in cloud computing have been studied and evaluated successfully [17]. To gather different application peripheral interfaces (API) and firewall logs the FROST, a forensic enabled gizmo has been established by researchers [14] [17]. But, a strong trust is needed in different layers of the tool. Correspondingly, to deliver several activity logs to cloud consumers securely, novel APIs have been proposed which consider data in different phases like rest, motion, and execution [6]. In [35] Distributed denial of service (DDoS) attack detection mechanism has been implemented using Syslog on the eucalyptus cloud computing platform. The task of inner and outer activities observation by means of transmission capacity and CPU utilization is feasible in eucalyptus cloud computing software [35]. To procure the various logs from network segments, virtual file systems (VFS), and system call interfaces the supervision level over the Infrastructure as a Service is needed [36]. However, this

aforementioned layer may be a residence of weakness for enemies [12] [30]. A lot of forensic experts have put forward the idea to use Trusted Platform Module (TPM) to execute procedures and methods of digital forensics assuming the cloud service provider is a reliable participant in the cloud computing environment [29]. Few researchers were worked on the investigation of logs for several attack recognition [35]. Delegation of log controlling and its supervision instead of building activity log supervision for cloud environment is a price-saving job. Mysterious networks like TOR can be utilized for mockups [37] [38]. To maintain the order of VMs dealings, happened-before relationships are positioned in [41]. However, this relationship is not suitable in each criminal study. Zawoad and Ahsan have established Secure Logging as a Service (SecLaaS) [12] and CLASS [19], integrity safeguarding and verification way with the help of probabilistic data structures in cloud computing which is raising false positives and they are not publicly verifiable.

Cucurull et. al [42] proposed a secure logging method by using Bitcoin to record the history of events on local log chains. Sutton et. al [43] engage graphs to store the information of logs and offload the integrity proof digests on the Bitcoin network for audit trail. Since these methods depend on the Bitcoin blockchain, they cannot scale much by their block size and throughput. Other researchers explored the usage of permissioned blockchain framework i.e. Hyperledger Fabric. Ahmad et al. [44] worked on the database tracking by uploading the changed evidence information on Hyperledger Fabric. Shekhtman et. al [45] store the log files information straight away on the Hyperledger blockchain. Permissioned blockchain has been used for secure logging; however, the implemented methods are not scalable because the scalability parameters like throughput and storage are not undertaken. On the other hand, scalability is the utmost parameter to handle the huge number of log data in real-world secure logging management. SDN and blockchain has been used for secure logging with graphs in [46].

Cloud is a mixture of multifarious virtual systems and their linkages. Thus, it is exposed to cyber-attacks [28] [39] [40]. Currently, establishments can manage to pay for the additionally incurred care of safety and secure logging facilities. Though, a great amount of study is being accompanied in this region, for safeguarding reliable indications and marks in the cloud; but without considering collusion of multiple parties. Building a mechanism to make verifiable pieces of evidence presented to everyone in the system is what requires more research [12]. Trustworthiness and privacy maintenance specifically with logging in a virtual setting like a cloud is still an imperative topic to work upon [16]. Few schemes like SecLaaS and CLASS are based on centralized systems which can be down due to a single point of failure. As much existing work is based on internet protocols like HTTP may get affected due to DDOS attacks which lead to data unavailability. Privacy of the cloud consumers' data is also a major issue. Till now, cloud consumers have to depend on cloud providers to get the logs of their activities. Many of the approaches are assuming logger as a trusted entity.

Above mentioned research works precisely motivated us to work on the coherent readiness of logs; by looking at compelling problems of secure logging in spite of the collusion of multiple parties in a cloud that means no stakeholder of the cloud system is trusted and collusion may happen. Thus, there is a strong need for a scalable, efficient, and provable logging model in the distributed environment. The kind of system needs the proper procedures and forensic practices to be applied. A summary of the most recent and relevant approaches is given on the next page TABLE I. We considered the paper name, publication year, paper objective, service, advantages, and limitations for comparison.

4. THREAT MODEL & SECURITY PROPERTIES

In this section, we define the important notations used in the proposed secure logging model. After that, we narrate the threat model and security properties required in our projected system.

A. Threat Model

1. Confidentiality Violation: The confidentiality violation occurs when the cloud consumers' logs information retrieved by the invaders without consumers' consent. Though some confidentiality violations are unintentional, cloud consumers can suffer from financial losses.

2. Integrity Violation: The integrity violation of cloud consumers' logs is misconduct on their data to damage it. Such misconduct can be achieved by a single or group of entities by colluding with each other.

3. Availability Violation: The availability violation takes place by using unauthorized access to data which makes the cloud consumers' logs unavailable to the actual stakeholder of cloud systems.

4. Privacy Violation: The privacy violation of cloud consumer' logs occur when exuded log files can lead to creating a link or direct identification of cloud consumers' identity and data.

5. Repudiation by CSP: The cloud service provider can deny the logs and the proofs of consumers' actions in cloud computing.

TABLE I. A SUMMARY OF THE MOST RECENT AND RELEVANT APPROACHES FOR SECURE LOGGING

Ref.	Year	Paper Objective	Services	Advantages	Limitations
[12]	2016	Secure Logging as a Service	Centralized	Preservation of Integrity and Confidentiality, Method for publishing and verifying the logs.	The system may get down due to a single point of failure, Suffers from false positives, privacy issues of the cloud users' logs, and the possibility of collusions may lead to data leak. A trusted third party is required for forensic analysis.
[42]	2016	A Bitcoin-based secure logging technique to record the history of events on local log chains.	Decentralized	Provides a method for data auditability.	Since this method depends on the Bitcoin blockchain, it cannot scale much by its block size and throughput. Optimized implementation is required, Required huge amount of gas and transaction fee.
[47]	2017	Graphs to store the information of logs and offload the integrity proof digests on Bitcoin network for audit trail.	Decentralized	Maintenance of Integrity proof using graph approach.	Logging data transactions will be very huge which can place a storage burden on the blockchain. Off-chain storage methods are not used, Since this method depends on the Bitcoin blockchain, it cannot scale much by its block size and throughput. Optimized implementation is required. Required a huge amount of gas and transaction fee.
[43]	2017	Database operations tracking using graphs and Bitcoin network	Decentralized	Discussed the Database operations tracking and its security.	They have shown the viability of logging audit method using permissioned blockchain; however, the implemented methods are not scalable because the scalability parameters like throughput and storage are not undertaken, Required huge amount of gas and transaction fee.
[19]	2018	To develop cloud log assurance soundness and secrecy	Centralized	Preservation of log integrity, confidentiality, and privacy of consumers' data through encryption.	The storage is completely centralized and thus may suffer from a single point of failure which leads to data unavailability; Use of probabilistic data structures which may give wrong results. The log inspection process was very tedious.
[46]	2018	Secure storage of the log files on the Hyperledger Fabric.	Decentralized	Metadata is stored on the on-chain storage of blockchain.	Permissioned blockchain has been used for secure logging; however, the implemented methods are not scalable because the scalability parameters like throughput and storage are not undertaken.

[45]	2018	Data Integrity Validation	Decentralized	Validation of data integrity using blockchain is valuable.	Only data validation method is presented. The method works on few assumptions. Data Storage on a blockchain is very expensive. IPFS data storage is suggested in the future scope of the paper.
[48]	2019	Challenges and Opportunities in Distributed Cloud Storage Forensics	Decentralized	Explain Cloud Storage Forensics using STORJ case study.	The guidelines have been given for cloud storage forensics but implementation details are missing.
[49]	2020	Implementation for secure Logging Service	Decentralized	Isolation of logging service, reconstruction of event timeline, Resiliency to log manipulation, privacy, and data confidentiality.	Vulnerable to DDOS attacks. Only the on-chain storage layer is discussed; Data packing load is very high on a blockchain which is uneconomical solution.
[50]	2020	concrete transparency and compliance architecture	Centralized	List of data processing events and their sharing and compliance. Special Architecture for compliance checking.	A policy vocabulary and language has been given for logging. Integration of it is not described anywhere. Does not directly deal with the integrity and privacy of the data. Dashboard creates a new place for attackers.
[51]	2020	Network Log Management	Decentralized	This technique provides transparency, and preserves confidentiality & data accountability.	Not presented off-chain storage of records and also provided only on-chain storage for pre forensic data files. Solution is not cost effective.
[52]	2020	Method for collection of evidence and Preservation of Provenance in Cloud	Decentralized	Authentication, Encryption and optimal key generation algorithms have been implemented.	Not presented off-chain storage for evidences thus it is uneconomical solution, Logical graph of evidence visualizations is not up to the mark.

6. Repudiation by CSC: A cloud consumer may assert that the said consumers' log information is not his own and can pin the ownership on some other user considering the fusion of cloud data.

B. Security Properties

1. Admissibility (A): Prospective pieces of proof have to be safeguarded, for viable enough to be admissible in the law court for criminal examinations.

2. Correctness (C1): A Correctness possession upholds the eminence of restricted to faults, errors & conformism towards the acceptance of the proof for criminal inquiries.

3. Tamper Resistance (TR): TR is the property of security which quantifies the confrontation to interfering of cloud consumers' log files or whichever reliable proofs on cloud computing.

4. Confidentiality (C2): This property is a state of being kept secret of the cloud consumers' logs to authorized entities only, while others cannot ensure secured access.

5. Verifiability (V): Every single secured proof of activity must be verifiable while considering virtuous precision and performance.

TABLE II. NOTATIONS

Notation	***Meaning***	***Notation***	***Meaning***
CSP	Cloud Service Provider	H(M)	Hash Function
CSC	Cloud Service Consumer	E	Events
CFI	Cloud Forensics Investigator	O	Objects
PK_{CSP}	Public Key of CSP	L	Activity LogInfo
SK_{CSP}	Private Key of CSP	R	Event Request
PK_{CSC}	Public Key of CSC	D = {accept, reject}	Decision
SK_{CSC}	Private Key of CSC	$M = R^I$	Request Queue
PK_{CFI}	Public Key of CFI	$N = D^I$	Decision Queue
SK_{CFI}	Private Key of CFI		

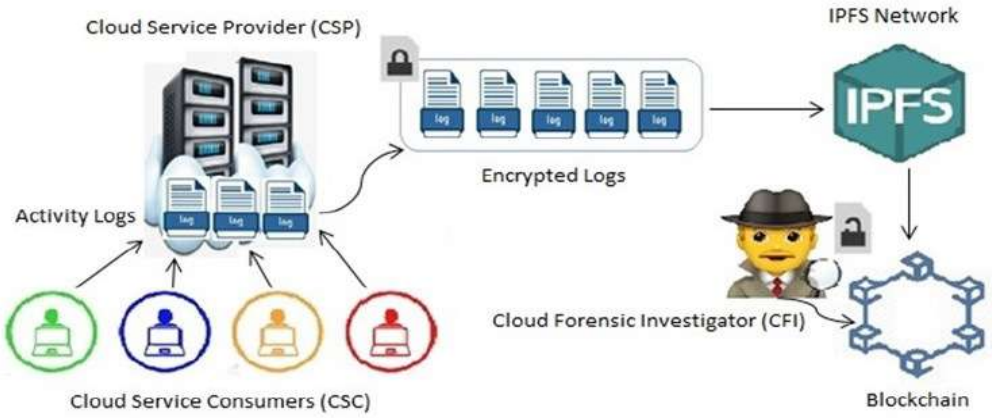

Figure 4. Proposed Blockchain Driven Secure and Efficient Cloud Logging

5. PROPOESED TECHNIQUE

Cloud service consumers (CSCs) make use of the cloud daily, for the consumer as well as business activities. For every single action happening in the cloud computing environment, we capture produced action occurrence into the log file. Afterward, we collect these logs, encrypt them and accumulate them on the IPFS network to reduce the storing load of the blockchain. Finally, the highest hash will get stored on to the blockchain network which is essentially publicly verifiable as shown in Figure 4. The flow of the scheme is shown in Figure 5. We assume that, CSP is honest for collecting the logs, publishing the proof of past logs, but during an investigation they can collude with other parties as discussed in hypothesis. We also assume that, in the Service Level Agreements (SLA), CSP is agreed that he will be responsible for logging all the events.

A. System Model

Definitions, Notations, and Assumptions: We take for granted the nature of the entire cloud stakeholders is untrusted. PK_{CSP}, $SK_{CSP,}$ $PK_{CSC,}$ $SK_{CSC,}$ $PK_{CFI,}$ and SK_{CFI} *are* public and private keys of CSP, CSC, and CFI respectively. H (D): This generates the hash for a given data. $Encypt_{PK}$ (D): This is the encipherment of data D using the public key PK. $Sign_{SK}$ (D): This signifies the signature over data D using the private key SK. D1 || D2: shows the consistency between two data/ messages/proofs.

B. Proof Creation

Cloud service consumers $CSC = \{CSC_1, CSC_2, CSC_3 \dots CSC_n\}$ send an event $E = \{e_1, e_2, e_3 \dots e_n\}$ for requesting R *(*which will be initially resides in the queue, $M \rightarrow R^I$*)* to data objects $O = \{o_1, o_2, o_3 \dots o_n\}$ in cloud to perform various actions for which system captures the activity logs $L = \{l_1, l_2, l_3 \dots l_n\}$.

a) Log File Creation

The scheme catches every incident that happened in this environment into the log file LF, $E_i \rightarrow L_i$ in which i is starting from 1 for the very first action. The scheme will be incrementally captured the events and creates a log file over the time T. Index i is assigned to each event E. Thus the scheme is maintaining the sequence of events $L.Seq\{L_i, L_{i+1}, L_{i+2}, \dots L_{i+n}\} \rightarrow PS$; in which PS is the proof of sequence where $i \leq i+1$.

b) Partial Proof Generation

In the second step of proof creation, the scheme is storing m number of events in one file. This will create a partial proof of events in the system. Partial Proof Generation is represented as $LF.insert \{E_1, E_2, E_3 \dots E_m\} \rightarrow PP1$; where PP1 is the partial proof of events E_1 to E_m and so on for remaining events.

c) Partial Proof Encryption

In the third step, considering data privacy concerns of cloud customers, the scheme encrypts the partial proofs using CSCs' public key, $Encrypt_{CSC}(PP1) \rightarrow EP1$ where EP is the Encrypted Proof which is signed and as per its sequence number i. Thus only CSC will be able to decrypt the logs which will preserve their privacy. The creation of EP1 and other partial proofs accumulatively will give P_n. it will get added into the IPFS network. Therefore, EP1 || EP2, EP2 || EP3 and the rest similar for all the proofs.

d) Add Encrypted Proofs on IPFS Network

In the end, all the proofs from $P_1 \dots P_i, P_{i+1}, P_{i+2} \dots P_n$ which are reliable and scrambled are pushed on an interplanetary file system network. For insertion of a piece of proof, interplanetary file system returns a hash which CSCs' may use for auxiliary checking in future. Command to add proof on IPFS is *$ ipfs add P.log*. At the end of the day, for one IP, the scheme uploads the final hash or root hash of all the proofs onto the blockchain. Algorithm-2 shows

that how the system starts the IPFS daemons and when it is ready system uploads the log files into the IPFS. IPFS return the content hash of the file. With the help of geth console; after completion of mining process content hash get offloaded on blockchain which results the transaction hash.

Algorithm-2: Storing log hash in ethereum blockchain

```
Input: log-hash from IPFS
Output: Transaction hash
Begin
  Start all Daemons D in the IPFS nodes M
  if D == Ready then
  Upload the file in one of the IPFS nodes
  M (1)
  Get the log-hash from IPFS node M (1)
  end if
  Start geth console in one of the Ethereum
  nodes N (1)
  if account == locked then
    Unlock the private account
  end if
  Start the mining process
  while mining == True do
      Make a transaction to store the log-hash
      Wait for the block to get mined
      Get transaction hash
  end while
End
```

C. *Eclectic Proof Verification*

The second half of our scheme offers an eclectic verification of the integrity of the potential items as well as trustworthy proofs. In our work, every block consists of four things. 1. TS is the block creation timestamps; 2. PH stand for the previous hash is a hash address that locates the preceding block. 3. L_Root is the topmost hash that comes from the hash of all the transactions of the logs in a block. 4. Nonce is the number to the block which is an arbitrary number and only uses once. It also maintains the difficulty level restrictions.

In our proposed work, the scheme is built to provide two-step integrity verification. It comprises engagement of Interplanetary File System and blockchain. IPFS has the feature of versioning the data. The first phase of the scheme stocks the encrypted log files into the IPFS as shown in Algorithm-2. If some adversary tries to tamper it generates the different modified copy by keeping the actual log file unaltered. Therefore, the scheme can definitely trail the hashes of altered and unaltered files. In the same situation, the logs are encrypted with CSCs public key so only authorized CSC can decrypt that log with forensic investigators at the time of the investigation. Thus, the privacy of the cloud consumers gets preserved. As shown in Figure 6, in the subsequent period the scheme is pushing the topmost combined log hash L_Root to the blockchain. Even minuscule alterations in the log data will consequence the completely dissimilar hash. Therefore, eventually succeeding hash data of the hierarchy become altered. In this phase, the cloud forensic investigator is authorized to do the verification in the cloud. When CSC wants to verify the integrity of their activity logs, they send a request to CFI. After receiving the request CFI asks CSP to give the logs of the period in which malicious activity happened.

When any malicious activity happens cloud forensic investigator randomly take few logs L = $\{l_1,\ldots, l_k\}$ for k logs, where $1 \leq l_i \leq n$. First, Cloud Forensic Investigator takes MHT root from IPFS and blockchain. CSP generates the new hash for asked logs. Here, the eclectic verification process starts which is the novelty of our scheme. After getting the root value from CSP, CFI matches that root value with blockchain root. If that matches all logs stored in the cloud system are not tampered otherwise logs get tampered with. And therefore forensic investigators can release decision D in terms of either positive or negative. Decision D will depict the reliability of proofs. We signify the queue of results by N -> D^I. Hence, CFI can smoothly confirm the truthfulness of log files & other pieces of evidence. We demonstrate the safety of the proposed scheme with below-mentioned security properties. Algorithm-3 describes that how we system is retrieving L-Root log-hash from blockchain and Algorithm-4 shows the log validation function so as to get accurate transactions.

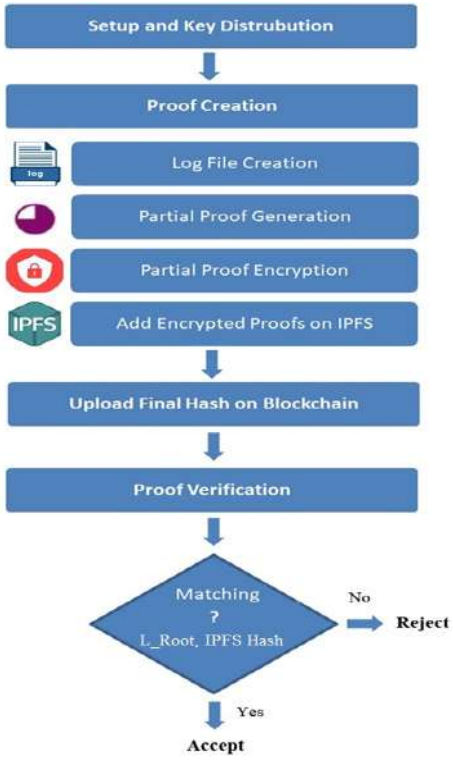

Figure 5. Flowchart for working of a BlockSLaaS

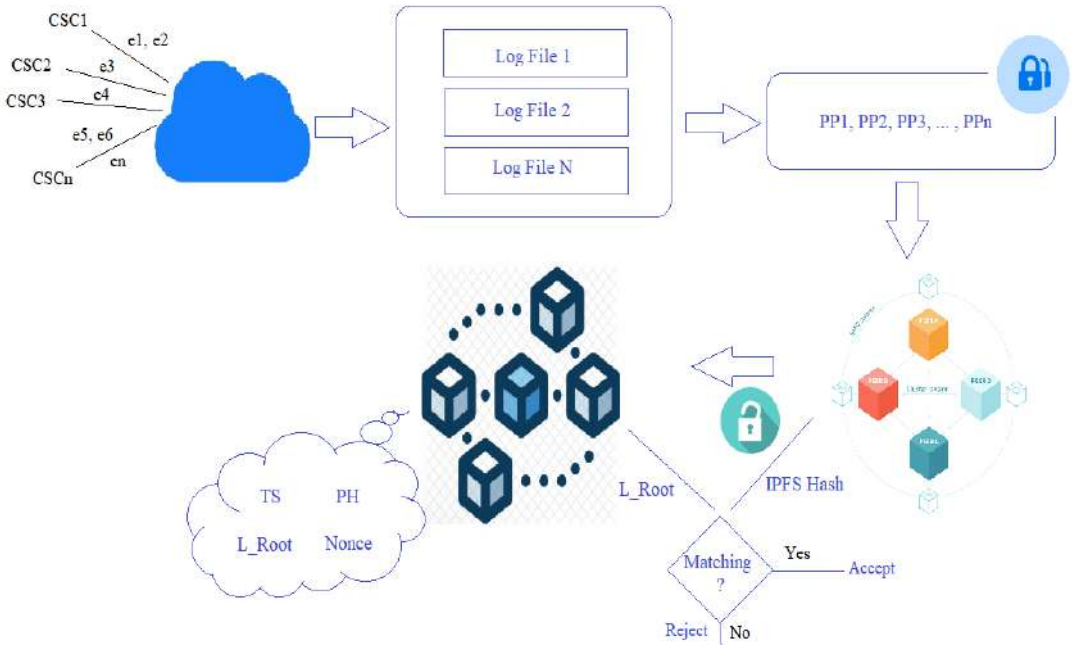

Figure 6. Secure Logging and Eclectic Proof Verification

Algorithm-3: Retrieving log-hash from blockchain

Input: Contract address, Blockchain nodes N
Output: log-hash stored in blockchain
Begin
Start geth console in one of the Ethereum nodes N (1)
if account == locked **then**
Unlock the private account
end if
Start the mining process
while mining == True **do**
if N (1) requires log-hash **then**
Make a transaction to retrieve log-hash by submitting the contract address
else
Send bin, abi and the contract address to other peers
Call the function which retrieves the log-hash
end if
Wait for the block to get mined
Return log-hash
end while
End

Algorithm-4: Validating log-hash stored in blockchain

Input: Transaction hash Tx, IPFS log-hash i
Output: Validation Result
Begin
Start geth console
Start mining process
if mining == True **then**
receipt ← Retrieves the transaction receipt of Tx from blockchain
endif
h ← receipt [input]
if i == h
return true
else
return false
end if
End

6. SECURITY ANALYSIS

In this paper, as shown in Figure 1. Multi-stakeholder collusion model, there are basically three entities are involved: Cloud Service Provider, Cloud Service Consumer, and Cloud Forensics Investigator. All above mentioned entities can do malicious activities individually or can collude with each other for their personal benefits as mentioned in hypothesis. As a host cloud service providers have complete control over the logs stored in interplanetary File System. Thus, CSP can be able to add / modify / delete the activity logs. After obtaining logs from CSP, Cloud Forensic Investigator may be motivated to modify the log data beforehand providing in front of court. Thus, we presented the interference stopping scheme using block chain and IPFS. Violation of the any property by CSC, CFI and CSP, as mentioned in threat model, can be reveal in the verification process.

In this segment, we converse on how our novel scheme guarantees all the security properties and essential to defend against collusion between CSP, CSC & CFI. In Figure 11, we have shown the multiple-party collusion model, the variety of probable assaults which can take place over cloud & the necessity of security property. In this, we symbolize a truthful cloud service provider as P, a fraudulent cloud service provider as $\bar{P}$, a truthful cloud consumer as C, a fraudulent cloud user as $\bar{C}$, a truthful forensic investigator as I, and a fraudulent forensic investigator as $\bar{I}$.

(Correctness, Tamper Resistance, Confidentiality):
Security is always an important concern in a cloud-based system where sensitive data should maintain in an appropriate way to tackle different attacks and guarantee cloud service consumers' data integrity and confidentiality. Assume that a malicious insider or external entity can get into the IPFS data storage, such a malicious insider or entity struggles for getting the sensitive information using BlockSLaaS. Because, in our proposed scheme, all log file records $L = \{l_1, l_2, l_3 \dots l_n\}$ are hashed using a one-way hash function i.e. H ($l_1, l_2, l_3 \dots l_n$) where $l_i \in L$. One way hash functions are irreversible and thus, difficult to find the content of log file. Also, the log files are enciphered with the public key of CSC, PK_{CSC} for uploading to the IPFS. To get these trustworthy logs data, any attackers should know the secret key PK_{CSC} of a particular CSC for decryption operation. Thus, through BlockSLaaS, it's very hard for the malicious insider or outside invader to guess/find the private key PK_{CSC} to decrypt and obtain the sensitive logs data. Only authorized users with the keys can access the log files. It ensures confidentiality property.

In the Interplanetary File System, activity log files LF are get chunked and saved on various storage machines. Now, the log files are already encrypted using the RSA algorithm and stored in IPFS storage machines. Other machines of the system can only see a part of scrambled data, $Encrypt_{CSC}$ (PP1) -> EP1 and cannot obtain any useful insights from the log files. The root of these proof files $P_1 \dots P_i$, P_{i+1}, $P_{i+2} \dots P_n$ are stored on the blockchain network nodes. This is computationally impractical to alter the log information on blockchain. If adversary tries to tamper t block, hash value of t+1 block will automatically change and so on. Thus, our scheme ensures tamper resistance property. Authentic stakeholders of the cloud system can get access to complete log records and retrieve correct logs using our system which provides the access control mechanism by preserving integrity and confidentiality. After applying one way function H (L) to logs; log contents will be irreversible. As shown in Figure 6, adversary cannot tamper the logs; and checks for the proof hash available with blockchain. Forensic Investigator will get correct logs through our system and thus ensures correctness property.

(Verifiability, Admissibility):
In our proposed scheme, Cloud Service Provider constructs the Merkle Hash Tree (MHT) with the hash of different leaf and intermediate nodes using IPFS log files and finally creates the root node say L_Root and stores it into the blockchain network. If any adversary tries to alter the IPFS logs, it generates a new copy of that log file, say IPFS_Root. It happens due to the versioning nature of IPFS. Still, if someone tampers the logs data MHT hash values will get change, and subsequently, the root of MHT will get changed. So, the root of the IPFS logs file and associated blockchain root will either match or not. If L_Root = IPFS_Root then content is not changed otherwise got tampered. Using this principle system can easily verify that the IPFS logs are authentic or not. Thus, the scheme ensures verifiability property as shown in Algorithm-4. Each and every secure evidence is verifiable while considering good accuracy and performance. Potential items of evidence i.e. logging proofs $P_1 \dots P_i$, P_{i+1}, $P_{i+2} \dots P_n$ are got secured using our blockchain-driven secure logging scheme in such a way that they are viable enough to be acceptable for law enforcement. Thus, it guarantees the admissibility property. With these security properties, the significance of security properties can be seen as stated in the threat model. The BlockSLaaS scheme empowers the security belongings by conserving & confirming integrity, the confidentiality of responsible indications and marks in the cloud system, hence making the cloud more secure & forensic friendly.

7. IMPLEMENTATION AND RESULTS

For the implementation purpose, we used the open-source OpenStack software to form a cloud with I9 Machine, 32GB Random Access Memory, 2TB Hard Disk, Linux 18 versioned OS, and Oracle VirtualBox 6.1.18. RSA public-key cryptography algorithm and Secure Hash Algorithm of 256 bits, a hash function has used for encipherment and hash creation correspondingly.

Figure 7 depicts the integrity and signature proof verification of logs through the proposed BlockSLaaS scheme. The overall time required for these operations is also calculated and shown in the same figure. The time taken to complete both the verification processes are also shown. X and Y-axis display the number of actions in a chiliad and the time required to finish the proof verification in seconds respectively. Our results indicate that the projected novel method is efficient. So, this BlockSLaaS setup on OpenStack open-source cloud computing platform and its results reflect the feasibility for giving safety to reliable pieces of evidence and marks in the cloud.

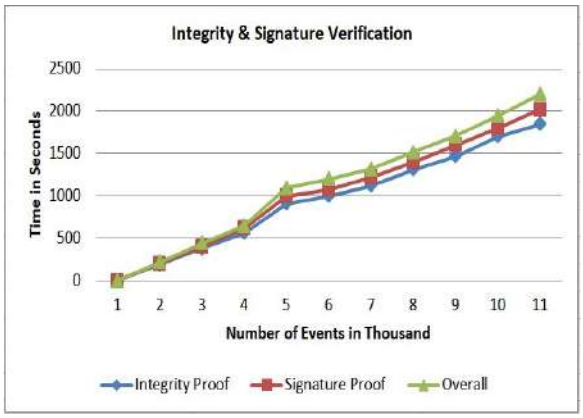

Figure 7. Integrity and Signature Proof Verification

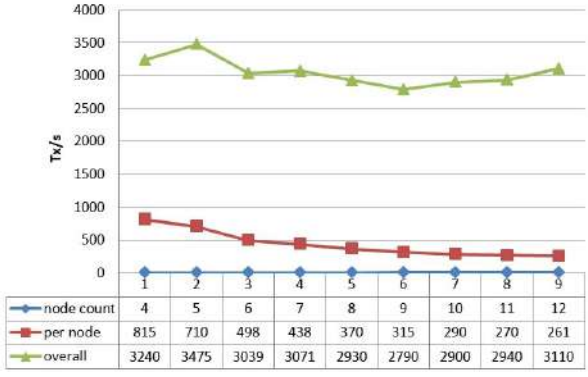

	1	2	3	4	5	6	7	8	9
node count	4	5	6	7	8	9	10	11	12
per node	815	710	498	438	370	315	290	270	261
overall	3240	3475	3039	3071	2930	2790	2900	2940	3110

Figure 8. Transaction per second for varying node count

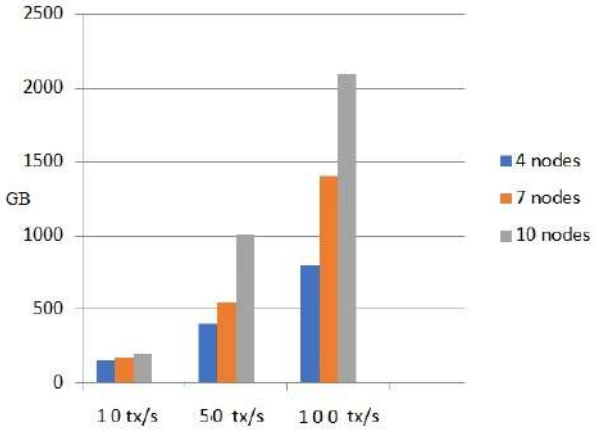

Figure 9. Storage requirements for varying average throughput and node count

In this implementation ethereum testnet blockchain was used to serve the purpose. Figure 8 shows the transactions per second completed for varying node count. It is showing that the system is performing fewer transactions per second after increasing few nodes and then it is stable. Overall transaction per second reflects the same analysis but transaction per second increases slightly at the end. Figure 9 shows the storage requirement for varying average throughput from 10tx/s to 100tx/s and node count from 4 to 7. Integration of IPFS is with blockchain greatly reducing the storage burden of blockchain and thus its efficient and cost-effective scheme. The above implementation results and security analysis proves that our system is efficient & secure.

Sample setter function statistics
Without IPFS
Gas used 12355552
Transaction cost 12355552 gas
Data size = 37kb
Mining time = 59 sec

With IPFS
Gas used 75896
Transaction cost 75896
Data size = 37kb
Mining time = 11 sec

We measured the time required to send the log data to IPFS and then on Ethereum. We also calculated the transaction validation time and the total time required for the whole execution process. The analysis has been done for 20 times; 4 times each for the following number of files.

TABLE III. EXECUTION TIME OF PROOF CREATION AND VERIFICATION IN SECONDS FOR VARYING NO. OF LOG FILES

No. of Log Files	IPFS	Etherium Sent	Etherium Confirmed	Total
5	2.85	1.284	32.125	36.259
10	1.323	1.191	49.411	51.925
15	3.774	1.273	25.992	31.039
20	2.124	1.194	27.004	30.322
30	1.395	1.282	30.939	33.616

Above mentioned result is an average execution time in seconds. The TABLE III. depicts the etherium confirmation time is high in the validation process by varying number of log files.

We did some experiments to check the performance of the BlockSLaaS scheme by uploading, reading and downloading the file by varying the node count. The results are shown in Figure 10, 13 and 14. The log files were uploaded using one machine and accessed by another two machines. At each step we increased the number of nodes in the BlockSLaaS as shown in figure. We observed that if the number of increases the transaction time slightly increases. This signifies that the extra overhead does not degrade the overall performance of the system. Thus, our system nature is scalable. The logging process generates a tremendous amount of logs on daily basis. Inspecting these logs for forensic purposes is a hectic process. To overcome this problem we have developed a consumer activity log visualization mechanism on top of IPFS using BlockLaaS. Figure 12. shows a sample visualization of few events that happened in our system. These events can be retrieved easily through the content hash of a log file. This will be a great help for forensic investigators in identifying the suspects early stages.

We did a comparison with the well know techniques CFLOG [51] and DFeSB [53] in terms of complete response time, proof insertion time and proof verification time as shown in TABLE IV. For inserting the evidence CFLOG and DFeSB taken 88.5 ms and 63 ms time respectively considering 100 users on the system. BlockSLaaS get the response from the system in 38.3 ms only which is very less time as compare to other two. Evidence insertion time for CFLOG and DFeSB was 71 ms and 43.5 ms respectively. BlockSLaaS requires only 29.7 ms as it is based on off-chain data storage.

TABLE IV. PERFORMANCE COMPARISON WITH EXISTING TECHNIQUES

Performance Metric (ms)	CFLOG	DFeSB	BlockSLaaS
Response Time	88.5	63	**38.3**
Proof Insertion Time	71	43.5	**29.7**
Proof Verification Time	70	42.8	**26.3**

Verification time in BlockSLaaS is 26.3 which is also very less as compare to CFLOG and DFeSB for 10 users. The major impacts on results were due to integration of IPFS. Thus, our system performs better in all the aspects. Our scheme reduced block chain storage burden up to large extent. Thus, our proposed system is more efficient than existing systems. performance Comparison with existing techniques.

TABLE V. COMPARISON WITH EXISTING TECHNIQUES BASED ON SECURITY AND PERFORMANCE FEATURES

Ref.	Year	VL	I	C	A	P	O	D	V	S
[19]	2018	×	✓	✓	×	×	×	×	✓	×
[46]	2018	×	✓	✓	×	×	×	✓	✓	×
[48]	2018	×	✓	×	×	✓	×	✓	✓	×
[53]	2018	✓	✓	✓	✓	✓	×	✓	✓	✓
[50]	2019	×	✓	×	×	×	✓	✓	✓	✓
[44]	2020	×	✓	✓	✓	✓	×	✓	✓	×
[47]	2020	×	✓	×	✓	×	×	×	✓	×
[49]	2020	×	✓	✓	✓	×	×	✓	✓	×
[51]	2020	×	✓	✓	✓	✓	×	✓	✓	×
Our	2021	✓	✓	✓	✓	✓	✓	✓	✓	✓

VL- Visualization I - Integrity, C - Confidentiality, A - Availability, P - Privacy, O - Off-Chain Storage, D - Decentralized, V - Verifiability, S - Scalability

In this section, we have shown TABLE V. comparative analysis of most recent and relevant approaches used for secure logging. Most of the above-mentioned schemes are not scalable as they are centralized. Very few authors used off-chain data storage with blockchain. The proposed model addressed the limitations of existing work. We are the first to develop and point out the usefulness of log activity visualization for calm forensic analysis. Our scheme facilitates the secure, efficient, provable model for cloud forensics. The above analysis shows that our scheme is performing better as compared to existing techniques and methods.

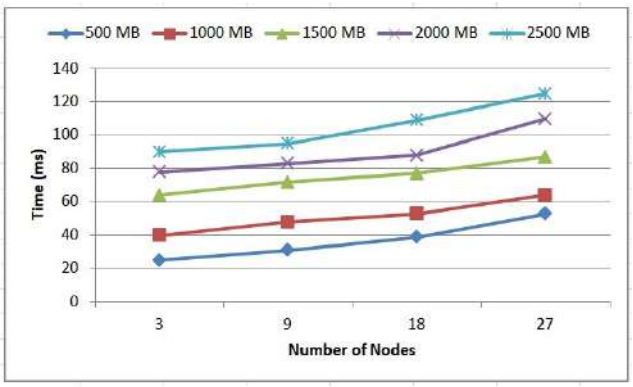

Figure 10. Time required uploading the file

Is Honest?			Notation	Possible Attacks	Required Security Properties
CSP	CSC	CFI			
Y	Y	Y	P C I	Attack free	None
N	Y	Y	$\overline{P}$ C I	Consumers activity disclosure from logs	C2
Y	N	Y	P $\overline{C}$ I	Other consumers' log recovery from proofs	C2
Y	Y	N	P C $\overline{I}$	Add, modify, delete logs	C1, TR, V, A
Y	N	N	P $\overline{C}$ $\overline{I}$	Add, update, delete logs, other consumers' log recovery	C1, C2, TR, V, A
N	Y	N	$\overline{P}$ C $\overline{I}$	Add, modify, delete logs, repudiate proofs, and disclose consumer activity	C1, C2, TR, V, A
N	N	Y	$\overline{P}$ $\overline{C}$ I	Add, modify, delete logs, repudiate proofs, other consumers' log recovery and consumers' activity disclosure	C1, C2, TR, V, A
N	N	N	$\overline{P}$ $\overline{C}$ $\overline{I}$	Add, modify, delete logs, repudiate proofs, other consumers' log recovery and consumers' activity disclosure	C1, C2, TR, V, A

Figure 11. A Cloud Stakeholders Collusion, Possible Attacks and Required Security Properties

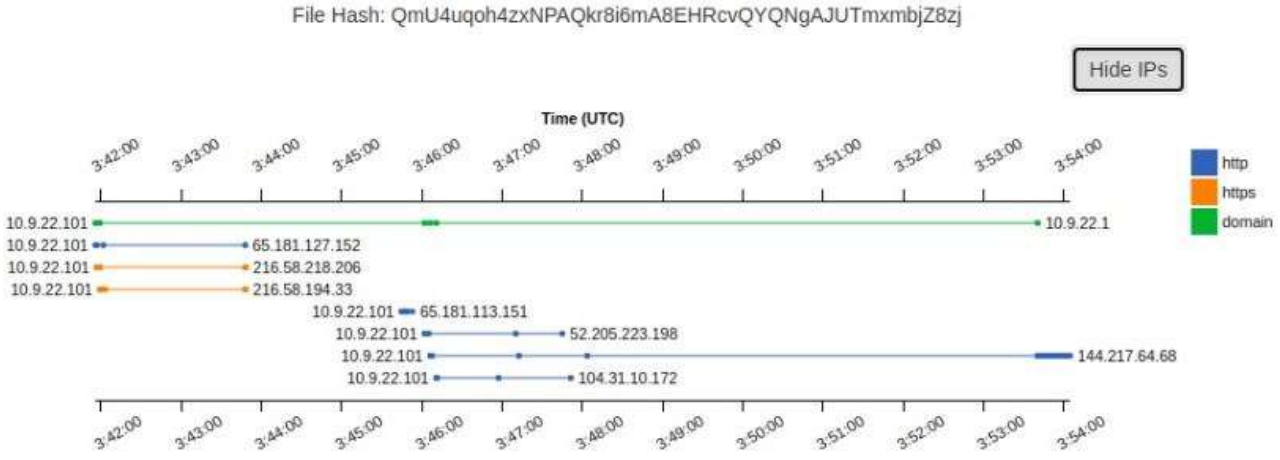

Figure 12. Forensic Data Visualization on top of IPFS in BlockSLaaS

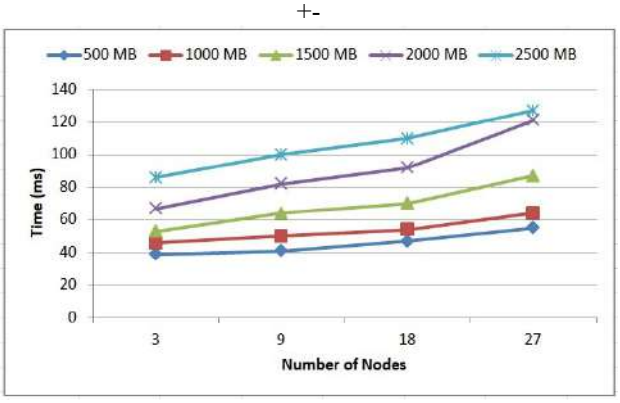

Figure 13. Time required reading the file

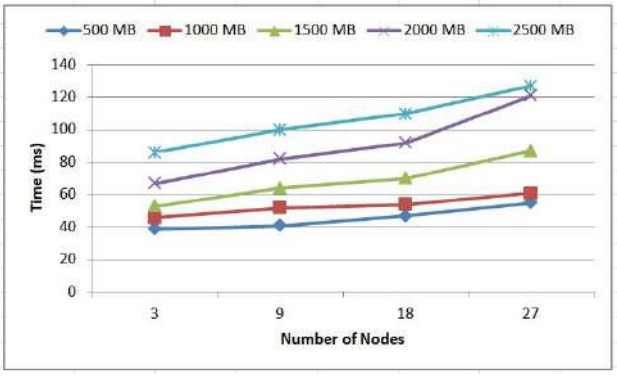

Figure 14. Time required downloading the file

8. Conclusion and Future Work

In this paper, we introduced BlockSLaaS, a blockchain-driven efficient and tamper-proof distributed log storage model while preserving the confidentiality of cloud consumers' logs. Unlike other centralized techniques, the proposed method integrated the IPFS with a fully decentralized blockchain that takes control from a single authority and provides a fair service. The IPFS along with smart contracts preserves an immutable record of cloud consumers' activities on the blockchain. With this scheme only authorized stakeholders can check the historical records stored in the blockchain. The proposed scheme is resilient as no malicious stakeholder of the cloud system can alter cloud consumers' logs despite the collusion of multiple parties.

Our analysis of the number of transactions per second, storage requirements, uploading, reading, and downloading of log files for varying node count and file size validates the viability of the proposed scheme. This work compared the proposed method with nine existing systems based on 9 security and performance features. The BlockSLaaS response, proof insertion, and proof verification times are 38.3, 29.7, and 26.3 milliseconds respectively which beat existing CFLOG and DFeSB methods. Our method adds security which enables a transparent system to obey the audit requirements. The visualization mechanism on top of IPFS gives better readability to the log evidence while doing forensic investigations. A comprehensive performance evaluation shows that our scheme is scalable, efficient, and assures high performance than existing schemes.

As future work, the evidence visualization techniques can be strengthened by implementing a better user interface and mapping logical shreds of evidence. Machine learning algorithms can be explored for the same. Attribute and role-based encryption techniques can be applied for better access control management over forensic data. The current scheme is completely based on IPFS so the drawbacks of IPFS need to be taken care of and other off-chain data storage models can be explored.

References

[1] P.Melland, T.Grance, "Nist Cloud Computing Forensic Science Challenges," NIST Cloud Computing Forensic Science Working Group, Information Technology Laboratory, Draft NISTIR 8006, June 2014.

[2] Kolhar, M., Abu-Alhaj, M. M., & El-atty, S. M. A. (2017). Cloud data auditing techniques with a focus on privacy and security. IEEE Security and Privacy, 15(1), 42–51.

[3] Nasscom, "India's cloud market to cross 7 billion dollar by 2022", https://economictimes.indiatimes.com/tech/internet/indias-cloud-market-to-cross-7-billion-by-2022-nasscom/articleshow/68689359.cms. [Accessed May 08, 2020].

[4] MRM, "Market Research Media, Global Cloud Computing Market Forecast 2019-2024", https://marketresearchmedia.com/global-cloud-computing-market/ [Accessed May 08, 2020].

[5] P. J. Sun, "Privacy Protection and Data Security in Cloud Computing: A Survey, Challenges, and Solutions," in IEEE Access, vol. 7, pp. 147420-147452, 2019, doi: 10.1109/ACCESS.2019.2946185.

[6] D. Birk and C. Wegener, "Technical issues of forensic investigations in cloud computing environments," in SADFE. IEEE, 2011, pp. 1-10

[7] M. Balduzzi, J. Zaddach, D. Balzarotti, E. Kirda, and S. Loureiro, "A security analysis of amazon's elastic compute cloud service," in Symposium on Applied Computing. ACM, 2012, pp. 1427-1434.

[8] S. Subashini and V. Kavitha, "A survey on security issues in service delivery models of cloud computing," Journal of Network and Computer Applications, vol. 34, no. 1, pp. 1\textendash11, 2011.

[9] D. Zissis and D. Lekkas, "Addressing cloud computing security issues," Future Generation Computer Systems, vol. 28, no. 3, pp. 583\textendash592, 2012.

[10] Tang, J., Cui, Y., Li, Q., Ren, K., Liu, J., & Buyya, R. (2016). Ensuring security and privacy preservation for cloud data services. ACM Computing Surveys, 49(1), 1–39.

[11] Tari, Z. (2014). Security and privacy in cloud computing. IEEE Cloud Computing, 1(1), 54–57.

[12] S. Zawoad, A. Dutta, and R. Hasan, Towards Building Forensics Enabled Cloud through Secure Logging-as-a-Service, IEEE Transactions on Dependable and Secure Computing, preprint, \DOI:10.1109/TDSC.2015.2482484. 13(2):148-162 (2016)

[13] K. Kent and M. Souppaya, "Guide to computer security log management," Tech. Rep. 800-92, NIST Special Publication, 2006.

[14] J. Dykstra, A Sherman, Understanding Issues in Cloud Forensics: Two Hypothetical Case Studies Cyber Defense Lab, Department of CSEE, University of Maryland, Baltimore County (UMBC).

[15] Varghese, B., & Buyya, R. (2018). Next generation cloud computing: New trends and research directions. Future Generation Computer Systems, 79, 849–861.

[16] S. Zawoad and R. Hasan, Cloud Forensics: A Meta-Study of Challenges, Approaches, and Open Problems arXiv: 1302.6312v1 [cs.DC] 26 Feb (2013)

[17] J. Dykstra and A. Sherman, Acquiring forensic evidence from infrastructure-as-aservice cloud computing: Exploring and evaluating tools, trust, and techniques, Journal of Digital Investigation 9 S90-S98, DOI: 10.1016/j.diin.2012.05.001 (2012).

[18] Wang, B., Li, B., & Li, H. (2015). Panda: public auditing for shared data with efficient user revocation in the cloud. IEEE Transactions on Services Computing, 8(1), 92–106.

[19] M. A. M. Ahsan et al., "CLASS: Cloud Log Assuring Soundness and Secrecy Scheme for Cloud Forensics," in IEEE Transactions on Sustainable Computing, doi: 10.1109/TSUSC.2018.2833502.

[20] Wang, Q., Wang, C., Ren, K., Lou, W., & Li, J. (2011). Enabling public auditability and data dynamics for storage security in cloud computing. IEEE Transactions on Parallel and Distributed Systems, 22(5), 847–859.

[21] Zhu, Y., Ahn, G. J., Hu, H., Yau, S. S., An, H. G., & Hu, C. J.(2013). Dynamic audit services for outsourced storages in clouds. IEEE Transactions on Services Computing, 6(2), 27–238.

[22] Jiang, T., Chen, X., & Ma, J. (2016). Public integrity auditing for shared dynamic cloud data with group user revocation. IEEE Transactions on Computers, 65(8), 2363–2373.

[23] Tian, H., Nan, F., Jiang, H., Chang, C. C., Ning, J., and Huang, Y. (2019). Public auditing for shared cloud data with efficient and secure group management. Information Sciences, 472, 107–125.

[24] Hao, Z., Zhong, S., & Yu, N. (2011). A privacy-preserving remote data integrity checking protocol with data dynamics and public verifiability. IEEE Transactions on Knowledge and Data Engineering, 23(9), 1432–1437.

[25] Wang, C., Chow, S. S. M., Wang, Q., Ren, K., & Lou, W. (2013). Privacy-preserving public auditing for secure cloud storage. IEEE Transactions on Computers, 62(2), 362–375.

[26] Rane S., Dixit A. (2019) BlockSLaaS: Blockchain Assisted Secure Logging-as-a-Service for Cloud Forensics. In: Nandi S., Jinwala D., Singh V., Laxmi V., Gaur M., Faruki P. (eds) Security and Privacy. ISEA-ISAP 2019. Communications in Computer and Information Science, vol 939. Springer, Singapore.

[27] Sagar Rane, Sanjeev Wagh and Arati Dixit (2020) Design of Forensic Enabled Secure Logging, in Proceedings of the 21st International Conference on Distributed Computing and Networking, Article No.: 61, Pages 1, DOI: https://doi.org/10.1145/3369740.3373803

[28] Keyun Ruan, Jeo Carthy, Tahar Kechadi, Mark Crosbie ,Cloud Forensics Chapter 2, Advances in Digital Forensics.

[29] S. Thorpe and I. Ray, "Detecting temporal inconsistency in virtual machine activity timelines." Journal of Information Assurance and Security, vol. 7, no. 1, pp. 24-31, 2012.

[30] S. Thorpe, I. Ray, T. Grandison, A. Barbir, and R. France. 2013b. Hypervisor event logs as a source of consistent virtual machine evidence for forensic cloud investigations. In Data and Applications Security and Privacy XXVII. Springer Berlin Heidelberg. 97-112.

[31] S Khan, A Gani, and A Wahab et al., Cloud Log Forensics: Foundations, State of the Art, and Future Directions ACM Computing Surveys, Vol. 49, No. 1, Article 7, \DOI:http://dx.doi.org/10.1145/2906149 (2016).

[32] Satoshi Nakamoto, Bitcoin: A peer-to-peer electronic cash system. Consulted, 1:2012, 2008.

[33] Juan Benet, "IPFS - Content Addressed, Versioned, P2P File System draft 3, arXiv:1407.3561v1, July (2014)"

[34] R. Marty, Cloud application logging for forensics, Proc. of the 2011 ACM Symposium on Applied Computing (SAC11), Taichung, Taiwan. ACM, March 2011, pp. 178-184.

[35] Z. Zafarullah, F. Anwar, and Z. Anwar, "Digital forensics for eucalyptus," in FIT. IEEE, 2011, pp. 110-116.

[36] A. Patrascu and V.-V. Patriciu, "Logging system for cloud computing forensic environments," Journal of Control Engineering and Applied Informatics, vol. 16, no. 1, pp. 80\textendash88, 2014.

[37] Dıaz, M., Martı´n, C., & Rubio, B. (2016). State-of-the-art, challenges, and open issues in the integration of Internet of things and cloud computing. Journal of Network and Computer Applications, 67, 99–117.

[38] I. Ray, K. Belyaev, M. Strizhov, D. Mulamba, and M. Rajaram, Secure logging as a service delegating log management to the cloud, IEEE Syst. J., vol.7,no. 2,pp.323-334, Jun. (2013)

[39] A. Khajeh-Hosseini, D. Greenwood, and I. Sommerville, Cloud migration: A case study of migrating an enterprise it system to iaas, in proceedings of the 3rd International Conference on Cloud Computing (CLOUD) IEEE, 2010,pp. 450-457.

[40] George Grispos, W Glisson, Tim Storer, Calm before the Storm: The Emerging Challenges of Cloud Commuting in Digital Forensics University of Glasgow.

[41] S. Thorpe and I. Ray, "Detecting temporal inconsistency in virtual machine activity timelines." Journal of Information Assurance and Security, vol. 7, no. 1, pp. 24\textendash31, 2012.

[42] Cucurull J., Puiggalí J. (2016) Distributed Immutabilization of Secure Logs. In: Barthe G., Markatos E., Samarati P. (eds) Security and Trust Management. STM 2016. Lecture Notes in Computer Science, vol 9871. Springer, Cham. https://doi.org/10.1007/978-3-319-46598-2_9

[43] Sutton A., Samavi R. (2017) Blockchain Enabled Privacy Audit Logs. In: d'Amato C. et al. (eds) The Semantic Web – ISWC 2017. ISWC 2017. Lecture Notes in Computer Science, vol 10587. Springer, Cham. https://doi.org/10.1007/978-3-319-68288-4_38

[44] Ahmad, Ashar & Saad, Muhammad & Bassiouni, Mostafa & Mohaisen, David. (2018). Towards Blockchain-Driven, Secure and Transparent Audit Logs. MobiQuitous '18: Proceedings of the 15th EAI International Conference on Mobile and Ubiquitous Systems: Computing, Networking and Services. 443-448. 10.1145/3286978.3286985.

[45] Shekhtman, Louis & Waisbard, Erez. (2018). Securing Log Files through Blockchain Technology. 131-131. 10.1145/3211890.3211921.

[46] Ameer Pichan, Mihai Lazarescu, Sie Teng Soh, Towards a practical cloud forensics logging framework, Journal of Information Security and Applications, Volume 42, 2018, Pages 18-28.

[47] I. Zikratov, A. Kuzmin, V. Akimenko, V. Niculichev and L. Yalansky, "Ensuring data integrity using blockchain technology," 2017 20th Conference of Open Innovations Association (FRUCT), 2017, pp. 534-539, doi: 10.23919/FRUCT.2017.8071359.

[48] J. Ricci, I. Baggili and F. Breitinger, "Blockchain-Based Distributed Cloud Storage Digital Forensics: Where's the Beef?," in IEEE Security & Privacy, vol. 17, no. 1, pp. 34-42, Jan.-Feb. 2019, doi: 10.1109/MSEC.2018.2875877.

[49] Rosa, M., Barraca, J.P. & Rocha, N.P. Blockchain structures to guarantee logging integrity of a digital platform to support community-dwelling older adults. *Cluster Comput* **23,** 1887–1898 (2020). https://doi.org/10.1007/s10586-020-03084-4.

[50] Kirrane, Sabrina & Fernández, Javier & Bonatti, Piero & Milošević, Uroš & Polleres, Axel & Wenning, Rigo. (2020). The SPECIAL-K Personal Data Processing Transparency and Compliance Platform.

[51] M. H. Rakib, S. Hossain, M. Jahan and U. Kabir, "Towards Blockchain-Driven Network Log Management System," 2020 IEEE 8th International Conference on Smart City and Informatization (iSCI), 2020, pp. 73-80, doi: 10.1109/iSCI50694.2020.00019.

[52] M. Pourvahab and G. Ekbatanifard, "Digital Forensics Architecture for Evidence Collection and Provenance Preservation in IaaS Cloud Environment Using SDN and Blockchain Technology," in IEEE Access, vol. 7, pp. 153349-153364, 2019, doi: 10.1109/ACCESS.2019.2946978.

[53] A. Patil, A. Jha, M. M. Mulla, D. G. Narayan and S. Kengond, "Data Provenance Assurance for Cloud Storage Using Blockchain," 2020 International Conference on Advances in Computing, Communication & Materials (ICACCM), 2020, pp. 443-448, doi: 10.1109/ICACCM50413.2020.9213032.

APPENDIX

Algorithm-1: Creation of a new block in blockchain

Input: BI, TS, data, PH
Output: CH, nonce

```
1. nonce = 0;
2. BD = concatenate (BI, TS, data, PH);
3. BD = H (BD);
4. Repeat
5.     nonce = nonce++;
6.     CH = H (concatenate (nonce, BD) );
7. until prefix of CH = DT;
8. return CH, nonce;
```

BI – block _index, TS – timestamp, PH – previous_hash, CH – current_hash, BD – block_data, H – Hasher, DT – difficulty_target

Sagar Rane received the B.E. and M.Tech. degrees in computer engineering from Savitribai Phule Pune University, India in 2013 and 2015 respectively. He is pursuing Ph.D. degree in computer and information technology at Savitribai Phule Pune University, India. He worked at Government Polytechnic Pune as a Lecturer in 2014. He was research intern at Center for Development of Advanced Computing (CDAC) headquarters, Pune, India in 2015. Since 2015 he is working as an Assistant Professor in Army Institute of Technology, Pune, India. His current research interest is in Information Security, Cloud Forensics, Blockchain and Web Development. He has published 20+ research papers in reputed journals and conferences. He has three books on his name. He has received various grants from national and international organizations for conducting research activities. He has delivered many sessions in information security and digital forensics domain. Mr. Sagar Rane was a recipient of Sahara Welfare Foundation Fellowship.

Sanjeev Wagh, working as Professor and Head in Department of Information Technology at Govt. College of Engineering, Karad. He has completed his BE(1996), ME(2000) and PhD(2009) in Computer Science & Engineering from Govt. College of Engineering, Pune & Nanded. He was full time Post Doctorate fellow at Center for Tele-Infrastructure, Aalborg University, Denmark during 2013-14. He has also completed MBA in IT from NIBM 2015, Chennai. Also, honored as D.Sc. Award (Honorary). He has total 25 years of experience in academics & research. His research interest areas are Network Security, Natural Science Computing, Internet technologies & Wireless Sensor networks, Data Sciences & Analytics. He has 100+ research papers to his credit, published in International/National Journals & conferences. He has visited various universities in different countries.

Arati Dixit received the B.E. and M.Tech. degrees in computer science and engineering from Pune University and IIT Bombay, India, in 1994 and 1999 respectively. She has completed the certificate in scientific computing program and Ph.D. degree in computer engineering at Wayne State University (WSU), Detroit, MI, USA in 2007 and 2010 respectively. Currently she is a Senior Scientist, Predictive Analytics and Modeling Group at Applied Research Associates Inc., Raleigh and a Teaching Associate Professor, Electrical and Computer Engineering Department, North Carolina State University. Until January 2018, she worked as a Professor at the Department of Computer Engineering, PVPIT, Pune, India. She has published more than 80 research papers in reputed refereed national/international conferences and journals. Her areas of interest are AI and Security Analytics, Cyber Security, Digital Forensics, Cyber Physical Systems and Education Technology. She is ACM Senior member, Chairperson of ACM-W(ACM Council on Women in Computing) India, supporting and advocating full engagement of women in computing. She has been active volunteer and founding Vice-Chairperson of ACM iSIGCSE(India SIGCSE) and Chairperson, ACM Pune Professional Chapter. She has been on ACM India Eminent Speaker Program (ESP) since June 2015, with more than 50 talks delivered. She has received many prestigious awards.

Army Institute Of Technology (AIT), Dighi Camp, Pune - 15.
Director : 7249250115, Joint Director : 7249250117, Principal : 7249250186
Exch : 7249250183, 7249250184, 7249250185
Website : www.aitpune.com Email : ait@aitpune.edu.in
Recognised by AICTE and DTE Maharashtra and affiliated to Savitrabai Phule Pune University

ONWARD TO GLORY

Dr. Ashok Kr Singh (ASGE)

- PhD Certificate
- Publication Copy

Savitribai Phule Pune University

(formerly University of Pune)

Declaration of Result of the Doctor of Philosophy (Ph.D.)

Ashok Kumar Singh (अशोक कुमार सिंह)

Mothers Name: Champa (चंपा)

University has accepted thesis submitted by the above-mentioned candidate for award of Ph. D., as per reports of referees and examiners of open defence of the thesis. Accordingly, it is hereby notified that, the above-mentioned candidate is declared to have passed the examination of Ph. D. and has become eligible for the award of Ph. D. Degree.

RELEVANT DETAILS ARE AS UNDER:

1.	Faculty	:	Science and Technology
2.	Subject	:	Mathematics
3.	Title of the Thesis	:	"Wavelets and the Uncertainty Principle."
4.	Place of Research	:	Department of Mathematics, Savitribai Phule Pune University Pune-411007.
5.	Name and Address of the Guide	:	Dr. Hemant Bhate, Department of Mathematics, Savitribai Phule Pune University Pune-411007.
6.	Date of Registration	:	22nd August, 2011
7.	Date of Re-Registration	:	22nd August, 2016
8.	Date of Declaration of Result	:	31st July, 2020

SAVITRIBAI PHULE PUNE UNIVERSITY Admission Section PUNE-7.

Ganeshkhind, Pune - 411007.
Ref. No. PGS/Ph.D./ 229
Date: 17 AUG 2020

16/8/2020
For Director
Board of Examinations and Evaluation

International Journal of Applied Engineering Research, ISSN 0973-4562 Volume 13, Number 11 (2018) pp. 9091-9102

Wavelets As Minimizers Of Uncertainty From The Kinematical Group

Ashok Kumar Singh[1] and Hemant Bhate
Department of Mathematics, University of Pune.

Abstract: In this paper we propose a method of obtaining a family of wavelets. The members of the family are tagged by the time parameter. We obtain these wavelets as minimizers of an uncertainty principle. The wavelets are directional in nature. As the family depends on the time parameter, each value of time parameter associates with it a wavelet and because of this scenario the method suggests utility of the idea in motion tracking, video analysis and other such situations.

AMS subject classification: 42C40.
Keywords: Kinematical Group, Uncertainty Principle, Wavelets, Minimizers, Unitary Representation, Commutation Relations, Admissibility Conditions, Kinematical Wavelets.

INTRODUCTION

J P Leduc in his paper [6] analyses rotational motion in image sequences. His paper introduces Lie theory as the actual mathematical foundation of all observable kinematics embeded in spatiotemporal signals. In another paper [7] the same author designed a new family, the Galilean wavelets, using transformation groups and representation theory. In their paper [10] the authors study wavelet based spatiotemporal decomposition techniques for dynamic texture recognition. Murenzi et al. in [15] apply spatiotemporal wavelets to analyze moving patterns. The authors F Mujica et al. in [11], [12] apply continuous spatiotemporal wavelets to missile warhead detection and tracking. Kazuyoshi and Bin Wang in [13] have applied spatiotemporal wavelets in the field of geophysics to analyse multiscale phenomena in ocean currents. The authors in [14] attempt to understand brain function with reported success using spatiotemporal wavelet transform as compared to other techniques.

In this paper we study the spatiotemporal wavelets that arise from a unitary representation of the kinematical groups in dimensions one to four.

We present here a brief note on the kinematical group in n-dimensions. We refer to [1], (Chapter 15, page 342). The wavelets traditionally have been used for analysing static signals or images. To analyse moving objects, changing images or signals one considers $s \in L^2(\mathbb{R}^{n+1}, d^n x dt)$, the space of time dependent signals of finite energy. The operations one would like to carry out on such signals are space translations, time translation, space dilation, time dilation, and space rotations. In the stated reference, it is mentioned that in order to be visible, a fast moving object needs to be wide and narrow objects have to be slow. The transforms that reflect such behaviour are modelled by the following operators.

Define $\mathcal{D} : L^2(\mathbb{R}^{n+1}, d^n x dt) \to L^2(\mathbb{R}^{n+1}, d^n x dt)$ by $(\mathcal{D}^a s)(x,t) = a^{-\frac{n+1}{2}} s(a^{-1}x, a^{-1}t)$, where $a > 0$, $x \in \mathbb{R}^n$ and $t \in \mathbb{R}$. This operator is called the operator of global dilations. Define $\mathcal{A} : L^2(\mathbb{R}^{n+1}, d^n x dt) \to L^2(\mathbb{R}^{n+1}, d^n x dt)$ by $(\mathcal{A}^c s)(x,t) = s(c^{\frac{1}{n+1}}x, c^{-\frac{n}{n+1}}t)$, where $c > 0$, $x \in \mathbb{R}^n$ and $t \in \mathbb{R}$. This operator is called the operator of speed tuning. It is easily checked that these two operators commute indicating the independence of the scale and speed analysis which could be desirable from the physics point of view.

The calculations that follow are promising as they suggest a method of obtaining a family of wavelets depending on the time parameter.

[1] Department Of Applied Sciences and General Engineering, Army Institute Of Technology, Dighi, Pune, Maharashtra, India, 411015.

Dr. S. Tiwari
Offg. HOD-ASGE